Organs-on-chips technologies – A guide from disease models to opportunities for drug development

Anna Grazia Monteduro [1, Δ], Silvia Rizzato [1, Δ], Giusi Caragnano [1], Adriana Trapani [2], Gianluigi Giannelli [3] and Giuseppe Maruccio [1*]

[1] *Omnics Research Group, Department of Mathematics and Physics "Ennio De Giorgi", University of Salento and Institute of Nanotechnology, CNR-Nanotec and INFN Sezione di Lecce, Via per Monteroni, 73100, Lecce, Italy;*

[2] *Department of Pharmacy-Drug Sciences, University of Bari "Aldo Moro", Bari, Italy;*

[3] *National Institute of Gastroenterology "Saverio de Bellis", Research Hospital, Castellana Grotte, Bari, Italy*

* *Correspondence: giuseppe.maruccio@unisalento.it*

[Δ] *These authors equally contributed to the work*

Abstract

Current in-vitro 2D cultures and animal models present severe limitations in recapitulating human physiopathology with striking discrepancies in estimating drug efficacy and side effects when compared to human trials. For these reasons, microphysiological systems, organ-on-chip and multiorgans microdevices attracted considerable attention as novel tools for high-throughput and high-content research to achieve an improved understanding of diseases and to accelerate the drug development process towards more precise and eventually personalized standards. This review takes the form of a guide on this fast-growing field, providing useful introduction to major themes and indications for further readings.

We start analyzing Organs-on-chips (OOC) technologies for testing the major drug administration routes: (1) oral/rectal route by intestine-on-a-chip, (2) inhalation by lung-on-a-chip, (3) transdermal by skin-on-a-chip and (4) intravenous through vascularization models, considering how drugs penetrate in the bloodstream and are conveyed to their targets. Then, we focus on OOC models for (other) specific organs and diseases: (1) neurodegenerative diseases with brain models and blood brain barriers, (2) tumor models including their vascularization, organoids/spheroids, engineering and screening of antitumor drugs, (3) liver/kidney on chips and multiorgan models for gastrointestinal diseases and metabolic assessment of drugs and (4) biomechanical systems recapitulating heart, muscles and bones structures and related diseases. Successively, we discuss technologies and materials for organ on chips, analyzing (1) microfluidic tools for organs-on-chips, (2) sensor integration for real-time monitoring, (3) materials and (4) cell lines for organs on chips. (Nano)delivery approaches for therapeutics and their on chip assessment are also described. Finally, we conclude with a critical discussion on current significance/relevance, trends, limitations, challenges and future prospects in terms of revolutionary impact on biomedical research, preclinical models and drug development.

Keywords: *organ on chip, lab on chip, microphysiological systems, drug screening, drug research, cancer, disease models*

42 # Summary

65
66

Introduction

Fighting human diseases and improving life expectations are key challenges for the modern society. In these efforts, two major routes can be identified: on one side, a better understanding of disease mechanisms and the involved pathological processes; on the other, the development of effective therapeutic strategies for disease treatment with limited side effects and impact on life conditions. Organs-on-chips (OOC) technologies have the ambition to provide a resource-efficient response to this demand in the form of miniaturized microphysiological systems for biomedical research.

In this review, we provide an overview on the current status and latest trends in on-chip disease models with special attention to opportunities for drug development. As sketched in the graphical summary in **Figure 1**, we will start with **(1)** an analysis of OOC technologies with applications for testing the major drug administration routes: **(1.1)** intestine-on-a-chip (oral/rectal route), **(1.2)** lung-on-a-chip (inhalation), **(1.3)** skin-on-a-chip (transdermal) and **(1.4)** vascularization models (intravenous). Here, we will consider how drugs can penetrate in the bloodstream, directly or across relevant blood organ barriers and be conveyed to their targets, including analysis of inflammatory processes.

Then, we will focus on **(2)** microphysiological systems for (other) specific organs, processes and diseases studies: **(2.1)** neurodegenerative diseases (with brain models and blood brain barriers), **(2.2)** tumor models (including their vascularization, spheroids/organoids, engineering and screening of antitumor drugs), **(2.3)** biomechanical systems recapitulating heart, muscles and bones structures and related diseases, **(2.4)** liver/kidney on chips and **(2.5)** multiorgan models for gastrointestinal diseases and metabolic assessment of drugs.

In section 3, we will discuss **(3)** technologies and materials for organ on chips, analyzing **(3.1)** microfluidic tools for organs-on-chips, **(3.2)** sensor integration for real-time monitoring, **(3.3)** materials and **(3.4)** cell lines for organs on chips. Finally, we conclude

with a critical discussion on current significance/relevance, trends, limitations, challenges and future prospects in terms of revolutionary impact on biomedical research, preclinical models and drug development.

This review is not intended to provide exhaustive information on the OOC research (an impossible task for this fast-growing field) but takes the form of an atlas for both researchers approaching the topic and advanced users, providing useful introduction to major themes and indications for further readings.

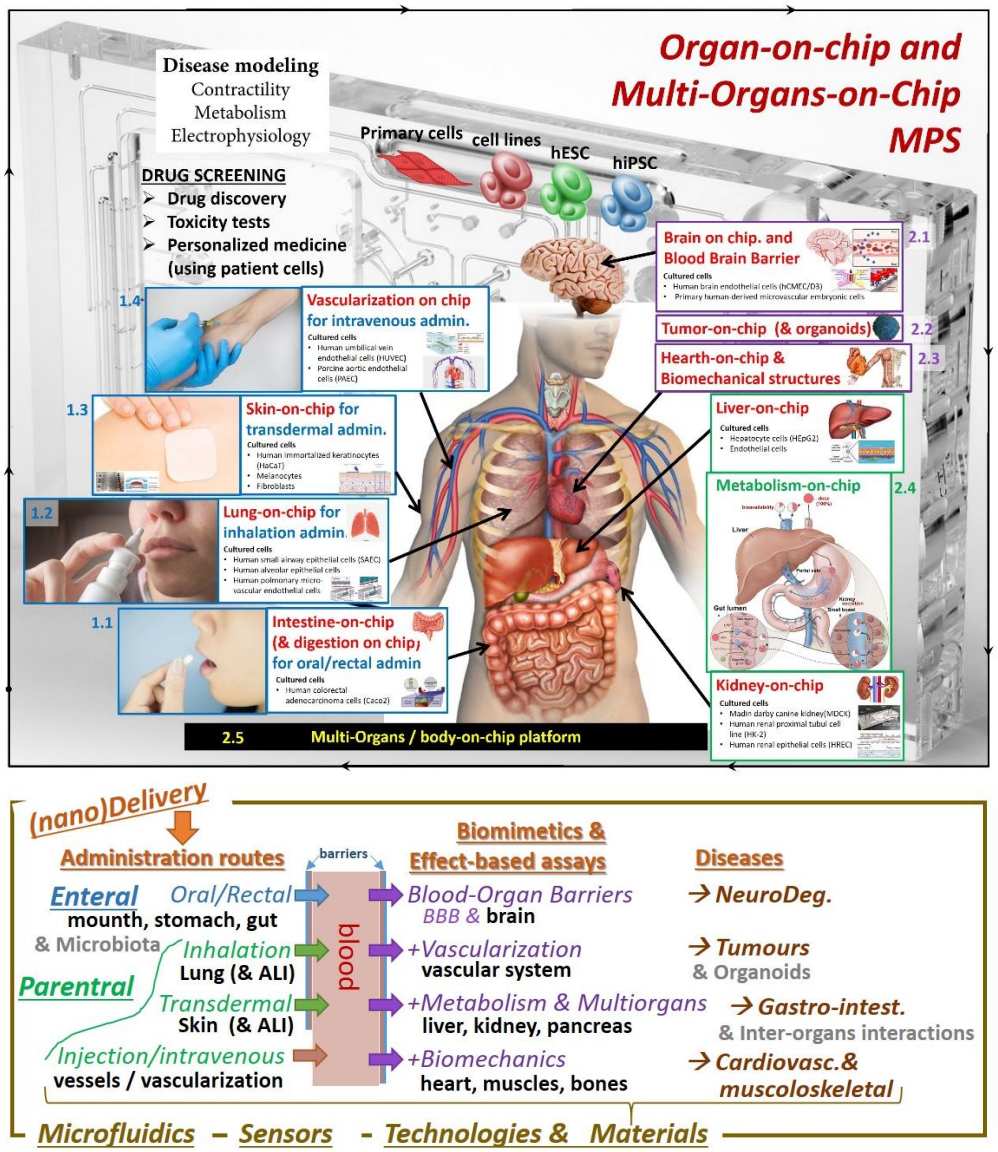

Figure 1. *Graphical summary and main topics covered by the present review, from enteral (oral/rectal) and parenteral (inhalation, transdermal, injection/intravenous) administration routes with relevant organ models (see Section 2) to biomimetics and effect-based assays with relevant organs and related diseases (see Section 3). These sections include discussion also on aspects related to relevant blood organ barriers to cross, vascularization, organoids, metabolisms, multiorgans models. In the external frame are then reported the microfluidics and sensor technologies and materials available for the development of organs-on-chips and automated platforms for high-throughput screening (see Section 4).*

1. Microphysiological systems for testing drug administration routes

The development of new drugs from discovery within proper candidate libraries to preclinical and clinical phases is a quite inefficient, long and costly process (**Figure 2 A**). Indeed, establishing one new drug typically requires several years of research and hundreds of millions of dollars/euros, with the involvement of specialized personnel and a validation procedure characterized by strictly regulated clinical phases and high risk in front of such huge investments. The success rate of new compounds is as low as 5% resulting in significant resources' loss every year. In addition, in the search for novel drugs, another crucial issue to improve therapeutic efficacy concerns the availability of effective routes for pharmaceuticals delivery in patients, e.g. by oral/rectal, inhalation, transdermal or intravenous administration (**Figure 2 B**). Organ-on-chip devices can provide useful support in both these directions, since they allow to recapitulate intrinsic and extrinsic features of an organ/tissue/construct, its microenvironment and biological barriers and enable testing drug efficacy, solubility, permeability, targeted delivery and toxicity in a more appropriate and reliable way [1-7].

Today, drug research relies on the use of conventional in-vitro 2D cell cultures and animal experiments which are not able to properly predict clinical efficacy, toxicity and side effects of therapeutics in humans since they are inadequate to reproduce human physiology. For these reasons, organs-on-chips technologies recently attracted considerable attention as alternative platforms for drug development with research grown tremendously worldwide. The interest is motivated by their potential use for high-throughput, high-content and resource-efficient screening (**Figure 3**). This represents a paradigm change and is important to review recent innovations and advances in the field in order to catch the opportunities provided by most appropriate disease models which are becoming more and more accepted by pharmaceutical companies as novel tools able to accelerate the drug development process towards more precise and eventually personalized standards [8].

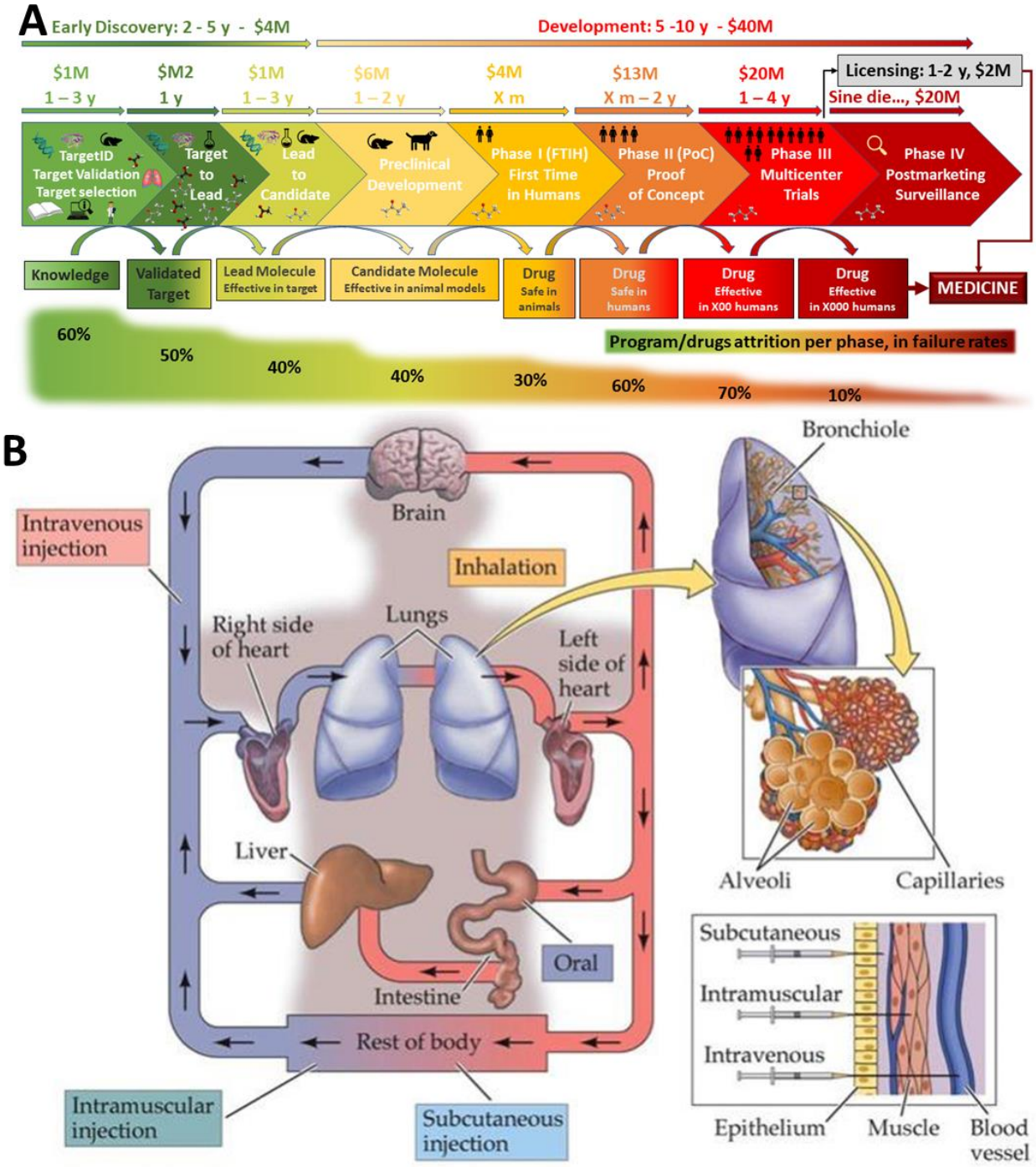

Figure 2.A. *The drug discovery process [https://doctortarget.com/machine-learning-applied-drug-discovery/] and major drug administration routes (beyond the involved organs/barriers, also the time until effect changes with the administration routes from short to long (30-60 s for intravenous administration; 2-3 min for inhalation; 5-30 min for rectal; minutes to hours for transdermal).* ***B*** *Routes of drug administration.*

Before starting to review cases relevant for various organ and diseases, it is worth noticing that a general classification of OOC architecture can be done in terms of ECM dimensionality distinguishing among 2D, 2.5D and 3D models [9]. In 2D models, a

synthetic membrane separates two vertically-stacked compartments and ECM provides coating, favors cell adhesion/growth and participates in defining the barrier and transport properties with respect to nutrients and drugs. 2.5D models are realized either using multiple ECM coated membranes or replacing the membrane with a thin hydrogel film. Instead, in 3D models, thick 3D hydrogel layers are used so that stromal cells can be incorporated to better recapitulate the interstitial matrix [9].

Model properties/ applications	Animals	2D cell cultures	3D cell cultures	Spheroids/ Organoids	Single OOC	Multiple OOC
Biomimetics / Recapitulation	–	✗	–	✓	✓	+
Complexity	✓	✗	–	✓	✓	+
Disease models	–	–	–	✓	✓	✓
Drug research	–	–	–	✓	✓	+
Cell-cell interactions	✓	✗	✓	✓	✓	✓
Organ-organ interactions	✓	✗	✗	✗	✗	✓
Vascularization	✓	✗	✗	–	–	✓
Integration of biosensors for real time	–	✓	✓	✓	✓	✓
Throughput	✗	✓	✓	✓	✓	✓
Costs	✗	✓	✓	–	–	–
Ethics	✗	✓	✓	✓	✓	✓

Figure 3. *Advantages of OOC and MoC platform in comparison to other methodologies.*

156 **1.1 Intestine-on-a-chip for testing oral/rectal administration**

157 A major route for drug administration relies on oral/rectal delivery. Thus, in this
158 section, we focus on intestine-on-a-chip models. Key challenges in this case are represented
159 by gastro-intestinal drug solubility and permeability since drugs must enter the blood
160 circulation upon intestinal absorption in order to become effective. Moreover, potential
161 side effects must be evaluated, in particular on the involved organs (see **Section 2.4 and**
162 **2.5** for metabolism-on-chip, digestion-on-chip and toxicity studies involving liver, kidney
163 and multiorgans microphysiological systems).

164 The intestine plays a fundamental role mediating nutrient, water and drug uptake,
165 performing a critical immunological function and hosting a complex pattern of commensal
166 and mutualistic microorganisms (gut microbiota). Thus it is a relevant model to reproduce
167 in terms of barrier function (from 2D cell cultures to 3D villi microstructures) and
168 physiological conditions including oxygen gradient, shear stress and mechanical
169 deformations [10-13].

170 Various intestine-on-a-chip / gut-on-a-chip designs were reported in literature
171 integrating 3D compartmentalized systems, perfusable chambers, 3D hydrogel scaffolds
172 and stretchable materials for mimicking peristaltic movements [11, 12, 14-16]. 3D
173 compartmentalized systems with upper and bottom chambers separated by a porous
174 membrane provide a simple, popular strategy for organ-on-a-chip layout and the
175 implementation of biological barrier models. Ingber group employed this approach
176 modifying their previously reported breathing lung-on-a-chip [4] (see **Section 1.2**) in the
177 form of gut-on-a-chip [17]. In particular, Kim et al.[17] integrated an ECM-coated
178 polydimethylsiloxane (PDMS) membrane among two PDMS microfluidic channels to
179 obtain two vertically stacked chambers (**Figure 4 A1-A3**). Caco-2 cells were used as
180 human intestinal epithelial cells. The addition of two vacuum chambers on the channel
181 sides permitted to mimic the peristaltic motions, while a strain of Lactobacillys rhamnosus

182 was added to simulate intestinal native microbes. Polarized Caco-2 cells were instead
183 seeded by Kimura et al. to better mimic human intestine [18] since they express
184 morphological and functional characteristics of mature small intestinal enterocytes with
185 better barrier functions.

186 Focusing on drug delivery, the oral uptake of the chemotherapeutic agent SN-38 (7-
187 ethyl-10-hydroxycamptothecin) was investigated by Pocock and coworkers using an
188 intestine-on-chip model [19] which improves conventional Caco-2 Transwell approach by
189 better mimicking the biological barrier function (**Figure 4 B1-B3**). In more detail, they
190 differentiated an epithelial cell monolayer using external mechanical stimuli and obtained
191 a 3D rippling morphology mimicking microvilli expression. Then, they investigated the
192 structure permeability for SN38 modified with fatty acid esters of different lengths and at
193 different positions, demonstrating that lipophilic prodrugs can contribute to tackle low oral
194 bioavailability issues. These models are also applicable to nanoformulations and biological
195 entities.

196 The transport of both high- and low-permeability drug compounds across the intestinal
197 barrier was studied by Kultong et al. [20] with a dynamic gut-on-chip model (**Figure 4 C1-**
198 **C3**). Specifically, the investigated compounds were antipyrine, ketoprofen, digoxin, and
199 amoxicillin with concentrations up to 500 μM, 300 μM, 250 μM, and 500 μM, respectively,
200 for 24 h on a differentiated monolayer of human colorectal adenocarcinoma cells (Caco-2).
201 The authors compared the apparent permeability (P_{app}) values of the four compounds and
202 observed that for antipyrine and ketoprofen, P_{app} values were lower in Caco-2 cells under
203 dynamic flow conditions than under static conditions in transwell systems. These
204 differences may be due to the effect of the chip design, the material composing the diffusion
205 membrane, and the presence of laminar flow. For amoxicillin which is a low permeability
206 compound, the P_{app} values are instead similar under both dynamic and static flow
207 conditions. Based on a comparison of OOC approach with the static transwell model,

208 Kultong et al. concluded that their gut-on-chip model was adequate to study drug transport
209 [20].

210 Notably, gut-on-a-chip models were likewise employed to study (with improved
211 efficacy) the response to nutrients and to emulate gut inflammation, host-microbiota
212 interplay as well as interactions with environmental factors where the imbalance between
213 pro-inflammatory and anti-inflammatory cytokines and alterations of the composition and
214 function of the gut microbiota (dysbiosis) play a pivotal role [15, 21-23]. As a result, OOC
215 can provide valuable insights on intestinal dysfunction and physiopathology, the involved
216 pathways and their relation to severe and chronic gut diseases with complex etiology from
217 early stage to full manifestation and eventual worsening [12-15]. In this respect, OOC are
218 expected to overcome animal models which often fail when extrapolated to humans due to
219 the differences in microbiota composition and immune system. Furthermore, OOC models
220 are expected to overcome limitations of 2D and 3D cultures, such as the lack of cell-matrix
221 interaction and mechanical stimuli respectively [24, 25].

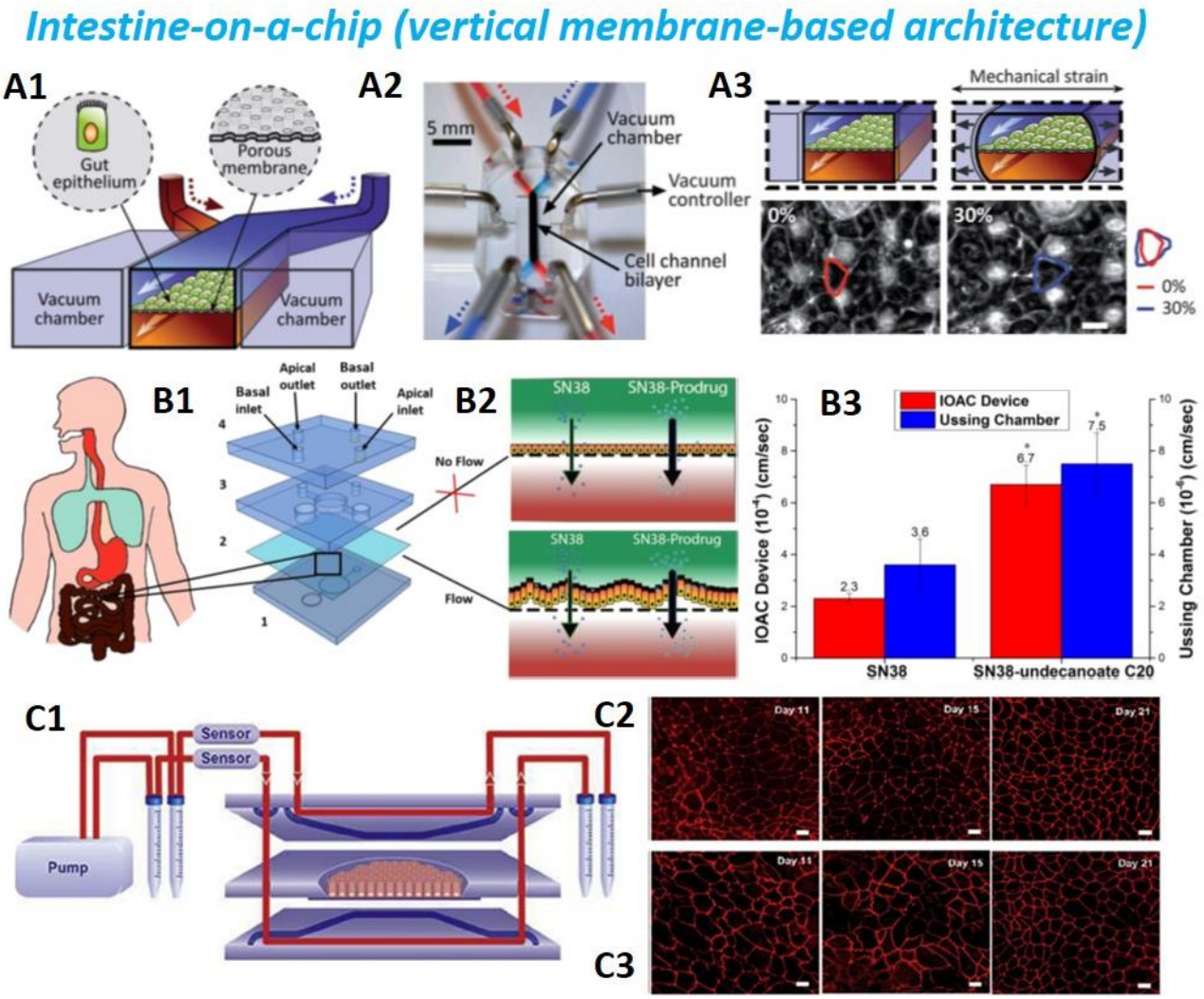

Figure 4. (A1) *Schematic representation of the gut-on-a-chip device in which the ECM membrane is covered by gut epithelial cells and cross the central microchannel between two vacuum chamber.* ***(A2)*** *A photo of the gut-on-a-chip device. Blue and red dyes flow through tubing to the upper and lower microchannels, respectively, to visualize these channels.* ***(A3)*** *Schematic (top) and phase contrast images (bottom) of intestinal monolayers cultured within the gut-on-a-chip in the absence (left) or presence (right) of mechanical strain. Reproduced from Ref. [17].* ***(B1)*** *Structure of the intestine-on-a-chip reported by Pocock et al. with apical and basal chambers separated by a PC membrane.* ***(B2)*** *Scheme of the performed permeability assay for chemotherapeutic agent SN38 through Caco-2 cell monolayers.* ***(B3)*** *Comparison among results from the OOC platform and rat intestinal mucosal membrane mounted in an Ussing Chamber. Reproduced from Ref. [19].* ***(C1)*** *Microfluidic gut-on-chip realized by Kulthong et al. and consisting of three re-sealable glass slides resulting in two microfluidic chambers separated by a polyester (PET) membrane where Caco-2 cells were cultured. The flow was injected by use of a multichannel air pressure pump. Confocal microscope images of top view of the Caco-2 cells layer, evidencing tight junction patterns (ZO-1/TJP1) in red, cultured for 21 days in a static Transwell system* ***(C2)*** *or a gut-on-chip system* ***(C3)*** *under a continuous flow of 100 µL/h. Reproduced from Ref. [20].*

237 **1.2 Lung-on-a-chip for testing inhalation administration**

238 Administration by inhalation provides another important route which is particularly
239 relevant for respiratory and pulmonary diseases including viral and bacterial lung
240 infections, chronic obstructive pulmonary disease (COPD), pulmonary edemas,
241 tuberculosis and lung cancer which are among the top 10 causes of death according to
242 World Health Organisation [26]. Against these diseases, inhaled drugs can be
243 advantageous for rapid delivery/action and in terms of targeted instead than systemic
244 exposure with drugs directly deposited within the airways. In this case, the absence of
245 interaction with liver or kidney can result in reduced toxicity and side effects and thereby
246 improve therapeutic efficacy, patient outcomes and patient quality of life [27, 28]. By
247 reproducing human in vivo pulmonary microenvironment, the air-liquid interface and the
248 lung-blood barrier for inhaled agents, lung-on-chip platforms facilitate research [4, 9, 29-
249 32].

250 Major difficulties in recapitulating lungs airways lies in their morphological and
251 histological complexities with the presence of different types of cells and epithelium in
252 addition to mucus and the relevance of branching and breathing movements. Remarkably,
253 in their seminal work, Huh et al. [4] demonstrated a breathing lung-on-a-chip (**Figure 5**
254 **A1-A2**) having the form of a compartmentalized system with vertically-stacked chambers
255 separated by a porous membrane. Specifically, the upper and bottom chambers were
256 seeded with human alveolar epithelial cells and lung capillary endothelial cells respectively.
257 An air-liquid interface (ALI) mimicking the alveolar-capillary barrier was then reproduced
258 by depleting the cellular media in the upper compartment. Two side vacuum chambers
259 were also realized to reproduce the cyclic strain and mechanical forces on the culture
260 membrane associated to breathing (**Figure 5 A1**). This architecture then became very
261 popular and extensively used in OOC models, beyond the lung-on-a-chip case [33, 34].

262 Known biomarkers (e.g. fluorescent albumin, transferrin and dextrans) are habitually

263 employed to evaluate the barrier permeability and the influence of shear stress on
264 paracellular and transcellular transport, i.e. between epithelial/endothelial cell junctions
265 or through cell lacking the required active transporters [4, 33]. In this respect, confocal
266 microscopy is a valuable technique since it permits localization of the biomarkers in the
267 different compartments to investigate transport across the barrier. In general, the alveolar
268 barrier permeability was found to be significantly smaller than in the case of liquid cultures
269 [4]. Trans-epithelial electrical resistance (TEER) measurements provide an useful
270 alternative to confocal microscopy for evaluating the barrier characteristics since the
271 resistance correlates to the tightness of the cell junctions [4, 35, 36] (**Figure 5 A3**).

272 A model of drug toxicity–induced pulmonary edema was also implemented by Ingber
273 group using a similar alveolar-capillary interface with human pulmonary epithelial and
274 endothelial cells that experience both air and fluid flow. In this study, the applied cyclic
275 mechanical forces [37] mimicking the breath were found to play a relevant role in the
276 edema formation and the authors had the possibility to test some therapeutic approaches.

277 This membrane-based architecture, however, does not exhaust all the proposed
278 approaches. Various models and interfaces have been reported using different
279 architectures and types of cell culture. They span from simple monocultures for the
280 epithelium [38, 39] to co-cultures for epithelial-endothelial (in alveolar-capillary [4, 40-
281 43] and small-airway models [44]) and epithelial-mesenchymal [45] interfaces. Tri-
282 cultures with epithelial, fibroblast and endothelial cells were instead employed for
283 recapitulating epithelial-stromal/vascular tissue interfaces [46-48]. In this way, through
284 an appropriate cell selection, lung barrier function, inflammation, immune response and
285 injury were modeled in lung-on-a-chip format providing unprecedented tools for
286 physiopathological investigations, drug development, inhalation assays, exposure studies
287 and airborne toxicological assessment [4, 9, 30, 49, 50].

288 In particular, microphysiological models of human asthmatic and COPD airways are

289 relevant for better understanding and contrasting diseases which have a high personal,
290 societal and economic impact and are associated to inflammatory processes affecting the
291 whole respiratory tract, from central to peripheral (small) airways [51] which have sizes <2
292 mm in internal diameter and include bronchioles and alveoli. Remarkably, an organotypic
293 small-airway-on-chip was reported by Ingber group using membrane-separated chambers
294 and microvascular endothelium and mucociliary bronchiolar epithelium from patients
295 (**Figure 5 B1-B3**) [44]. Interestingly, the authors analyzed the exposure to interleukin-13
296 (IL-13, which has a key role in asthma), viral mimic poly(I:C) (an analogue of dsRNA
297 produced by cells infected by respiratory viruses) and lipopolysaccharide endotoxin (LPS,
298 a bacterial wall derived component) in terms of effect on inflammatory
299 cytokine/chemokine secretion, decreased ciliary function, globet cell hyperplasia and
300 neutrophil recruitment. Then, they used the same platform for drug discovery applications
301 and in particular testing therapeutic agents capable to contrast the inflammation. Viral-
302 induced exacerbation of asthma was investigated by Nawroth et al. too [52]. Stucki et al.
303 instead employed micro-diaphragms and an electro-pneumatic setup to stretch the alveolar
304 barrier and showed the effect of these mechanical cues on metabolic activities and cytokine
305 secretion [42]. A layout with three vertically stacked chambers with arrayable suspended
306 gels was realized by Humayun et al. to examine the interactions among airway epithelial
307 cells and smooth muscle cells which are relevant in chronic lung diseases [45].

308 Injuries, alveolar epithelial wound healing under mechanical strain and intravascular
309 thrombosis were another subject of study for the development of new anti-inflammatory
310 therapeutic agents [38, 53]. The inclusion of fibroblasts in these models is important to
311 contemplate their interactions with epithelial and immune cells and their role in airway
312 repair through ECM deposition and degradation, once triggered by epithelial cells after an
313 injury [9]. In this respect, Sellgren et al. employed an architecture with three vertically
314 stacked chambers to produce an airways model with epithelial cells, lung fibroblasts and

315 polarized microvascular endothelial cells [46]; while Bovard et al. combined lung/liver-on-
316 a-chip for toxicity studies [54] (for multi-organ on chips models see **Section 2.5**). Other
317 recent reports focused on modeling fibrotic diseases [55], investigated endotheliitis and
318 vascular damage during SARS-CoV-2 infection [56], and intriguingly the spontaneous
319 evolution of influenza viruses [57].

320 Beyond the membrane-based approach, different architectures with adjacent chambers
321 were recently reported with the target to provide improved 3D models able to better mimic
322 in vivo structures [31, 47, 48, 50]. In particular, Zhang et al. realized three parallel channels
323 (**Figure 5 C**) with a lung and a vessel side respectively lined with human pulmonary
324 alveolar epithelial cells and vascular endothelial cells. The middle ECM channel was then
325 filled with Matrigel to recapitulate the alveolar capillary barrier. This platform was
326 employed for nanotoxicity tests [50]. The bronchiole model by Barkal and colleagues has
327 some similarities and differences. This approach offers more physiologically relevant
328 microarchitectures in terms of sizes, geometries and 3D interactions as compared to flat
329 conformations with porous membranes. Furthermore, the various compartments can be
330 addressed separately and the cell types are exposed to different conditions thanks to gel
331 polymerization in a stable 3D structure and the presence of appropriate ports for
332 injection/removal/sampling. The counterpart is the inherent difficulty in collecting gel-
333 embedded cells since device disassembly for gel extraction and subsequent digestion is
334 required. This process became even harder in multicellular hydrogel-based models [48],
335 when cell collection is necessary before digestion or requires cell sorting method.

336 3D cell printing was employed by Park et al. to fabricate an airways model comprising a
337 blood vessel network made of human dermal microvascular endothelial cells and human
338 lung fibroblasts in decellularized ECM. Primary human tracheal epithelial cells were
339 instead seeded on a Transwell insert containing an ECM membrane [48]. The presence of
340 a vascular network improves the physiological relevance of this model, although the co-

culture of endothelial cells and fibroblasts complicate the analysis [9]. Recently, in the search for more physiologically relevant models and materials, alternative architectures were proposed using nanofiber membranes [58], reverse engineered hydrogels with inverse opal structure [39] and stretchable collagen-elastin biomembranes.

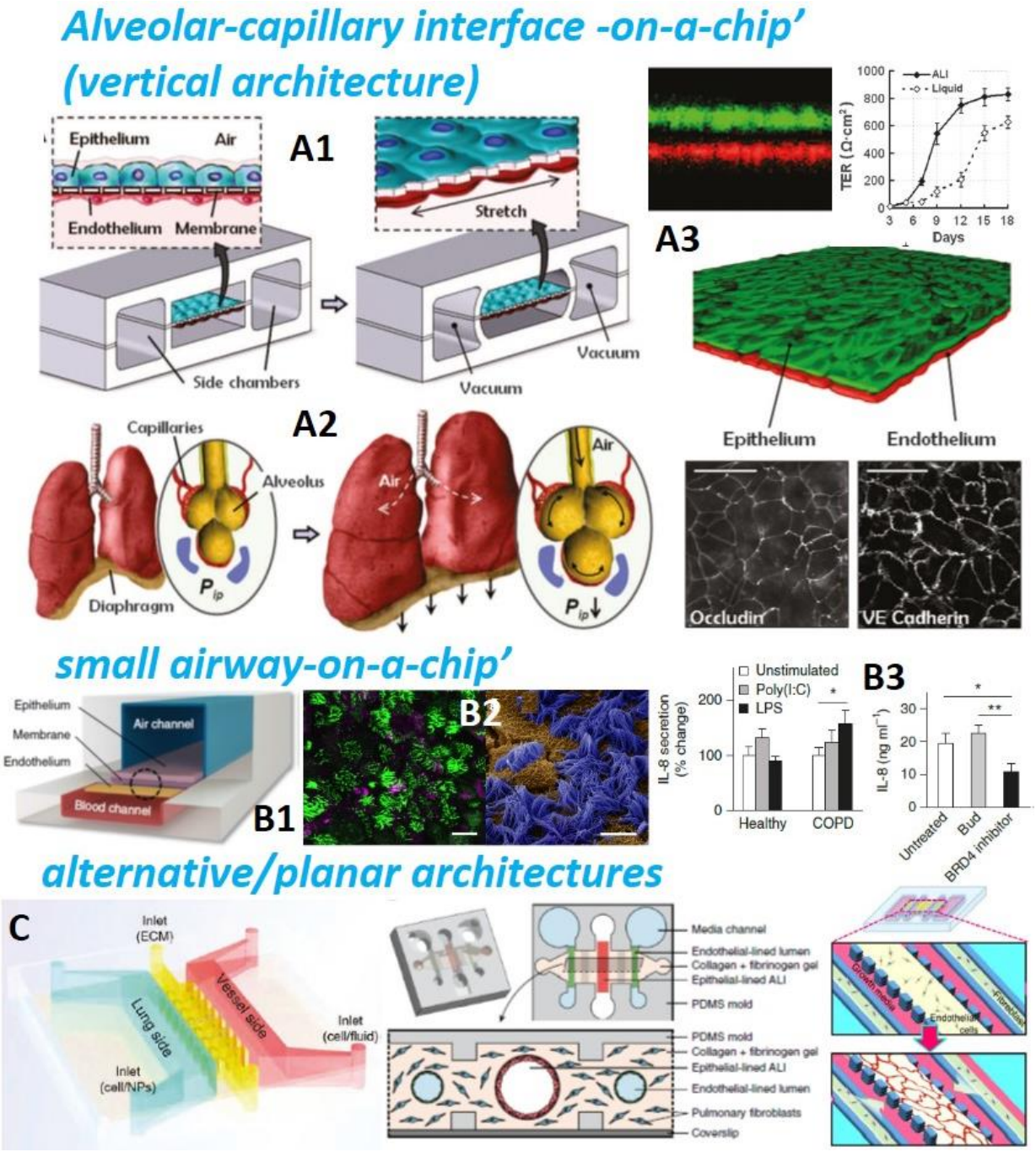

Figure 5. (A1-A2) *Alveolar air-liquid interface model reported by Ishahak et al. [34] which uses a cyclic pressure to mimic breathing.* ***(A3)*** *Assessment of the interface by TEER measurements and fluorescent staining. Reproduced from Ref. [34].* ***(B1)*** *Air-liquid interface model workflow with seeding of endothelial cells (LMECs) and then alveolar epithelial cells (AECs) on a transwell system.* ***(B2)*** *Human airway epithelium grown on chip (scale bar, 20 µm) and cilia (blue) on the apical surface of the airway epithelium (scale bar, 10 µm).* ***(B3)*** *Effects on production of the cytokines IL-8 on small airway chips lined by either normal or chronic obstructive pulmonary disease epithelial cells (left) and upon therapeutic modulation of cytokine inflammation (right). Reproduced from Ref. [44].* ***(C)*** *Schematic of structures of lung-on-a-chip with alternative/planar architecture. Reproduced from Ref. [47, 48, 50].*

354 **1.3 Skin-on-a-chip for testing transdermal administration**

355 Skin implements several functions for the body: (i) thermoregulation through sweat
356 glands, (ii) heat, pressure and strain sensing through several sensory receptors, (iii) vitamin
357 D synthesis. As a physical barrier, it preserves from dehydration, maintains gas
358 concentration gradients (for O_2, CO_2, N_2) and protects the body against exposure to external
359 agents and threats (including microorganisms, ultraviolet radiation, toxic and mechanical
360 agents). Within the therapeutic field, transdermal drug administration provides a mean for
361 administration of systemically acting drugs through vessels or adipose tissue after
362 overcoming the skin barrier.

363 Human skin-on-a-chip (SOC) models [59-64] attracted significant attention for
364 dermatological studies, wound healing, risk assessment for external agents/chemicals,
365 evaluation of cosmetic products and their ingredients and transdermal drug administration
366 research. In this case, differences with animal skin are considerable in terms of structural
367 and biochemical properties, lipid profile, hair density and stratum corneum thickness [60].
368 As the more external layer consisting of protein-rich dead cells in a lipid matrix, the stratum
369 corneum influences drug permeation with its thickness and lipid composition contributing
370 in establishing the barrier penetration characteristics. 2D cell cultures suffer in
371 appropriately recapitulating attachments and growth kinetics and the lipid profile and, for
372 example, can exhibit limitations in evaluating permeability of hydrophilic compounds
373 depending on the use of non-lipid or lipid-based membrane models. 3D skin-on-a-chip
374 models can better mimic in vivo physiological conditions.

375 Human skin consists of three structural compartments. The external, avascular
376 epidermis layer is mainly composed of keratinocytes producing keratin as a protective
377 protein. The intermediate dermis compartment is a connective tissue with fibroblasts as the
378 primary cell component in a collagen microenvironment, elastin fibers providing elastic
379 properties and hyaluronic acid involved in skin hydration. It is pervaded by blood and lymph
380 vessels and contains nerves, sensory receptors, sweat and sebaceous glands, hair follicles
381 and shafts. The inner subcutaneous tissue is predominantly made of adipocytes (fat cells) in

382 addition to fibroblast and macrophages and is characterized by larger nerves and blood
383 vessels. For widening the range of functions and possible investigations, it can be relevant
384 to include additional cell types (e.g. melanocytes and Langerhans cells in the epidermis)
385 [62]. Both skin biopsies or models generated off-chip were integrated in chip models.

386 Progress in the field came through the development of more and more appropriate and
387 complete models. We can distinguish different categories of in vitro skin models (**Figure 6**
388 **A**) with increasing physiological relevance and complexity and skin-on-a-chip followed a
389 similar development [59-61, 63, 64]:

390 • reconstructed human epidermis (RHE) models typically uses only one cell type
391 (keratinocytes): they provide a well-established and reproducible platform for risk
392 assessment and were employed in skin irritation, corrosion and sensitization studies in
393 toxicological and cosmetic research as well as transdermal drug delivery, phototoxicity,
394 metabolization assays [65]. With the incorporation of melanocytes, RHE models allow
395 skin lightening and pigmentation assays [66]. However, more advanced models are
396 needed for drug efficacy tests, recapitulating cross talk with other cell types;

397 • dermo-epidermal human skin equivalents (HSE) [64, 67] are cultivated in serum and
398 include the dermis compartment with collagen I and fibroblast cells in proximity to the
399 keratinocytes which are seeded in a second phase and cultivated at the air-liquid interface
400 to form the adjacent epidermal compartment. These models allow to investigate cell-cell
401 crosstalk and provide more biomimetic barrier properties. In vitro, they exhibit high
402 reproducibility and standardization and enable evaluation of wound healing and bacterial
403 adhesion. Major drawbacks concern the limited lifespan and the limited cell types
404 employed.

405 • human skin equivalents integrating other cell types to perform investigation of basic
406 melanogenesis and vitiligo pathogenesis (incorporating melanocytes), innate immune
407 response, irritant exposure and allergen assessment (incorporating immune or
408 Langerhans cells); epidermal development, wound healing, pigmentation disorders and
409 autologous transportation (incorporating stem cells) [64, 68-70]. Dorsal root ganglion

410 neurons were also incorporated to reconstruct a peripheral skin nerve system [63].
411 Models with trans-appendageal moieties were furthermore developed, e.g. hair follicles
412 for substance penetration studies [71]. Limitations include lower standardization and
413 limited tissue survival.

414 • vascularized human skin equivalents are the next technological step which allows
415 nutrients and oxygen supply and waste removal resulting in extended tissue survival. This
416 approach enables the assessment of transdermal penetration of drugs in the bloodstream,
417 angiostatic therapies and adipose metabolism, impact of drugs on adipose tissue and
418 angiogenesis. While long term cultivation becomes feasible, this technology is less
419 standardized than the previous ones.

420 • skin-on-a-chip models promise to provide the ultimate step of technological innovation
421 in the form of miniaturized microfluidic platforms which allow high throughput
422 physiologically relevant studies at reduced costs by applying different physical and
423 biochemical stimuli (including shear stress, mechanical forces and chemical gradients).
424 Skin fragments have been either transferred to the chip from a biopsy or a HSE [72, 73]
425 or directly generated in situ (in an open structure or in channels as tissue-holding
426 compartments) [74-82].

427 SOC advances underwent similar development phases from RHE [72, 83] to HSE and
428 integration of additional cell types, components and vascularization [60]. RHE-based SOC
429 employed young and mature keratinocytes with different level of stratification and
430 junctional tightness, exhibited stability above 24 h and were employed for in vivo irritation
431 assays [84]. HSE-based SOC exhibited better barrier functions due to an improved cell
432 viability and were used for transdermal/topical drug permeation studies (**Figure 6 B1-B7**)
433 [79, 85] and wound healing [86, 87] and skin microbiome investigations [88]. A 3D vinyl-
434 based bilayer tissue model made of an epithelial and a stromal component was reported by
435 Valencia et al. [89] using immortalized human skin keratinocytes (hKCs, HaCaT cell line)
436 and primary human dermal fibroblasts (hFBs). A microporous (polycarbonate) membrane
437 was again employed to separate the skin model from a blood vessel channel used to

recapitulate dynamic perfusion and drug delivery. Varone et al. introduced two vacuum channels around the epithelium chamber to apply mechanical forces [90].

Hair follicles were incorporated in SOC models by Atac et al.[91]. Integration of explants in SOC can provide access to all cell types and diseased skin but suffer for limited availability and donor variability. Multi-organ on chips integrating skin with other models (e.g. liver, intestine and kidney) to investigate their crosstalk are the next frontier [92-94] (see **Section 2.5**). Microfluidic arrays of dermal spheroids were implemented by Chen et al. as a screening platform for skincare products ingredients [95].

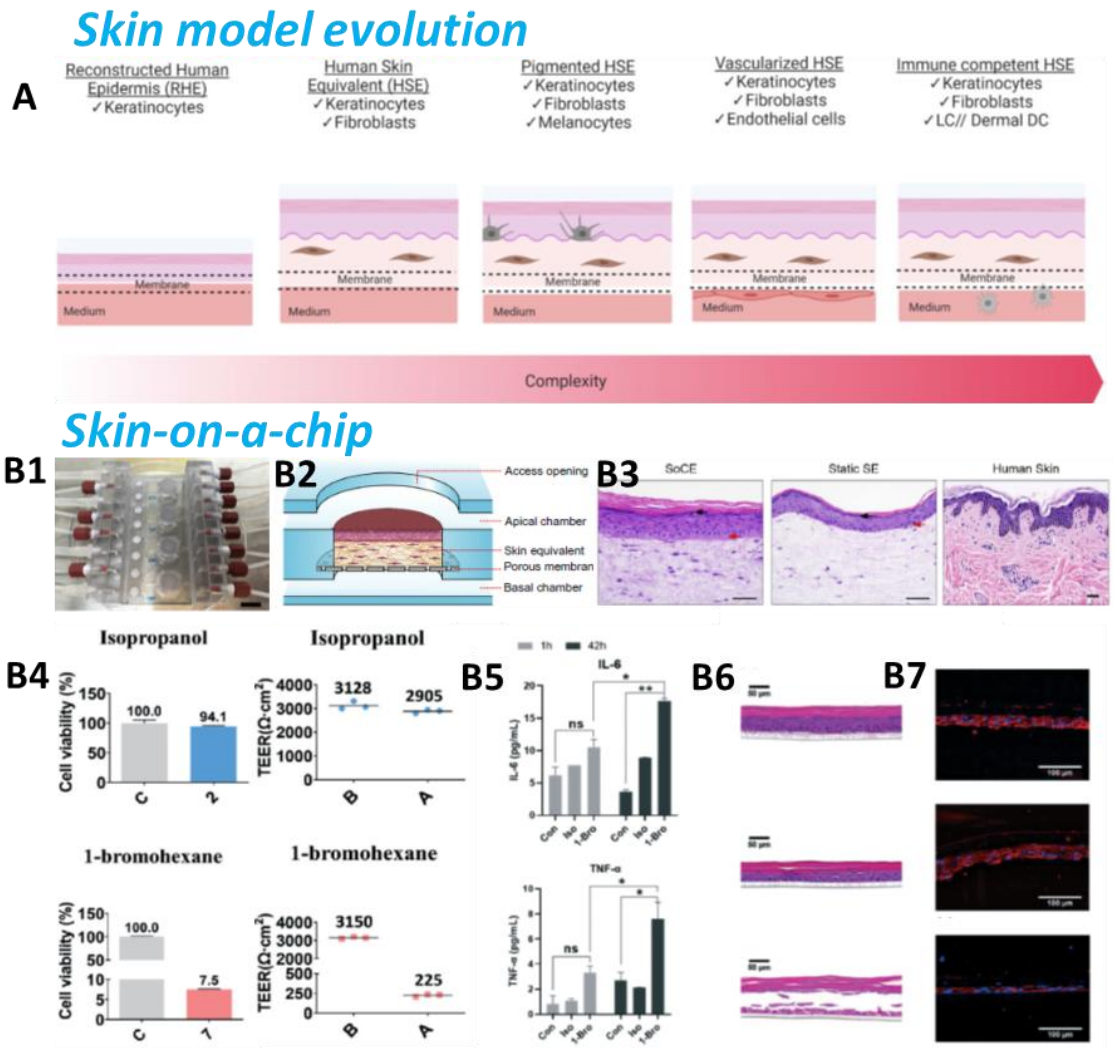

Figure 6. (A) *Summary of selected 3D in vitro skin tissue models, depicted with increasing biological complexity from left to right and their research applicability and predictability for NGRA using an open access OOC device for air–liquid culturing. Reproduced from Ref. [61].* ***(B1-B2)*** *Photographs and scheme of skin-on-chip equivalent (SoCE);* ***(B3)*** *Histological images representing epidermal morphogenesis in skin-on-a-chip equivalent compared to static human skin equivalents. Reproduced from Ref. [79]* ***(B4)*** *MTT Cell viability (C = negative control) and TEER values of the skin-on-chips before and after 42h exposure to isopropanol and 1-bromohexane irritation (label B means before, A means after).* ***(B5)*** *Inflammatory cytokine release following isopropanol and 1-bromohexane irritation.* ***(B6)*** *Hematoxylin–eosin staining of integrated epidermis-on-chip (iEOC) system:(from top to bottom) control, isopropanol irritation and 1-bromohexane irritation.* ***(B7)*** *Tight junction maker ZO-1 staining of integrated epidermis-on-a-chip: control, isopropanol irritation and 1-bromohexane irritation. Scale bars: 100 μm. Reproduced from Ref.* [84]

457 **1.4 Vascularization models for testing intravenous administration**

458 The vascular system has a critical role for maintaining homeostasis and organ-specific
459 functions [96]. Tissue survival in vivo is entirely dependent on delivery of nutrients through
460 blood vessels, while vascular dysfunctions are associated to various chronic or acute
461 disorders. Furthermore, several therapeutic agents are directly administered intravenously
462 instead than reaching the bloodstream across other biological barriers/organs. Compared
463 to oral administration, this route allows shorter times until effect and, importantly, permits
464 to overcome impediments related to low gastro-intestinal solubility and permeability [19].

465 Thus, it is not surprising that the recapitulation of micro-tissues and organoid
466 vascularization became focus of intense research as a key tool for providing suitable disease
467 models with superior biomimetic performance in investigating pathophysiology and testing
468 drug efficiency. In this respect, it is worth noting that vascularization additionally consents
469 to increase lifespan of OOC models and, for this reason, it is often integrated in various
470 microphysological systems (as already mentioned in some examples before). On the other
471 hand, on chip models are relevant for the investigation of specific diseases of the vascular
472 system such as atherosclerosis and deep vein thrombosis [7].

473 Various techniques were exploited and, in some cases, combined to produce network of
474 perfused microvessels, vascularized micro organs (VMO) and micro tumors (VMT) [97-99].
475 Vasculogenesis and angiogenesis are the biological processes responsible for in vivo
476 formation of new blood vessels leading respectively to de novo formation of vascular system
477 and growth of capillaries from pre-existing vasculature [100, 101]. Driving these processes
478 in vitro provides an effective strategy for a (random) formation of vessels by seeding
479 precursors, stem or endothelial cells inside extracellular matrix and exposing them to
480 vascular growth factor (e.g. VEGF) [102]. This approach permits to generate random
481 networks of sub-100 μm vessels but presents limitations when perfusable vascular lumens
482 are the target.

483 In this case, microfluidics, soft lithography, 3D printing and bioprinting provide useful
484 alternatives and support. For example, soft lithography allows to realize perfusable
485 microchannel networks by replica molding following an appropriately engineered CAD
486 design. In this case, the (already discussed) membrane-based layout is a widespread
487 strategy upon the pioneering work of Ingber group [4] and was employed in various organ-
488 specific models including lung, gut, liver, kidney, hearth, brain and blood-brain barrier. In
489 **Figure 7 A**, the case of application to liver is reported [103]. In particular, in the liver-on-
490 a-chip model by Du et al., the four major hepatic cell lines were grown in two membrane-
491 separated chambers to recapitulate liver functions (namely from base to top: hepatocytes,
492 hepatic stellate cells, the liver sinusoidal endothelial cells and Kupffer cells).

493 Other architectures are based on lateral/planar microchannels (e.g. interconnected by
494 sub-networks of smaller sizes) [98]. External pumps with valves or hydrostatic pressure
495 consent to drive the flow in the perfusable vascularized systems. In all these cases, the use
496 of scaffolds with predetermined geometries enables high control on lumen sizes, network
497 interconnections, flow rates and imposed shear stress. Direct micromachining of
498 microfluidic networks was also performed by laser patterning techniques with advantages
499 in realizing layer-by-layer architectures but at higher cost (**Figure 7 B**).

500 Templating and sacrificial molding methods are another option (**Figure 7 C**). In this
501 respect, 3D printing offers a cost-efficient approach through the use of cytocompatible
502 sacrificial templates in engineered tissues but presents limitations in terms of minimal sizes
503 (no less than ≈100μm) [104]. As examples, in skin-on-a-chip field, Abaci et al. and Mori et
504 al. [105, 106] exploited respectively micropatterned alginate sacrificial layers or nylon
505 threads successively removed in order to obtain hollow channels to be covered by
506 endothelial cells [105, 106]. A combination of 3D printing for the device layout and 3D
507 bioprinting of the cellular layers was exploited by some authors as a mean to achieve high
508 structural control [107].

509 In various reports, biological processes and engineered-based fabrication techniques
510 have been successfully combined to exploit the advantages of both worlds [98, 108, 109]
511 leading to microfabricated vessel scaffolds by lining microfluidic channels with endothelial
512 cells (**Figure 7**). For example, Hughes and Lee group realized perfusable microvascular
513 networks connecting microfluidic channels without noticeable leakage. The adopted
514 strategy was to pass through different stages of vascular development from vasculogenesis,
515 to endothelial cell (EC) lining, sprouting angiogenesis and anastomosis (**Figure 7 D**) [109].
516 Then, they employed this approach to support the in vitro growth of 3D (vascularized)
517 microtumors and to investigate the effect of drugs targeting growth factors in terms of
518 regressing the vasculature [110]. Tumor cell extravasation dynamics was also investigated
519 using on-chip microvascular models [111] (see **Section 2.2** for further details).
520 Remarkably, vascularized OOC are suitable for screening the efficacy/toxicity of libraries
521 of relevant compounds against multiple tissues in a more physiological environment.
522 Finally it is worth mentioning that Pradhan et al. investigated how hemodynamic forces
523 and vascular parenchymal mechanotransduction influences relevant pathways in organ-
524 specific niches and pathophysiological states, a possible way toward developing
525 mechanotherapeutics [96]. A further option is to transfer tissues on chip, where further
526 studies are then carried out.

527 In terms of bioavailability, blood organ barriers can however limit drugs in reaching
528 their targets. For these reasons, numerous studies focused on the accuracy of microfluidic-
529 based in vitro reproduction of these barriers in order to provide miniaturized and
530 controllable platforms for investigating drug delivery and pharmacokinetics as well as
531 nutrient/gas/waste exchange. The gut and lung cases were described before. Another
532 important case is represented by the blood-brain barrier which is relevant for
533 administering drugs to the brain and for developing therapies for neurodegenerative
534 diseases (see **Section 2.1** for details). Other examples of applications to liver and kidney

are reported in **Section 2.4** since these organs are key players in drug metabolism and clearance with impact on bioabailability and side effects/toxicity.

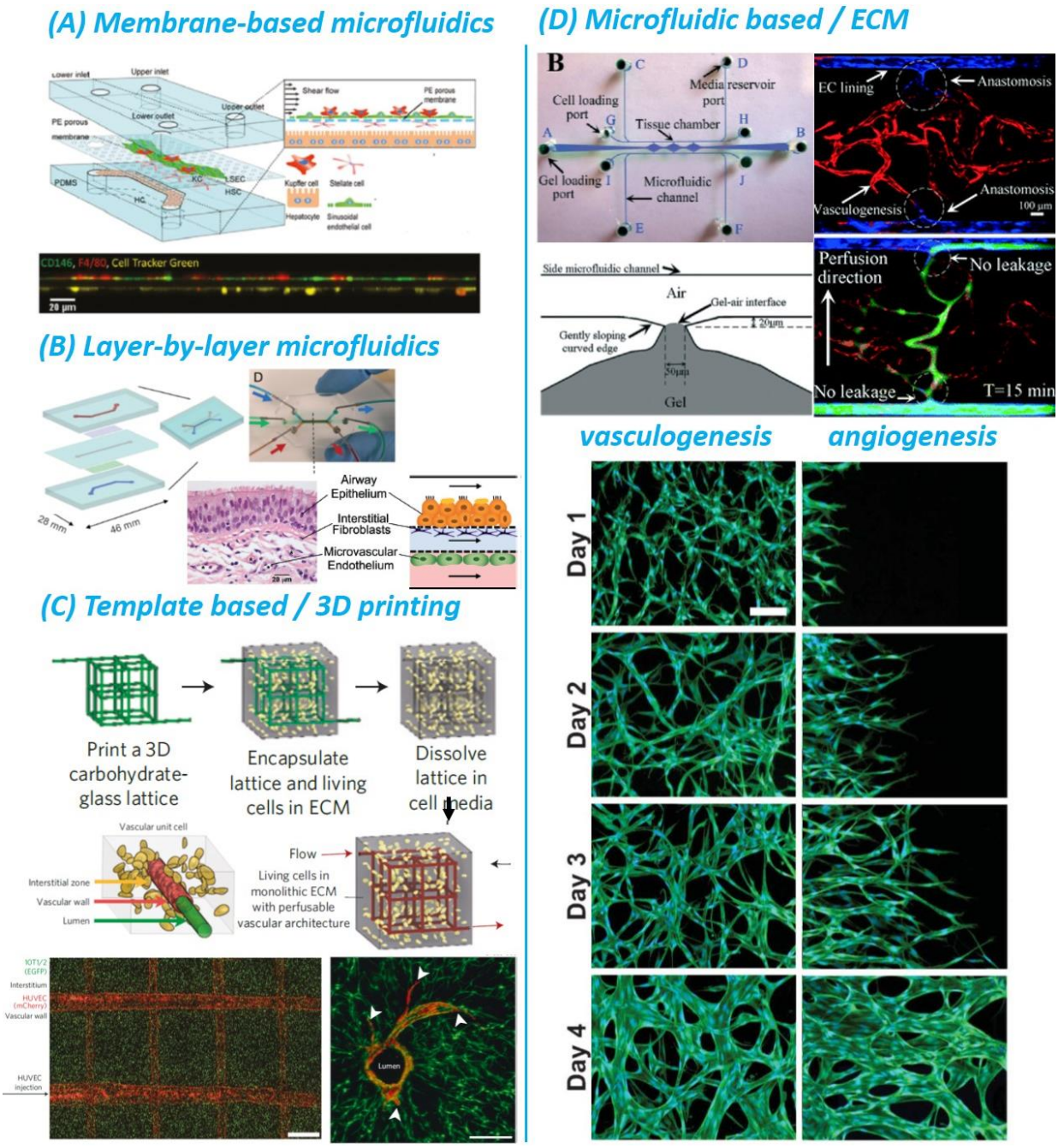

Figure 7. *Schematic representation of methods employed to vascularize 3D OOC models. These techniques can be divided into soft-lithography and 3D patterning approaches.* ***(A)*** *Membrane-based soft lithography technique in which a porous membrane is inserted among two microfluidic channels. Reproduced from Ref. [103].* ***(B)*** *Layer-by-layer microfluidics consisting of assembled modular layers. Reproduced from Ref. [46].* ***(C, top)*** *Templating approaches in which a matrix is cast around the template. The template is subsequently removed, generating hollow channels, which can be seeded and perfused.* ***(C, bottom)*** *Three-dimensional printing (bioprinting) in which vascular and cell inks are used to generate a 3D tissue with embedded, perfusable vascular channels. Reproduced from Ref. [104].* ***(D, top)*** *ECM-based soft lithography in which microfluidic channels are filled with ECM [109].* ***(D, bottom)*** *Micrographs of vasculogenic and angiogenic vessel formation in the fibrin matrix as a function of time. Reproduced from Ref. [108].*

547 ## 2. Microphysiological systems for (other) organs/disease studies and multi-
548 organs platforms

549 ### 2.1 Blood brain barrier and OOC for neurodegenerative diseases

550 The blood-brain barrier (BBB) separates bloodstream from brain tissue and is formed
551 by specialized endothelial cells, pericytes and astrocytes up to neurons, as illustrated in
552 **Figure 8 top** [112, 113]. Its study attracted significant attention as the BBB represents a
553 formidable challenge to access the central nervous system for delivery of pharmaceuticals
554 and therapeutic antibodies against neurological disorders. Indeed, by implementing its
555 neuroprotective function, the BBB tightly regulates transport of biomolecules and harmful
556 compounds. It is characterized by low permeability to most chemical compounds and
557 provides homeostasis for optimal neuronal function [112]. To increase the throughput of
558 present technologies and overcome their limitations, engineered microfluidic BBB models
559 have been proposed. However, they must satisfy a number of criteria: high-fidelity in
560 mimicking in vivo physiological microenvironment and relevant conditions/functions,
561 possibility for investigating organ-level functions, stability for a prolonged period to permit
562 real-time study, recirculating perfusion for drug permeability studies, and of course
563 standardization and reproducibility [112].

564 Various proposed BBB-on-a-chip models rely on co-cultures of neurovascular
565 endothelial cells and primary astrocytes on the two sides of a porous membrane [114]. This
566 approach was shown to better recapitulating in vivo conditions and to result in tighter
567 junctions and lower barrier permeability than the case with only endothelial cells [115].
568 Moreover, it allows recirculation at physiologically relevant perfusion rates and the
569 application of shear stress at in vivo levels. An example of this class of microfluidic BBB
570 models is reproduced in **Figure 8 A1** [114] which summarizes all the main components
571 and details of the layout used by Wang et al. for co-cultures of rat primary astrocytes and
572 brain microvascular endothelial cells (BMECs) derived from human induced pluripotent
573 stem cells (hiPSCs). Similarly, Park et al. combined hiPSC-derived human brain
574 microvascular endothelium with primary human brain astrocytes and pericytes [116].

575 Notably, differentiation under hypoxic conditions enhanced barrier functionality with high
576 levels of tight junction SLC and ABC proteins, functional efflux pumps and surface proteins
577 modulated transcytosis capabilities for drug, peptide, nanoparticle and antibody.

578 When characterizing barrier-forming tissues, a crucial step is the assessment of barrier
579 integrity and function, which should be maintained in time for the whole duration of the
580 study. For this purpose, various in vitro techniques are available, from microscopy imaging
581 of cell-cell adhesion proteins to measuring ionic currents, to flux of water or transport of
582 molecules across cellular barriers [117]. In their work, to evaluate barrier integrity, Wang
583 et al. performed time lapse studies by immunostaining for the tight junction proteins, ZO-
584 1 and claudin-5, while cell nuclei are stained in blue with DAPI as shown in **Figure 8 A2**
585 [114]. Recently, trans-endothelial electrical resistance (TEER) measurements (**Figure 8**
586 **A3**) are attracting strong attention as an alternative electrical procedure for assessment of
587 tight junction formation and comparison with in vivo conditions in various models
588 including the blood-brain barrier (BBB), gastrointestinal (GI) tract, and pulmonary models
589 [118]. Notably a tighter barrier was observed when using co-cultures.

590 To further analyze barrier function, permeability assays are commonly carried out using
591 fluorescent tracers, large molecules (FITC-dextrans) and model drugs (caffeine, cimetidine,
592 and doxorubicin) as well as permeability mediators with results compared with in vivo
593 permeability coefficients values [114]. In this respect, it is of particular interest an
594 electrochemical permeability assay introduced by Wong et al. as a method to overcome the
595 need for complex optical instrumentation and laborious manual sampling by using an
596 electroactive tracer [119].

597 Not all microfluidic BBB platforms with low permeability have been, however,
598 implemented with the membrane-based approach. For example, Bang et al. established a
599 3D blood brain barrier model by the direct contact between a perfusable vascular network
600 and astrocytes in an architecture comprising a vascular and a neural channel (**Figure 8**
601 **B1-B2**) [120]. These side channels were supplied by different media resulting in better
602 barrier properties and viability with respect to the single medium cases. Notably, the

603 vascular network permeability for FITC-dextrans was estimated to be similar to in vivo
604 values and the authors also observed a good neurovascular interfacing and the presence of
605 synapses.

606 Beyond facilitating the development of new treatments, the availability of such
607 microfluidic models of tissue barriers can facilitate an improved understanding of their
608 functionality and disruption which are associated to the pathophysiology of many diseases
609 [117]. For example, Brown et al. used a microfluidic model of the human neurovascular unit
610 to investigate the inflammatory disruption of the blood-brain barrier, its metabolic
611 consequences and repair mechanisms. Namely, a loss of barrier function associated to
612 increased diffusion and reduced presence of tight junctions was observed upon
613 inflammatory stimulation using lipopolysaccharides or a cytokine cocktail to mimic
614 systemic and local infections. Then, the authors demonstrated how metabolite analysis can
615 contribute to identify critical pathways in inflammatory response [121]. Present limitations
616 in BBB-on-chip field concern standardization of methods for quantification of relevant
617 parameters such as barrier permeability and shear stress, making difficult a direct
618 comparison in terms of performance [112].

619 Remarkably, microfluidic neurodegenerative diseases models for both the central and
620 peripheral nervous system focusing on Alzheimer's disease, Parkinson's disease, and
621 amyotrophic lateral sclerosis were implemented recapitulating their critical features with
622 compartmentalized microenvironments for the co-culture of neurons, glial cells,
623 endothelial cells, and skeletal muscle cells and the ability to reproduce chemical gradients
624 and mechanical features [113].

625 To summarize, different (vertical) and planar architectures have been implemented
626 with various cell lines co-cultured in order to model the BBB on chip. Other parameters to
627 take into account in the chip design include membranes selection and ECM coating. The
628 incorporation of physiological shear stress, inflammatory stimulation and the integration
629 of sensors for TEER measurements provide advantages with respect to traditional
630 methodologies.

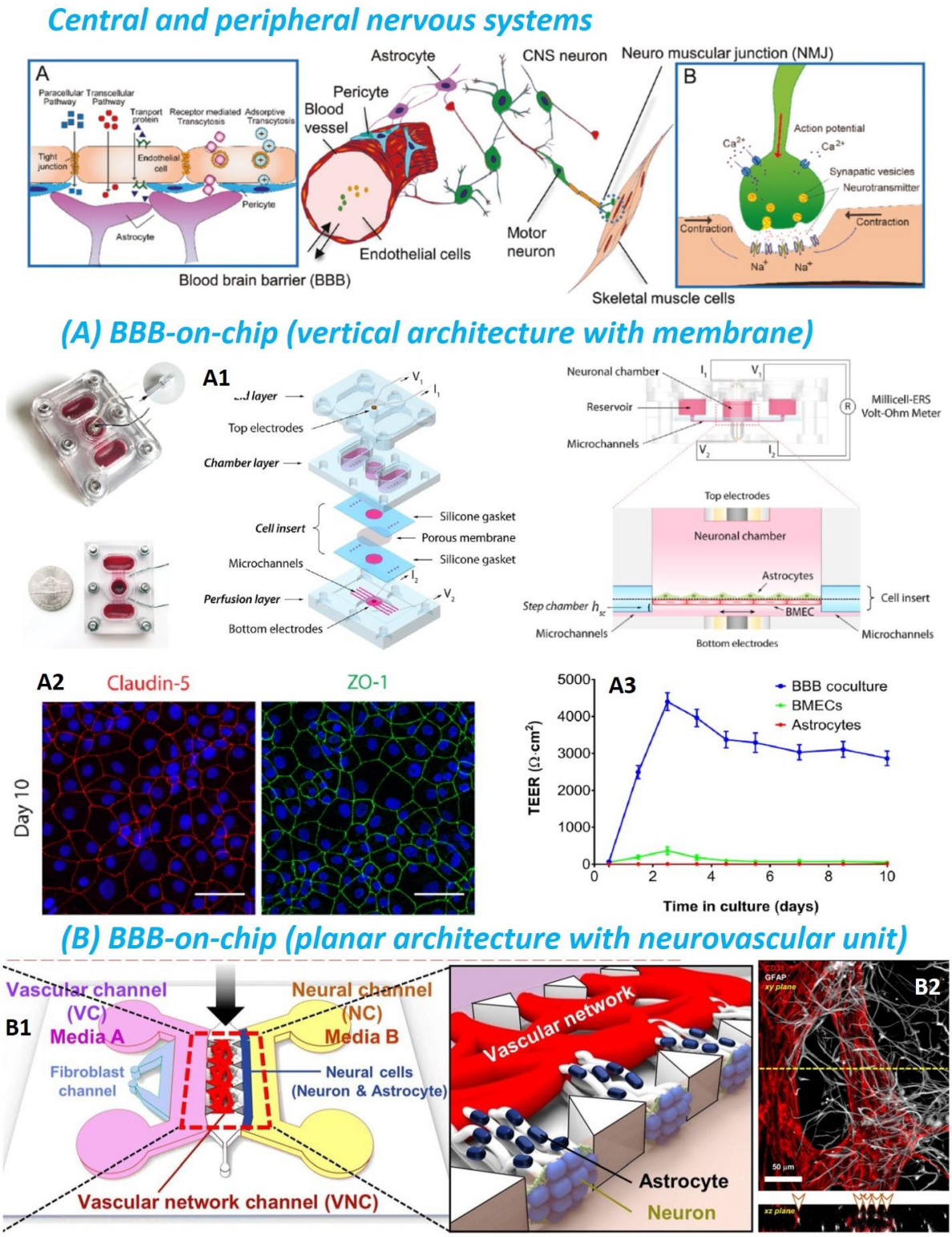

Figure 8. (top) *The main players at the central and peripheral nervous systems (CNS and PNS involved in neurodegenerative diseases [113].* ***(top left)*** *At CNS level, the blood–brain barrier (BBB) separates bloodstream from brain tissue. It is characterized by tight junctions and a very low permeability with access through paracellular and transcellupar pathways. It involves different cell types: endothelial cells, pericytes, astrocytes and CNS neurons.* ***(top right)*** *At PNS level, motor neurons and muscle fibers form the neuromuscular junction, which is a chemical synapse. Muscle contraction is driven by signals transmitted by the motor neurons to the muscle in the form of acetylcholine release. Reproduced from Ref. [113]* ***(A1)*** *Vertical structure of the BBB-on-chip reported by Wang et al. and evaluation of barrier integrity* ***(A2)*** *by immunostaining for the tight junction proteins Claudin-5 and ZO-1 and* ***(A3)*** *by TEER measurements. Reproduced from [114];* ***(B1)*** *Planar microfluidic platform for neurovascular unit containing blood-brain barrier.* ***(B2)*** *Confocal microscopy image of the direct vascular network-astrocyte interface that confirmed direct contact on two axes, with contact points indicated in the xz plane through arrows. Reproduced from [120].*

643 **2.2 Tumor models and organoids engineering for new drug development**

644 The development of cancer-on-chip models is of particular interest for their potentials
645 to recapitulate the cancer pathophysiology by reconstructing the highly complex tumor
646 microenvironment (TME) composed by several factors, including extracellular matrix
647 (ECM), blood vasculature, and multiple stromal cells, which control cellular function,
648 proliferation and cancer metastasis.

649 Conventional in vitro models based on monolayer cultures are unable to accurately
650 mimic the in vivo environment and, consequently, are less effective for drugs research. On
651 the other hand, the use of animal models has limitations for high-throughput screening in
652 preclinical drug testing because of high consumption of chemicals, time consuming
653 operations, constraints in study of the mechanisms at play and species-specific differences.
654 By combining modern microfluidic and tissue engineering technologies, tumors-on-chips
655 (ToC) provide more biomimetic and high-throughput in vitro models. ToC can recapitulate
656 the complex microphysiological features of disease microenvironments by enabling the
657 production of three-dimensional models and replicating tumor and vasculature
658 interactions, tumor angiogenesis and metastasis. As a consequence, they can accelerate drug
659 development and screening.

660 In this scenario, tumor spheroids/organoids are considered the best models for cancer
661 research. They are self-assembled cancer cells aggregates with diameters from 100 μm to
662 1000 μm. Tumor spheroid formation attracted significant attention because they are able to
663 better mimic the in vivo TME providing a more accurate platform for cancer investigation
664 and therapeutic testing. Indeed, they are able to reproduce the extracellular matrix
665 environment (ECM), cell–cell interactions and the presence of nutrients, metabolites and
666 oxygen gradients [122] beyond their 3D structure. Furthermore, they can be produced from
667 a variety of tumor cell lines including human and patient-derived cells.

668 Conventional homogeneous spheroids formation is achieved with techniques such as
669 hanging drop and rotating flask methods, and the use of external (e.g. electric field or
670 magnetic) forces or non-adhesive surfaces. These techniques allow drug testing and
671 performance analysis, and commercial systems are available on the market, such as
672 Insphero, Aggrewells (Stem Cell Technologies) and Nucleon Sphera (ThermoFisher).
673 However, they require frequent media exchange and are labor-intensive and time
674 consuming. On the other hand, in microfluidic systems, procedures can be automated and
675 the formation of tumor spheroids can be achieved from a small number of cells, with
676 continuous infusion of the culture medium ensuring high cell activity, small sample and
677 reagents volumes. This guarantees high sensitivity and integration, with advantages in terms
678 of arraying the samples and testing various combinatorial treatments with high throughput.
679 Other studies addressed on chip investigation of tumor and vasculature interactions,
680 tumor angiogenesis and metastasis. Among them, the self-assembly microvascular approach
681 allows to recreate on chip tumor angiogenesis and to emulate metastatic cascade [123] such
682 as invasion/intravasation [124], extravasion of tumor cell [111, 125, 126] and perivascular
683 niche [127-130]. Indeed, typically in a metastatic cascade, first tumor cells invade the blood
684 circulation passing the extracellular matrix and the vascular endothelium. Then cancer cells
685 extravasate at the distant site travelling across the endothelium blood vessel to leave the
686 circulation and colonize another tissue/organ giving rise to a new metastatic TME or
687 secondary tumor formation [131-136] (**Figure 9 top**).
688 In this respect, Du et al [124] reported a microfluidic co-culture system containing both
689 breast cancer cells (MDA-MB-231) and noncancerous cells (MCF-10A or HDF-n), which was
690 employed to investigate the influence of the tumor microenvironment on metastasis before
691 intravasation into the vessels. A vascular endothelial layer was also recreated in order to
692 mimic the semipermeable membrane function and the transendothelial nutrients transport
693 in blood vessels. The authors demonstrated the ability of the developed tool to study the

694 mechanism of tumor invasion into the stroma and to screen anti-metastatic drugs. Chen et
695 al [111] instead presented a microfluidic platform with self-organized perfusable human
696 microvascular networks formed over 4–5 days, after which the tumor was perfused and
697 extravasation events were tracked over 72 h via standard confocal microscopy (**Figure 9 A**).
698 This assay allows a rapid quantification of tumor cell extravasation kinetics and can be used
699 for the screening of therapeutic agents. As another example, Xiao. et al [127] reproduced on-
700 a-chip the microvasculature as a perivascular niche model to evaluate the ex vivo dynamics
701 of brain tumor stem-like cells (BTSCs) derived from glioblastoma patients. They found that
702 the degree of colocalization between tumor cells and microvessels depends on the genetic
703 and pathologic subtypes of the tumor samples and varies significantly across patients. These
704 findings demonstrate the potential of the developed assay for ex vivo analysis of tumor cell
705 dynamics and heterogeneity, representing a new route to study patient-specific tumor cell
706 functions.

707 As described above, considerable efforts were dedicated to combine tumor cells and
708 microvasculature on chip with the aim to achieve a more in deep understanding on the
709 angiogenesis processes, the interaction of the cancer cells with the microvasculature and the
710 metastasis cascade dynamics. However, the aforementioned models do not recapitulate the
711 pathophysiology of vascularized solid tumor tissue, but it is known that this is a critical
712 feature in cancer treatment. For this reason, novel technologies were developed to culture
713 3D solid tumor tissue (or tumor spheroids) with microvasculature on-a-chip [137-141].

714 In this respect, Nashimoto et al. interconnected a spheroid to a perfusable vascular
715 network inducing angiogenic sprouts from the microchannels up to reaching vessel-like
716 structures in the spheroid [142] (**Figure 9 B1**). Intriguingly, they demonstrated the
717 presence of a continuous interconnection available to deliver biomolecules and drugs. The
718 constructed vascular network allowed long-term perfusion culture of the tumor spheroids
719 which result in a significant enhancement of the proliferation activities of tumor cells and in

720 a non-conventional dose-dependent response to the anticancer drug, highlighting the
721 importance of vasculature network flow in evaluating tumor activities in a drug screening
722 platform [140] (**Figure 9 B2-B4**). This achievement allows to mimic in vivo TMEs and
723 represents an important achievement for all the studies on spheroids/organoids/ tumoroids.
724 Using a vascularized tumor model based on microtumors arrays with independently-
725 addressable elements, a blinded screen of both anti-cancer and anti-angiogenic drugs was
726 performed by Phan et al. [129] (**Figure 9 C**). Further efforts may be necessary in this
727 direction to develop more powerful tools for fundamental studies in tumor angiogenesis and
728 drug testing targeting a clinical personalized therapeutic treatment.

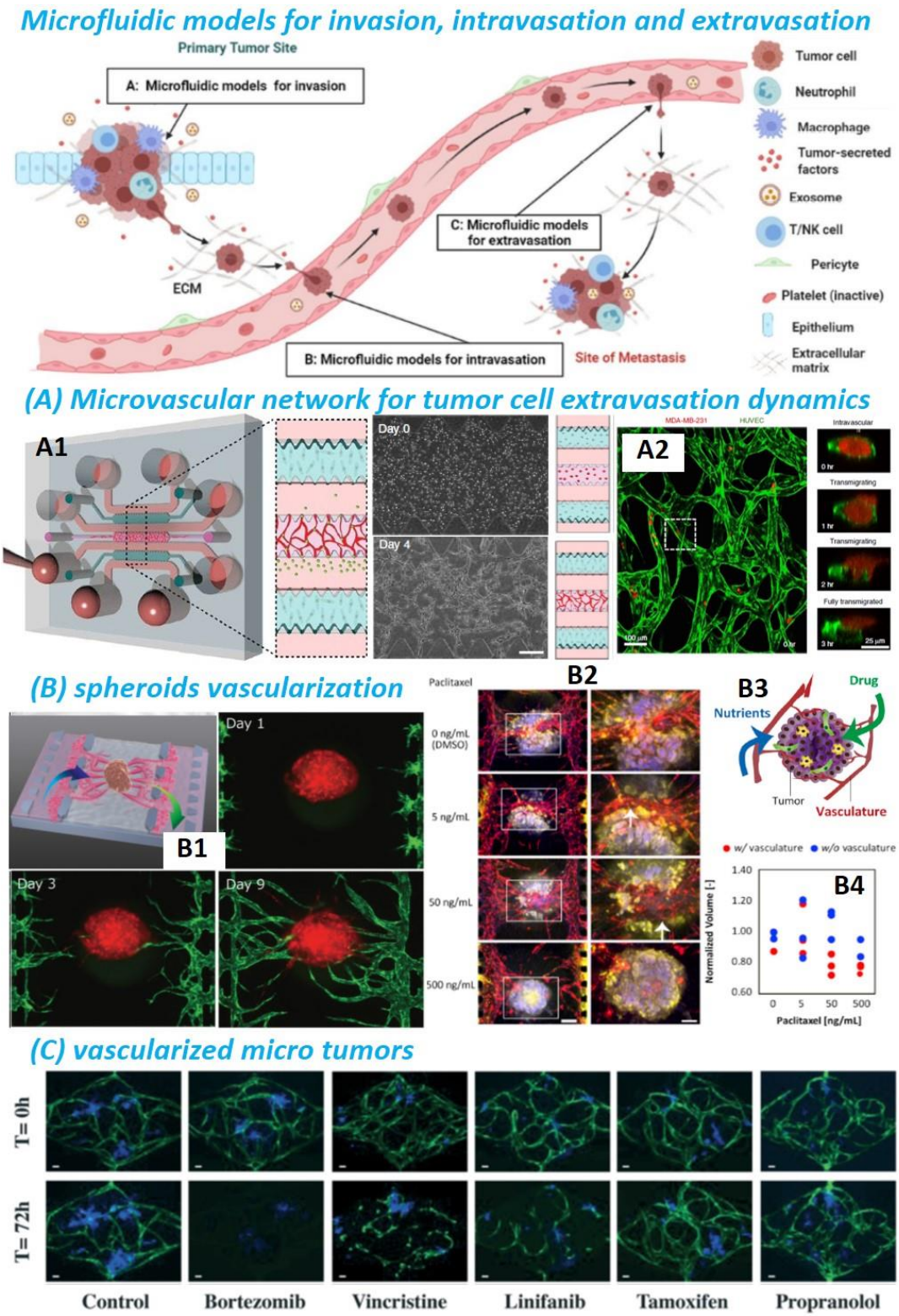

Figure 9. (top) *Microfluidic models including metastatic steps from invasion to intravasation and extravasation. Reproduced from Ref. [133]* ***(A1)*** *Microfluidic platform with self-organized perfusable human microvascular networks formed over 4–5 days.* ***(A2)*** *Confocal image of a region of tumor-perfused (red) microvascular network (green) and cross-sectional views of a transmigrating tumor cell (right sequence) with extravasation scoring. Reproduced from Ref. [111].* ***(B1)*** *Schematic diagram and fluorescent micrograph of a sferoid interconnected to a perfusable vascular network inducing angiogenic sprouts. Reproduced from Ref. [142].* ***(B2)*** *Immunofluorescence images of the tumor spheroid with the vasculature under drug administration at different doses.* ***(B3)*** *Tumor vasculature for nutrients and drugs.* ***(B4)*** *Spheroid volumes as a function of drug concentration calculated from sequential histological sections Reproduced from Ref. [140].* ***(C)*** *VMT arrays for drug screening with ECFC-EC formed vascular networks around HCT116 colorectal cancer cells and evaluation of drug efficacy on tumor growth and the associated vasculature quantified after 72 hours (reproduced from [129]).*

741 **2.3 Biomechanical structures - bone-on-a-chip and heart-on-a-chip**

742 Biomechanical structures represent key components of the human body and include
743 bones, muscles and tendons. Several 2D models for bones and cartilage employ a single
744 type of cells (chondrocytes for the cartilage; osteoblasts, osteocytes, and osteoclasts for the
745 bone) [143] with intrinsic limitations. Another important aspect is that a reliable in vitro
746 model must allow to investigate the influence of mechanical cues. This can be achieved in
747 different ways. An option consists in seeding bone cells on 2D membranes which are
748 pneumatically or electromagnetically deformed to introduce cyclical cell stretching. In
749 microfluidic systems, shear stresses can be recapitulated by means of fluid flow. Among the
750 co-cultures models, it is worth mentioning the work by Middleton and coworkers who
751 investigated osteocyte-osteoclast signaling under shear stress stimulation [144]. 3D models
752 were implemented using different scaffold materials, prevalently natural hydrogels (such
753 as collagen, gelatin, hyaluronic acid, alginate) and synthetic polymers (e.g. polyethylene
754 glycol, PNIPAM, PDLLA). The first class presents advantages in terms of biocompatibility,
755 permeability, similarity to natural tissues, presence of motifs for cell adhesion, non- or low-
756 immunogenicity. Furthermore, they are low cost and they properties can be tuned, e.g. by
757 chemical modification (e.g. ECM stiffness is relevant for osteoarthritis pathogenesis and
758 progression (see **Section 3.3** for details on Materials for OOC). Bone models were also
759 engineered using hydroxyapatite as a constitutive material resembling bone mineralization
760 products and favourable for proliferation and osteogenic differentiation of the human
761 foetal osteoblast cell line (hFOB) [145]. In particular, Tang et al. produced hydroxyapatite
762 microfluidic chips by ceramic stereolithography with a diffusive mixer to achieve a
763 concentration gradient of the model drug doxorubicin hydrochloride (DOX) and evaluate
764 its half maximal inhibitory concentration (IC50) [145]. Hydroxyapatite-based
765 nanocomposites are attractive materials for bone tissue engineering and their
766 cytocompatibility was demonstrated with respect to the MG63 osteoblast-like cell line [146].

767 Recently, vascularized bone-on-chip models attracted attention [147] and a neuro-
768 vascularized bone chip was implemented by Neto et al. with three channels comprising
769 nerve, vascular and bone unit in order to investigate the response to inflammatory bone
770 conditions and its effect first on the vascular unit and then on the nerve unit [148] (**Figure**
771 **10 A1-A2**). This platform can provide a useful tool for drug development and the authors
772 investigated anti-inflammatory drug nanodelivery by means of nanoparticles. In another
773 study, bone regeneration was also studied on chip [149].

774 Muscles are the other major biomechanical structures beyond bones. In this respect,
775 heart-on-a-chip models assume particular relevance since cardiac pathologies have high
776 impact on worldwide morbidity and mortality rates. Furthermore, there is a high incidence
777 of cardiovascular drug toxicity combined with the severity of adverse drug reactions in late-
778 stage drug development [150]. For these reasons, human heart muscle on chip models have
779 been developed to mimic healthy and pathological cardiac tissues and provide high-
780 throughput tools alternative to animal models for testing cardiovascular drugs,
781 cardiotoxicity and cardioprotective efficacy in preclinical trials [151]. In these studies, the
782 cardiac/myocardial mechanics and heart muscle contractility are central indicators and
783 contractile force development can be a phenotyping issue in cardiomyocyte-on-a-chip
784 models [151]. Microcantilevers are a hallmark of cardiac OOC. In a pioneering work, Legant
785 et al. reported 3D myotubes attached to MEMS microcantilevers as tissue gauges to
786 measure the microtissue-generated forces [152]. Few years later, Agarwal et al.
787 recapitulated heart ventricle architecture on flexible cantilevers of soft elastomers, whose
788 deflection was used to evaluate the generated diastolic and systolic stresses [153]. The
789 integration of flexible strain gauge sensors is a characteristics of the architecture from
790 Parker group to monitor the contractile stress and beat rate of the reconstituted cardiac
791 tissue [154] and how they are influenced by administration of bioactive compounds and
792 drugs (see also **Section 3.2** for discussion on sensors for OOC). The addition of endothelial

barrier model then permitted them to test the delivery through the blood vessels toward heart musculature [155]. A dose–response analysis on the effect of 12 cardiac and cardiotoxic drugs was instead carried out on a model of the ventricle laminar structure reconstituted by Lind et al using cardiomyocytes derived by human induced pluripotent stem cells [155]. In a recent work, Ren et al. validated the maturation and phenotypic changes of cardiomyocytes cultured in well-aligned structures and successfully reproduced their synchronous beating upon electrical pulse stimulations [156]. DOX-induced cardiotoxicity and the cardioprotective efficacy of CAR and IVA drugs were then assessed.

In terms of real time monitoring, transepithelial electrical resistance (TEER) sensors and multi-electrode arrays (MEAs) were used for evaluating tissue barrier function and recording cardiac activities (see **Section 3.2**) [157]. Photonic crystals provided alternative self-reporting monitoring tools of cardiomyocytes activity [158]. Furthermore, bioprinting is starting to have a significant impact on the field. Indeed, Zhang et al. fabricated endothelialized myocardium model capable of spontaneous and synchronous contraction by printing endothelial cells within microfibrous hydrogel scaffolds and then seeding cardiomyocytes [159] (**Figure 10 B1-B5**). An aorta smooth muscle-on-a-chip was implemented by Abudupataer and coworkers [160].

A further target for of large interest is represented by OOC models for amyotrophic lateral sclerosis (ALS) and neuromuscular development and disease which were developed combining human iPS-derived muscle cells and optogenetic motor neurons [161-163]. However, they are not discussed here for space constraints. In general, mechanobiology and mechanotransduction attracted large interest for the relevance in many biological processes. For this reason, biomechanical aspects have been also investigated in lungs and gut as discussed above (e.g. simulating breath and peristaltic stimuli). In this respect, OOC platforms provide advanced tools for investigation under well controlled and engineered conditions.

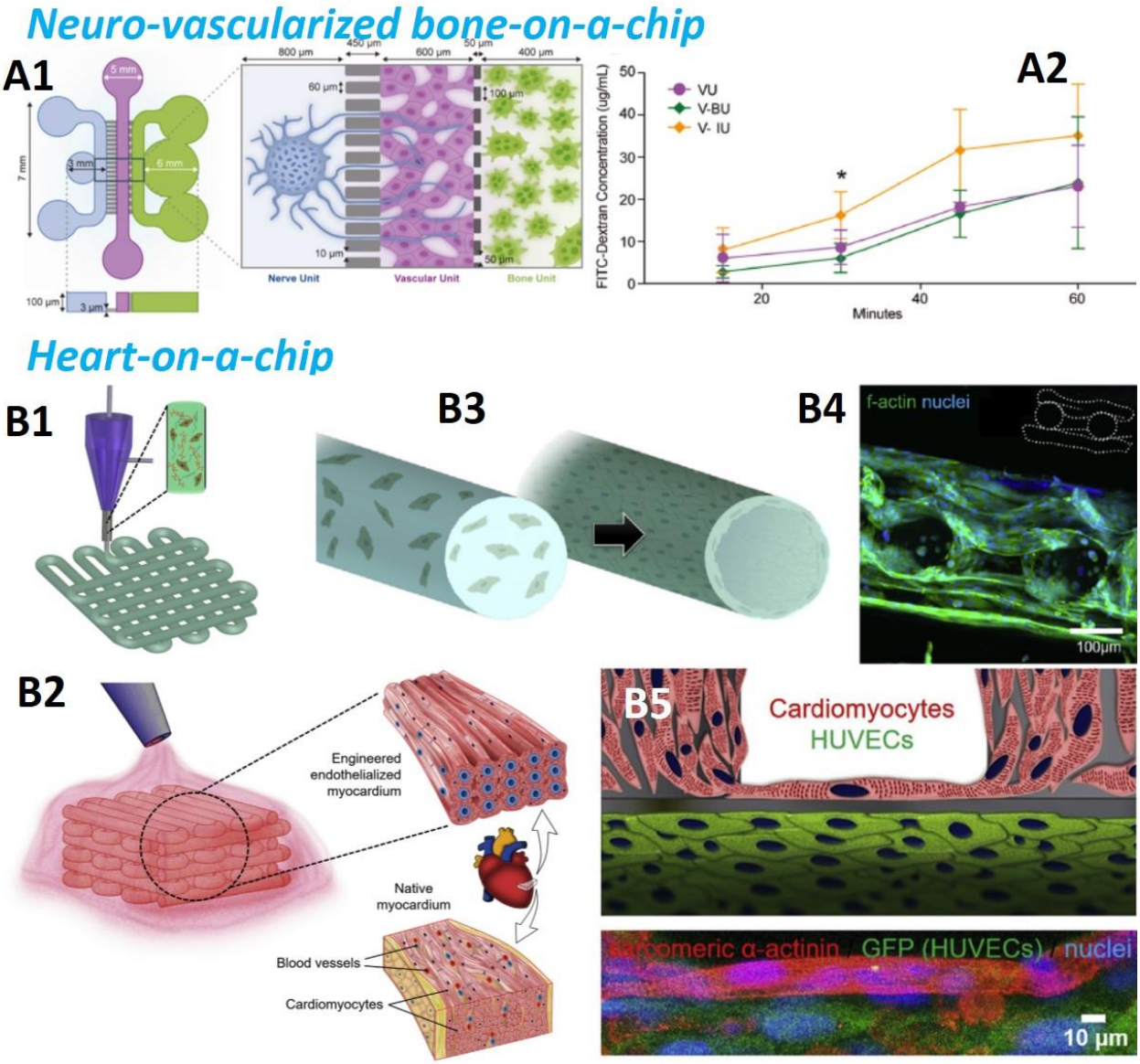

Figure 10 (A1) *Model of neuro-vascularized bone chip. Reproduced from Ref. [148].* ***(A2)*** *Permeability of the endothelial barrier evaluated at the vascular unit adjacent to the bone inflammatory unit (V-IU)—osteoclasts under IL-1β exposure—and compared to vascular unit adjacent to the physiological bone unit (V-BU)—osteoclasts in standard culture conditions.* ***(B1-B2)*** *Schematic diagrams of the process for fabricating endothelialized myocardium by 3D bioprinting.* ***(B3)*** *Schematics of the assembly of human umbilical vein endothelial cells encapsulated in bioprinted microfibers into a layer of endothelium.* ***(B4)*** *Confocal fluorescence micrograph indicating the formation of the endothelium by human umbilical vein endothelial cells.* ***(B5)*** *Schematic and confocal fluorescence images of an endothelialized myocardial tissue realized by seeding neonatal rat cardiomyocytes on to the bioprinted endothelialized microfibrous scaffold. Reproduced from Ref. [159].*

2.4 Metabolism-on-chip – Liver, Kidney and Multi-Organ models

Beyond the intestine, liver, kidney and pancreas on chip models were investigated. They are relevant for considering the role of drug metabolism/clearance beyond absorption, as well as for assessing potential organ damage and for evaluating multi-organ interactions (see **Section 2.5**) [54, 93, 164-188].

835 **2.4.1 Liver-on-a-chip**

836 The liver is responsible for various functions including the production of bile, serum
837 proteins (albumin), and lipoproteins, and it has a key role in the metabolism of amino acids,
838 lipids, and carbohydrates taken with food. It is also involved in the detoxification process
839 of endogenous (bilirubin) and exogenous products such as drugs. The detoxification
840 process can lead to drug-induced liver injury (DILI). Animal models and in vitro cell culture
841 models were used to evaluate drug-induced damage to the liver. However, due to the
842 species-specific differences that exist between animals and humans and due to the low
843 sensitivity in vitro models, neither type has led to good results in the prediction of DILI
844 [189, 190]. In this respect, Organ-on chips (OOC) can again provide useful tools to mimic
845 the functional and structural unity of the liver, including physical and chemical stimuli
846 [191].

847 A multispecies liver-on-chip could be helpful to understand toxicities detected in animal
848 models in order to better determine human safety. For this reason, Jang et al.[190] realized
849 a liver-on-chip to study the different types of toxicity in the liver of dogs, rats, and humans
850 when they are treated with different drugs. Their chip was composed of a top parenchymal
851 channel, where primary rat, dog or human hepatocytes were seeded on a porous ECM
852 (extracellular matrix)-coated membrane. Then in the bottom vascular channel below the
853 membrane, sinusoidal endothelial cells (LSEC), Kupffer cells and stellate cells were seeded
854 (**Figure 11 A**). To verify if this liver-on-chip could be helpful to predict species-specific
855 DILI responses, the authors evaluated the hepatotoxic effects caused by bosentan, an
856 endothelin receptor antagonist vasodilator, that induces cholestasis in humans but not in
857 dogs or rats, using the three species models. As shown in **Figure 11 B**, the administration
858 of Bosentan at 1, 10 and 100 μM led to a decrease in albumin secretion in dog and human
859 chips but not in rat chip. Moreover, the plasma concentration of bosentan that has been
860 associated with DILI in humans is similar to the concentration in the human liver-chip at

861 which they observed toxicity. The chip was also more sensitive compared to culture plates
862 and this could be due to the presence of a fluid flow and better hepatocyte functionality. In
863 another study, Jang et al. studied the toxic effect caused to the liver by the generic analgesic
864 acetaminophen (APAP), which through its toxic and reactive metabolite N-acetyl-p-
865 benzoquinone exhausts cellular glutathione and leads to oxidative stress in the cells. This
866 process was observed through a cellROX fluorescent probe that binds to reactive oxygen
867 species [190].

868 Hepatotoxicity tests were performed by Bircsak et al. [192] using a multiwell
869 microfluidic plate, Mimetas OrganoPlate® 2-lane (**Figure 11 C**). In this case, the liver-on-
870 chip is present in OrganoPlate 2-lane and consists of an organ channel where they seeded
871 clusters of pluripotent stem cell (iPSC)- derived hepatocytes (iHep) on an extracellular
872 matrix, and a perfusion channel where they seeded HMEC-1 endothelial cells and
873 differentiated THP-1 into macrophages. Cells were shown to remain viable for 15 days by
874 secretome measurements (albumin and urea secretion) and image-based analysis. To
875 demonstrate ability to discover hepatotoxicity, the authors treated the cells with
876 troglitazone (180μ M) as a hepatotoxin for positive control, and 0.5% dimethyl sulfoxide
877 (DMSO) as vehicle control. Then, similar conditions with 72 h exposure time and the same
878 assays were employed to validate the liver toxicity of a library of 159 compounds by means
879 of a Toxicological Prioritization Index (ToxPi score), which is a dimensionless weighted
880 linear combination of %live iHep, urea, iHep nuclear size and albumin. Among 159
881 compounds, 39 were found to be toxic and 34 of them showed a decrease in iHep viability
882 compared to vehicle control (DMSO). Then, for dose-response evaluation, the authors
883 considered 21 compounds from the previous screening and these studies confirmed all true
884 negative and true positive compounds, except hyproniazide. These results suggest that the
885 liver-on-chip created in the OrganPlate detects the hepatotoxicity of most compounds and
886 it is possible to perform more chronic exposure analysis with this platform using several

time points and additional readings [192].

Another intriguing study by Tsamandouras et al. [193] described hepatic drug metabolism changes in the human population using physiological microsystems with hepatocytes taken from different donors. For each donor, they analyzed the metabolic depletion profiles of six different drugs and confirmed that there is an inter-donor variability by comparing the expression levels of metabolism-related genes and other liver functions. Notably, TEER measurements and pH changes of HepG2 hepatoma cell line using a chip-embedded non-toxic sensor were employed by Farooqui et al.[194] for monitoring drug toxicity on cells exposed to various concentrations of drugs such as doxorubicin, epirubicin and lapatinib. Using this liver-on-chip, the authors demonstrated ability to provide real-time data on drug-induced liver injury in vitro (**Figure 11 D**).

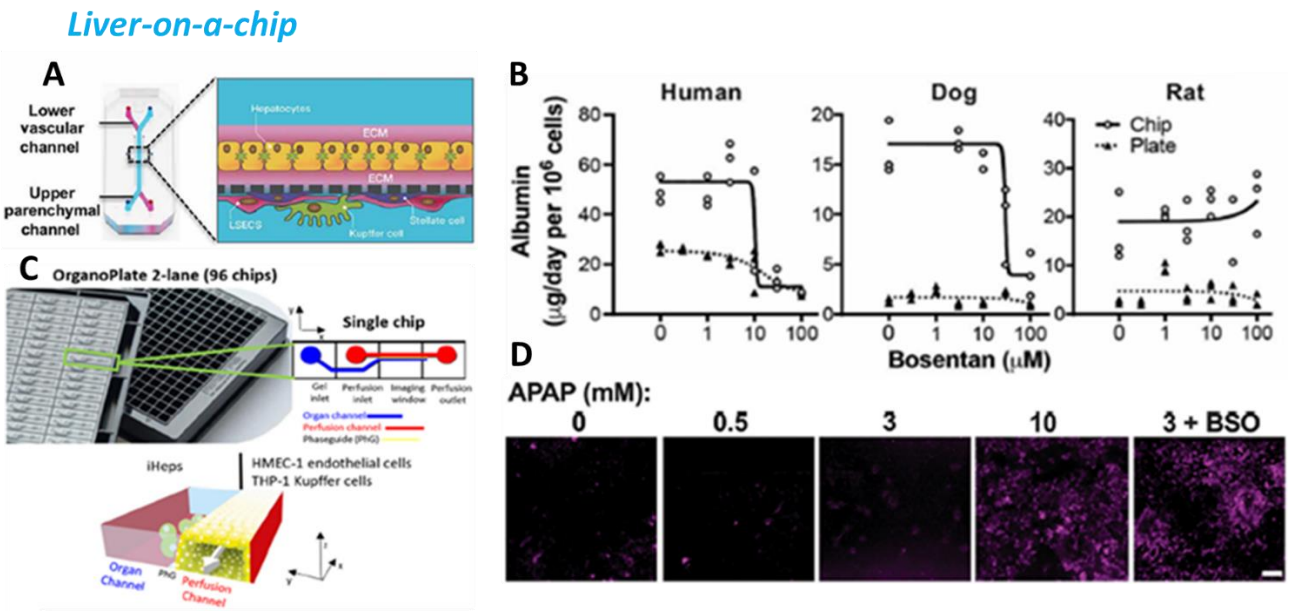

***Figure 11. Liver-on-chip**. **(A)** Liver-on-chip diagram showing which hepatocytes are seeded in the upper channel and Kupffer cells, Stellate cells and LSEC are seeded in the bottom channel. Reproduced from Ref. [190]. **(B)** Species-specific drug-toxicities in a rat,dog and human liver-chip. Albumin secretion after daily administration of Bosentan at 1,3,10 ,30 and 100 µM for 3 days in human chips with two kinds of cells (hepatocyte and LSEC), and plates only with hepatocyte monoculture, and for 7 days in dual-cell dog and rat chips and plates. Reproduced from Ref. [190]. **(C)** OrganPlate 2-lane. Image of OrganPlate 2-lane with 96 chips and schemes of organ channel and perfusion channel separated by a phaseguide(PHG). Reproduced from Ref. [192]. **(D)** Detection of liver injury caused by acetaminophen(APAP). Images of ROS intensity after daily administration of APAP at 0.5, 3 and 10 mM in human chips. Reproduced from Ref. [194].*

908 **2.4.2 Kidney-on-a-chip**

909 The kidneys have the task of filtering metabolic waste products from the blood and
910 expelling them through the urine. Through their functional unit, the nephron, the kidneys
911 maintain the correct hydro-saline balance in the body. Furthermore, they play a key role in
912 drug elimination and therefore may be susceptible to drug-induced nephrotoxicity, which
913 can lead to acute or chronic kidney injuries [195, 196]. Drugs that can cause nephrotoxicity
914 include antimicrobial, chemotherapeutic, immunosuppressive and analgesic agents [197].
915 Organ-on–chip (OOC) technology can provide useful tools to reduce the nephrotoxic
916 potential of novel drugs by mimicking organ functions and the complexity of the native
917 tissue better than animal models and 2D culture models due to the presence of a fluid flow,
918 pressure and a co-culture of various types of cells [198].

919 For example, Yin et al.[199] employed a kidney-on-chip model to evaluate
920 nephrotoxicity induced by some nephrotoxic drugs such as cisplatin (DDP), gentamycin
921 (GM) and cyclosporin A (CsA). Specifically, they developed a microfluidic platform, where
922 renal proximal tubule epithelial cells (RPTEC) were seeded in the upper layer on a
923 polycarbonate (PC) membrane coated with extracellular matrix (ECM) collagen, while
924 peritubular capillary endothelial cells (PCECS) were seeded in the bottom layer on another
925 PC membrane coated with ECM collagen (**Figure 12 A-B**). Their configuration comprised
926 a peristaltic pump that controls the flow rate of the cell culture medium into the chip, a
927 temperature control to maintain an optimal culture medium temperature and matching
928 catheters. The effects of different concentrations of DDP, GM and CsA were evaluated on
929 the kidney-on-chip and compared with results from the Petri dishes (in static condition)
930 with a live/dead assay and a cell counting kit-8 (CCK-8) (**Figure 12 C**). Remarkably, Yin
931 et al. demonstrated that the number of live cells was higher in the fluidic condition of the
932 chip than in the static group proving that the microfluidic system can be used for long-term
933 cell culture and nephrotoxic drug screening (**Figure 12 D**) [199].

934 In another study, Vormann et al. [200] used three-lane OrganPlate, purchased by
935 Mimetas, to create a 3D microfluidic platform for the detection of drug-induced kidney
936 injury (DIKI) in the development of new drugs (**Figure 12 E-F**). This platform presents:
937 (i) an upper perfusion channel, where they seeded the human primary renal proximal
938 tubule epithelial cells (RPTEC) and human immortalized proximal tubular epithelial cells
939 with organic anion transporter 1 (CiPTEC-OAT1), (ii) a central channel loaded with
940 extracellular matrix gel composed of collagen I and (iii) a bottom perfusion channel where
941 culture medium was added. The channels were divided by structures called Phaseguide that
942 work like pressure barriers. Afterwards, the cells were subjected to a treatment with four
943 nephrotoxic compounds (tenofovir, cyclosporin A, tobramycin and cisplatin) and various
944 assays were carried out to verify the damaging effect of these drugs on the kidney. Cell
945 viability was determined with the cell counting kit-8; instead membrane integrity was
946 observed with lactate dehydrogenase (LDH) activity and with the β-N-
947 acetylglucosaminidase (NAG) – assay kit. They also evaluated gene expression of toxicity
948 and nephrotoxicity markers and performed detection of miRNA in medium cell culture and
949 drug transporter assays. After having chosen certain concentrations of nephrotoxic
950 compounds, these have been shown to cause a decrease in Ci PTEC-OAT1 cell viability and
951 an increased release of LDH for tobramycin and cyclosporin A at the highest concentration
952 tested. With the same concentrations of nephrotoxic compounds administered to the
953 RPETC, reduced cell viability was instead seen only after exposure to tobramycin, thus
954 resulting in the RPETC being less sensitive than the CiPTEC-OAT1 [200].

955 In ref. [195], Kim et al. demonstrated the nephrotoxic effects of the antibiotic
956 gentamicin with cell injury markers, such as cell viability and membrane permeability, and
957 they also compared the nephrotoxicity of the gentamicin, using different systems that
958 simulate the pharmacokinetics of continuous infusion and bolus injection in humans. Of
959 the two systems, the one that causes less nephrotoxicity is the one that mimics a once-daily

bolus injection. This approach could be used in a large range of drug-induced nephrotoxicity studies. Other researchers used the kidney-on-chip approach to demonstrate the non-toxicity of a compound. For example, the microfluidic platform in ref. [201] presented human embryonic kidney cells encapsulated in gelatin methacryloyl (GelMA) to simulate the microenvironment and the main functions of the kidney. By administering 30 µM of kaempferol to the embryonic kidney cells for 12h, Li et al. did not notice any cell damage thus demonstrating the non-toxicity of kaempferol, a bioactive metabolite from spearmint.

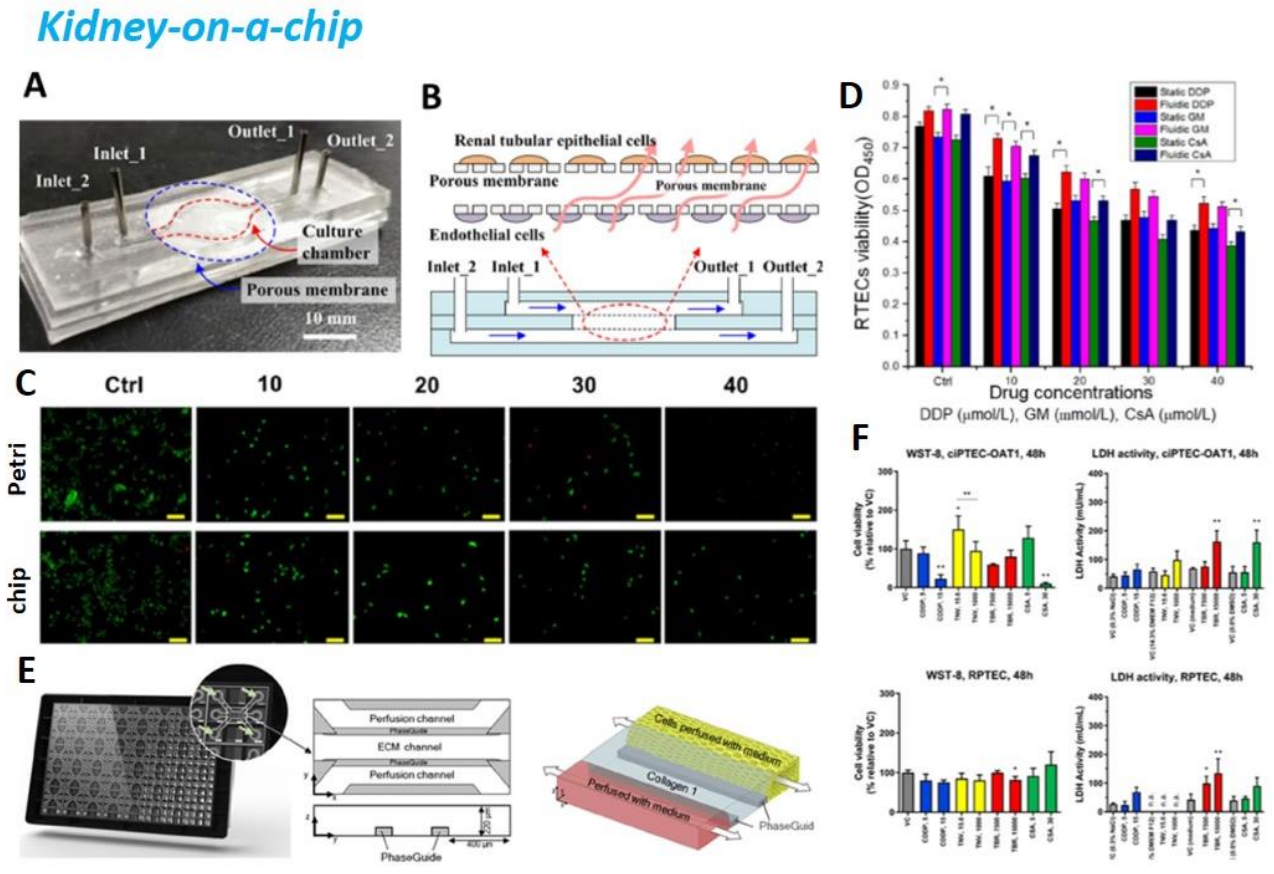

Figure 12. (A-B) *Image and scheme of a microfluidic kidney-on-chip made of three PDMS layers, two membranes, two inlets and two outlets. Reproduced from Ref. [199].* ***(C)*** *Live/dead cells (RPTECs) assay: live and dead cells (RPTECs) were labelled in green and red respectively. They used different concentrations (10,20,30 and 40 µmol/L) of DDP, under static conditions on Petri dishes and fluidic conditions on chip. Reproduced from Ref. [199].* ***(D)*** *Statistical analysis: CCK-8 of DDP, GM and CsA under static and fluidic conditions using a microplate reader (*p<0.05, **p<0.01). Reproduced from Ref. [199].* ***(E)*** *Scheme of the Mimetas kidney-on-chip.* ***(F)*** *Release of LDH and cell viability upon exposure to model nephrotoxicants cisplatin(CDDP), Tenofovir(TNV), Tobramycin (TBR) and Cyclosporin A (CSA) in RPTEC and in ciPTEC-OAT1 after 48 hours. *p<0.05, ** p<0.01. Reproduced from Ref. [200].*

978 **2.5 Multi-Organs on chip platforms**

979 Multiple organs on chip platforms (MOC) are the ultimate frontier in OOC research
980 where different organs compartments are interconnected into miniature 'body-on-a-chip'
981 microphysiological systems (MPS). The ambition is to recapitulate organ-organ
982 interaction/crosstalk, physiological relations, methabolic pathways, significant biological
983 barriers and whole-body drug response with an in vivo-like sequential organ-to-organ
984 transfer of media. Intestine models account for absorption and metabolism of drugs, liver
985 for their metabolism and kidney for clearance/excretion to enable a more appropriate
986 evaluation of systemic effectiveness, accuracy and safety of drugs [94]. In this section, we
987 describe this research keeping the focus on drug development from oral-administered (in
988 digestion-on-chip) to inhaled (e.g. lung/liver models) and transdermal-administered drugs
989 (integrating skin). Then some examples of MOC platforms for assessing drug availability
990 and cytotoxicity on tumors, brain and heart are discussed, including applications for brain
991 metastasis studies.

992 The bioavailability of two orally-administered small molecules (omeprazole and
993 verapamil) was analyzed by de Haan et al. [202]. Specifically, the authors employed a three-
994 stages compartmentalized chip to mimic the digestion chain representing mouth, stomach
995 and intestine. For this purpose, three y-shaped micromixers were connected in series
996 adding sequentially saliva, gastric juice and intestinal juice to the previously-treated
997 sample. Finally, the output chime and an additional cell culture matrix were inputted in a
998 fourth micromixer, whose outlet was connected to a flow-through transwell that contains a
999 co-culture of human colorectal adenocarcinoma cell line (Caco-2) and human colon
1000 adenocarcinoma mucus-secreting cell line (HT29-MTX-E12). Mass spectrometry (MS) was
1001 used for analysis. By means of this flow-based digestion-on-chip, the break down of
1002 omeprazole upon exposure to gastric acid was observed, while it arrives undamaged at the
1003 cell barrier if added in a way that emulates an enteric lining. Conversely, verapamil was not

1004 affected by digestion. A decreased absorption of verapamil was also noted when dissolved
1005 in apple juice as matrix [202].

1006 Toxicity studies on inhaled substances were instead the target for Bovard et al. [54], who
1007 combined lung and liver on a chip consisting of a fluidic plate and a reservoir made of
1008 polyetheretherketone (PEEK), a nonabsorbent material for small molecules. In the lung
1009 compartment, normal human bronchial epithelial (NHBE) cells were cultured at the air-
1010 liquid interface (ALI), while the liver compartment consisted of HepaRG liver spheroids.
1011 The aim was to mimic the human physiological response that occurs upon inhalation of
1012 substances, which are metabolized by both lung and liver CYP enzymes. In presence of liver
1013 spheroids, aflatoxin B1 (AFB1) toxicity decreased compared to NHBE lung cells alone due
1014 to crosstalk between the two cell types. Thus such lung/liver MOC platform may be useful
1015 for evaluating the toxicity of new inhaled drugs used in the treatment of lung diseases [54].
1016 Both inhalation- and intravenous administration were instead the target of comparison in
1017 terms of effectiveness and potentially toxicity in the study by Miller and coworkers, whose
1018 multi-organ platform integrated lung (including ALI), liver and breast cancer in a single
1019 chip [203]. The cultured cell lines were A549 for the lung, HepG2 C3A for the liver, and
1020 MDA MB231 for breast cancer, while curcumin, a natural compound from plants of the
1021 Curcuma longa species, represented the investigated drug. Inhalation therapy has the
1022 potential to be more economical if applied at home by the patient in contrast to intravenous
1023 therapy needing access to a clinical setting. Furthermore, for the same reason, it can be
1024 administered more frequently using lower drug level, as a way to reduce toxicity. In their
1025 study, the authors emphasized the importance of recirculating flow for more appropriate
1026 MOC platform and reported a small influence of curcumin administration on lung and liver
1027 viability while its effect was higher on breast cancer cells.

1028 In order to better testing systemic transdermal administration and subsequent drug
1029 metabolism, skin models were also integrated in multi-organ-chip. Marx group pioneered

1030 this field and in a first study realized a MPS combining skins with liver [92]. Successively,
1031 they improved this platform merging skin (with an air–liquid interface), reconstructed
1032 human intestinal barrier, liver (spheroids), kidney (in the form of a membrane covered by
1033 human proximal tubule epithelial cells) and vasculature mimicked with endothelial cells
1034 [93, 94].

1035 Multi-organ platforms have been also realized for predicting antitumor drug response.
1036 In the case of brain cancer treatments, in addition to the liver involved in drug metabolism,
1037 a key role is played by the blood-brain barrier, which selectively regulates the passage of
1038 chemicals to and from the brain. As an example, Li et al. [204] developed a multi-organ
1039 device to evaluate how the BBB and liver metabolism influence the availability and
1040 cytotoxicity of drugs used to treat glioblastoma (**Figure 13A**). Their biomimetic liver-brain
1041 chip consisted of microfluidic channels to create three compartments: the left one with
1042 human hepatocarcinoma cells (Hepg2) to mimic the liver, the right one with U87 cell to
1043 account for the glioblastoma. In between, a porous membrane and type I collagen were
1044 placed and rat brain microvascular endothelial cells (BMECS) and astrocytes were co-
1045 cultured to recapitulate the BBB. In this way, the chip recapitulated the drug pathway to
1046 reach both the liver and the brain upon oral administration. The brain-blood interface was
1047 characterized by TEER measurements and through the expression of proteins that
1048 constitute occluding junctions, such as ZO-1. Three anticancer drugs were tested in this
1049 study, namely Capecitabine, Temozolomide and Paclitaxel. Liver metabolism had limited
1050 effect on Temozolomide while resulted in a 30% enhancement of the Capecitabine
1051 cytotoxicity on U87 cells. The BBB instead reduced Paclitaxel cytotoxicity by 20%, but
1052 Temozolomide and Capecitabine effects were not significantly influenced. In conclusion,
1053 this chip allowed to evaluate how the efficacy of a drug targeting the brain is affected by
1054 both liver metabolism and the ability to cross the blood-brain barrier [204].

1055 A similar multi organ on-chip architecture was realized to assess the cardiac safety of an
1056 antidepressant drug (clomipramine) which is first metabolized by the liver. After
1057 administering 1 μM of drug in an upper compartment containing liver organoids, Yin et al.
1058 observed a reduced cell viability and an increased cardiocytotoxicity in the cardiac
1059 organoids located in the lower compartment [205]. Clomipramine also caused a reduction
1060 in intracellular calcium flux in the cardiac organoids monitored through a fluorescent Ca^{2+}
1061 indicator dye (Fluo-4 AM). Thus, the multi-organ chip permitted to predict the drug side
1062 effects both at the level of the main organ involved in its metabolism (the liver) and at the
1063 level of the target organ, in this case the heart.

1064 Coming back to cancer, metastasis formation is a key aspect to be addressed. It was
1065 discussed in **Section 2.2** in terms of interaction of cancer cells with the microvasculature.
1066 However, multi-organ models can contribute to gain further insight on the process. Liu et
1067 al. [206] implemented a platform for studying brain metastasis (BM) from primary tumor
1068 growth to its spreading by integrating an upstream lung compartment and a downstream
1069 brain including a functional BBB. In **Figure 13B**, the metastatic process and the MOC
1070 platform are illustrated. The lung model encompassed bronchial epithelial cells,
1071 fibroblasts, immune cells, pulmonary vascular endothelial cells, and tumor cells, and
1072 employed vacuum channels to account for breathing movements reconstituting the
1073 tumorigenesis and cancer intravasation. The brain model consisted of a brain parenchyma
1074 chamber surrounded by two vascular channels: (1) the left one connected to the upstream
1075 chamber in order to provide a pathway for metastatic cells, (2) the right one unconnected
1076 as a control. For cell co-culturing and tumor extravasation, the brain parenchyma
1077 compartment was interconnected to the vascular channels by micro-gaps. In their
1078 systematic study, the authors employed lung cancer cell lines with differing metastatic
1079 abilities and identified the Aldo-keto reductase protein family 1 B10 as a diagnostic

1080 biomarker showing higher expression in case of lung cancer BM and a prospective
1081 therapeutic target if silenced to limit BBB extravasation.

1082 In order to account for drug absorption, metabolism and clearance, Vernetti et al.
1083 reported a five organs platform including jejunum, liver and kidney models (respectively)
1084 in addition to skeletal muscle and neurovascular models [174]. The authors observed an
1085 organ-specific processing consistent with clinical data in their study of terfenadine for
1086 pharmacokinetics and toxicity; trimethylamine (TMA) as a potentially toxic microbiome
1087 metabolite; and vitamin D3. Furthermore, trimethylamine-N-oxide (TMAO) resulted able
1088 to cross the BBB. Co-culturing endothelial cells, fibroblasts and pericytes with (circulating)
1089 immune cells was also considered to investigate immune responses and its influence on
1090 disease progression and drug-induced response within an in-vivo mimicking
1091 microenvironment [358, 359]. The microbiota-gut-brain axis attracted large interest too
1092 [356, 357].

1093

1094

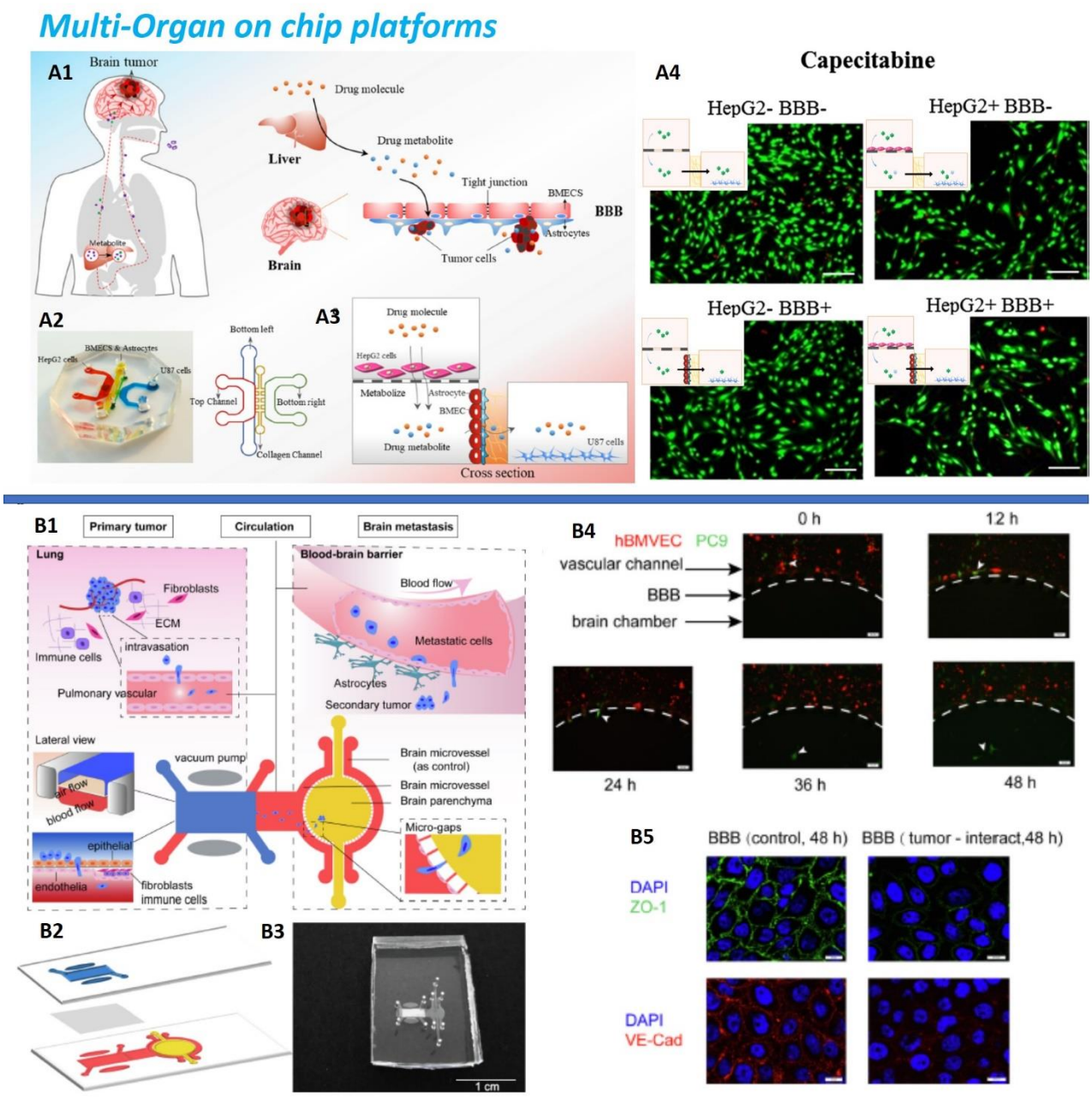

Figure 13. ***(A)*** *Multi organ-on-chip (liver and brain) platform:* ***(A1)*** *Pathway for oral drugs administration to brain tumors through liver metabolic activity and across the BBB.* ***(A2)*** *The MOC assembled by Li et al. to recapitulate this process using HepG2 cells in the top (liver) channel, brain microvascular endothelial cells (BMECS) and cerebral astrocytes in the bottom left and U87 cells in bottom right channels.* ***(A3)*** *MOC cross-sectional view.* ***(A4)*** *U87 cell viability in presence/absence of the liver compartment and the BBB upon administration of 80 µM CAP for 2 days. Live cells stained green, dead cells in red. Bar: 50 µm. Reproduced from Ref. [204].* ***(B)*** *MOC device for the investigation of lung cancer-derived brain metastasis.* ***(B1)*** *Pathological process and its recapitulation on chip by Liu et al. [206] through a upstream lung and downstream brain compartment.* ***(B2)*** *Structure of the MOC consisting of two PDMS layers and a membrane and* ***(B3)*** *its realization, scale bar 1 cm.* ***(B4)*** *Extravasation of PC9 lung cancer cells (green) through the BBB (red) in time-lapse images; scale bar, 50 µm.* ***(B5)*** *Confocal imaging of the expression of the tight junction zonal occludin-1 (ZO-1, green) and vascular endothelial -cadherin(VE-Cad, red) proteins in the control BBB (left) and in the BBB after tumor cells extravasation (right), evidencing a decrease in tightness upon vascular interaction with tumor cells; Scale bar, 20 µm. Reproduced from Ref. [206].*

1109 **3. Technologies and materials for Organs-on-Chips**

1110 **3.1 Microfluidic tools for Organs-on-Chips and drug research**

1111 A number of microfluidic tools have been optimized for Organs-on-Chips. A
1112 paradigmatic example concerns application to cancer field, where most of the tools were
1113 employed, from vascularization techniques and perfusable channels to administer
1114 nutrients and drugs (already discussed in **Section 1.4**) to microwell arrays, gradient
1115 generators and droplet microfluidics (described here). Thus we will draw this section by
1116 discussing the main microfluidic components to facilitate high-throughput drug screening
1117 with focus on the exemplary case of anticancer drug research.

1118 In particular, we can distinguish systems based on (i) microwells or U-shaped
1119 microstructures, or (ii) emulsion/droplets. Within the first category, the cancer cells are
1120 injected into the chip through a microchannel and captured by microwells arrays or U-
1121 shaped microstructures allowing their aggregation and tumor spheroid formation. This
1122 type of microfluidic chip is suitable for long-term culture, due to the continuum turnover
1123 of the culture media injected into the chip through the microchannel. For example, Khot et
1124 al. [207] used a 3D printed master to fabricate cell culturing wells in a PDMS layer
1125 sandwiched between two transparent PMMA layers, for direct microscope inspection
1126 (**Figure 14 A-F**). Using this device and culturing under static conditions, they reported
1127 on-chip generation of around 250 μm 3D spheroids from human colorectal HT29
1128 adenocarcinoma cell line. Then they demonstrated that seeding the cells through a port
1129 placed directly above the cell culturing wells improves the efficiency of 3D spheroids
1130 formation up to 100%, with respect to 68% observed in the case of flow-driven cell seeding.
1131 Following the culturing process, the HT29 spheroids were treated and analyzed on chip,
1132 through the perfusion of anti-cancer 5-Fluorouracil and the use of fluorescence microscopy
1133 for subsequent cell viability imaging confirmed by a Lactate dehydrogenase assay on the
1134 supernatant. In addition, in this work, two different methods were proposed for

administering cytotoxic treatment in the microfluidic devices, specifically limited-perfusion and continuous flow. In the first setup, allowing single endpoint experiments, single 3D spheroids were treated with 5-Fluorouracil under fluid flow (25 min at 20 µL/min) and then incubated under static conditions (for 24 h). In the second setup, spheroids on multiple devices were treated in parallel under continuous perfusion (up to 5 days at 20 µL/min) using a multichannel pump to better mimic systemic circulation in the body. Similar microfluidic chamber arrays were employed for on chip high throughput screening in other sectors/assays, such as screening of transient receptor potential channel modulators [208], screening of species differences in metabolism [209], screening of aggregation models [210], whole-organism behavior-based chemical screening [211] and single-embryo screening [212].

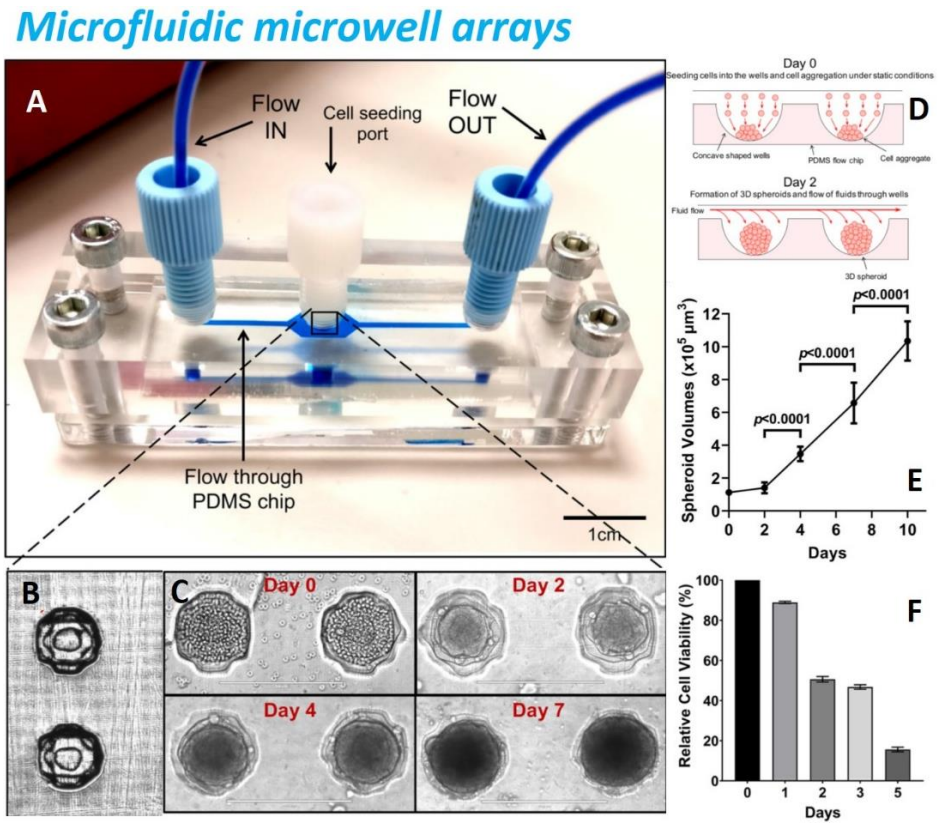

Figure 14. ***(A)*** *The PDMS 3D cell culturing microfluidic device developed by M. I. Khot et al., embedded between two PMMA layers and using standard UNF 1/4-28 flangeless fluidic fittings. Scale bar = 1 cm.* ***(B)*** *Optical microscopic image of the 3D cell culturing wells in the center of PDMS chip.* ***(C)*** *Progressive growth of 3D HT29 spheroids in images taken at days 0, 2, 4 and 7. Scale bar = 400 µm.* ***(D)*** *Scheme of the designed platform with concave shaped wells to favour cell aggregation at day 0. Then cell aggregates were cultured under static conditions to form 3D spheroids in the following two days and finally fluid flow was applied.* ***(E)*** *Progressive growth of HT29 spheroids cultured under static conditions for 10 days in the microfluidic devices.* ***(F)*** *The spheroids were treated with 5-FU (200 µM) through continuous perfusion at 20 µL/min for 5 days, and to monitor their chemosensitivity the supernatant was collected at the different time-points to perform a Lactate dehydrogenase (LDH) assay as reported in the histogram. Adapted from Ref. [207].*

1156 When the target is high-throughput screening, the use of gradient generators can be
1157 very effective. In this respect, Y. Fan et al. [213] developed a 3D brain cancer chip by using
1158 photo-polymerizable poly(ethylene) glycol diacrylate (PEGDA) hydrogel for high-
1159 throughput drug screening and prolonged drug release. The relevance of their device lies in
1160 the easy fabrication of the microfluidic device by simply a few seconds of photolithography
1161 without replica molding and plasma bonding which are instead required in the case of
1162 common PDMS microfluidic devices. 3D spheroid formation of glioblastoma multiforme
1163 cells (GBM, U87) was achieved into the microwell arrays and the authors investigated a
1164 combinatorial treatment with Pitavastatin and Irinotecan exploiting the integration of
1165 gradient generators on the chip (**Figure 15A-D**).

1166 Tumors, however, are complex tissues typically made of multiple cell types (e.g. cancer
1167 and stromal cells). Therefore, heterogeneous spheroids should be generated to explore
1168 mutual cell-cell interactions in both spheroids formation and anti-cancer drug screening
1169 response. In this respect, Yang et al. [214] reported the generation of heterospheroids
1170 consisting of MCF-7 (breast cancer) and L929 (fibroblast) cells, cultured for a long time in
1171 a microfluidic system and treated with Doxorubicin and Paclitaxel. Their device layout
1172 consisted of two (microwell and microfluidic) modules. Specifically, the microwell arrays
1173 were realized in PEGDA hydrogel, while the microfluidic module was realized in PDMS.
1174 Their drug screening study showed that heterospheroids of cancer and fibroblasts cells are
1175 characterized by a higher drug-resistance than homospheroids and combinatorial drugs are
1176 more effective than single drugs. In another study, Mazzocchi et al. [215] demonstrated the
1177 generation of 3D spheroids in a microfluidic device from cells derived by two mesothelioma
1178 biopsies to provide patient-specific models. In general, the microwells arrays approach is
1179 suitable for studies on a wider range of drugs, drug combinations and doses, and could
1180 represent a powerful tool to adjust patient-specific cancer treatments.

1181

Very promising for cancer research and drug development is the U-shaped microstructures technology reported by W. Liu et al. [216], who proposed a microfluidic strategy for large-scale and high-throughput in vitro anti-cancer investigation. An extraordinary large number of heterotypic 3D tumors (total of 672 tumors) with tissue-biomimetic phenotypes were produced in a single microfluidic device. Moreover, on-chip optical and fluorescent imaging were employed to analyze various 3D tumors characteristics such as growth dynamics, viability and apoptosis during cultivation and drug administration. These characteristics are advantageous for standardizing carcinogenesis, tumor progression and drug development studies by means of biomimetic organ-on-chip systems.

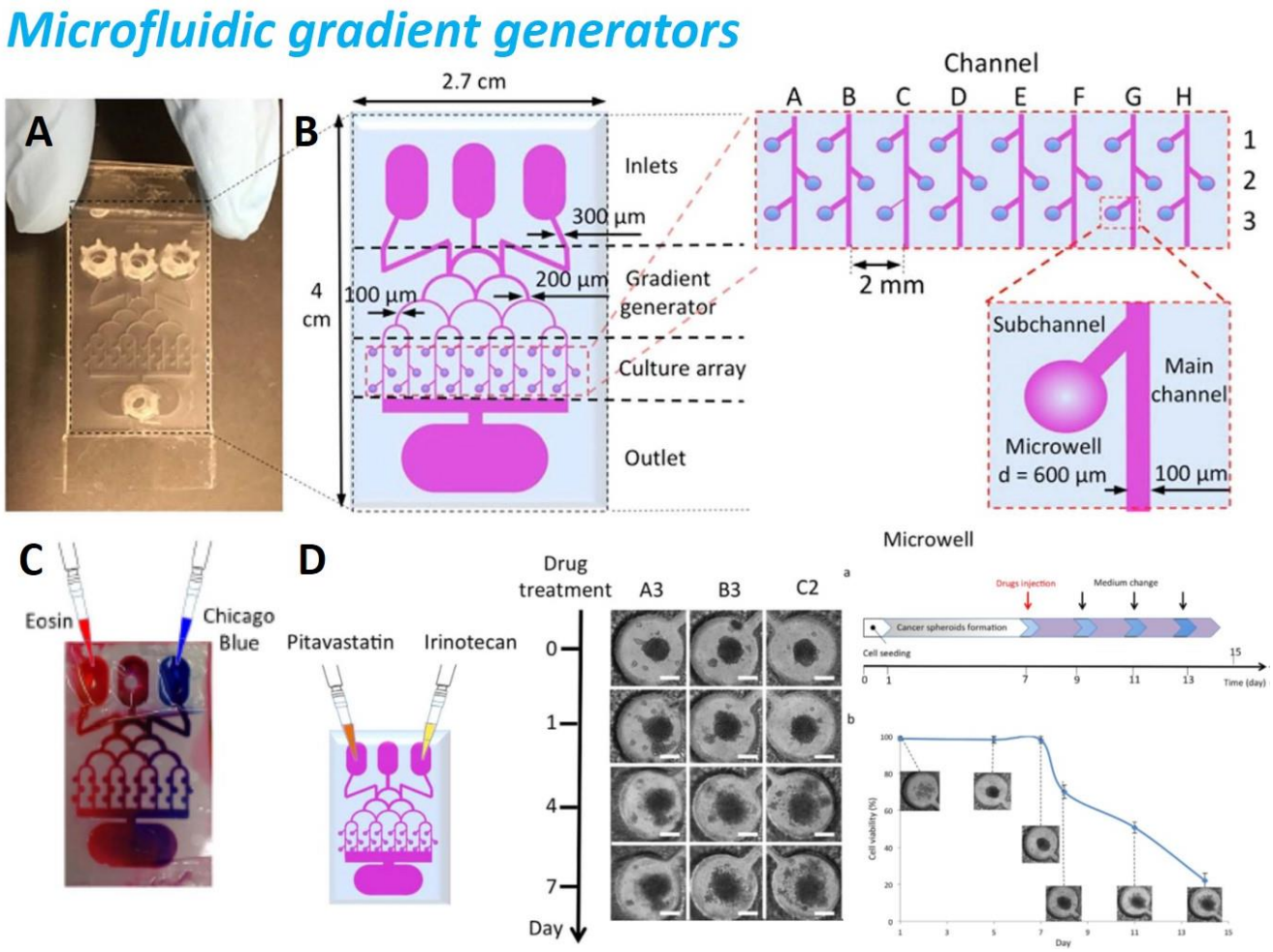

Figure 15 (A-C) *Gradient generator microfluidic chip designed by Fan et al. [213] and including individual culture chambers for brain cancer high-throughput combinatorial drug screening, performed with Pitavastatin and Irinotecan on cancer spheroids.* ***(D)*** *Time-lapse images and cell viability of U87 cancer spheroids upon continuous drug release. Scale bar, 200 µm. Adapted from Ref. [213]*

1197 Within the second category, droplets microfluidics is exploited. Usually, droplets are
1198 generated in a flow-focusing microfluidic device with two incompatible solutions injected
1199 in a microfluidic T-junction. At the cross junction, when the solution containing cells in
1200 aqueous medium meets the other solution, usually oil, emulsion droplets are spontaneously
1201 formed with cells trapped inside, due to their different interfacial properties. Then the
1202 droplets can be incubated to favor cells aggregation and tumor spheroid formation. With
1203 respect to microwells and U-shaped microstructures, the key advantage with droplets is the
1204 large number of microenvironments generated (tens of droplets per second) where cells
1205 can be encapsulated with high control on their number and in a rapid and efficient manner.
1206 In this frame, Lee et al. [217] reported a T-junction microfluidic system for large scale
1207 generation of cancer-cells embedded in micro-droplets with high generation frequencies
1208 (70 Hz) and a generation yield of about 20% higher than previously reported [218].
1209 Notably, they demonstrated the fabrication of brain tumor spheroids with diameter tunable
1210 between 100 and 130 μm by varying cell concentrations and as proof-of-concept they
1211 evaluated photothermal therapy and drug screening responses on brain tumor spheroids.

1212 To resemble the real tumor complexity and microenvironment, cell-laden hydrogel
1213 droplets were generated and investigated. In particular, Sabhachandani P. et al. [219]
1214 described the generation of cell-laden alginate droplets in a microfluidic device which
1215 combines a T-junction for droplet formation and a docking array which can house 1000
1216 droplets for gelation and spheroid formation and on chip drug screening (**Figure 16 A-D**).
1217 They demonstrated the generation of three spheroids models, drug resistant or drug
1218 sensitive breast cancer spheroids (MCF7) and co-culture spheroids consisting of drug
1219 sensitive breast cancer cells and fibroblast cells (HS-5). With this technology, they carried
1220 out on-chip cytotoxicity experiments using doxorubicin and paclitaxel chemotherapeutic
1221 drugs. Jang M. et al. [220] used a flow focusing microfluidic platform to generate two
1222 different types of 3D in vitro gastric cancer models by using the AGS (intestinal type) and

1223 Hs746T (diffuse type) cell lines encapsulated in Type 1 collagen beads (as ECM hydrogel).
1224 During droplets formation, the syringe filled with collagen solution was kept at low
1225 temperature by means of an ice bag, since collagen gels at 37 °C. Drug screening assays
1226 were then performed with 5-fluorouracil on the cultured microtumors. Another employed
1227 extracellular matrix component was matrigel, which is characterized by similar
1228 temperature dependent properties as collagen type I. Wu et al. [221] demonstrated the
1229 generation in matrigel droplets of tumor spheroids derived from patients' breast tumor
1230 tissues. A combined approach was proposed by Karamikamkar et al. [222], who produced
1231 breast cancer spheroids with alginate and collagen as ECM components, since the alginate
1232 helps to maintain the spherical shape of beads due to its fast gelling properties with respect
1233 to collagen I which gels more slowly and is temperature-sensitive. To reproduce the tumor
1234 complexity, Sun et al. [223] developed a microfluidic layout based on the flow-focusing
1235 principle for the preparation of core–shell alginate particles, which permitted the
1236 encapsulation of stromal fibroblast cells in the shell and tumor cells in the core (**Figure 16**
1237 **E-G**).

1238 To summarize, today several microfluidic tools are at the disposal of researchers for the
1239 implementation of OOC platform and to facilitate high throughput investigations. They
1240 include vascularization techniques and perfusable channels, microwell arrays, gradient
1241 generators and droplet microfluidics. Beyond them, it is worth mentioning also the
1242 availability of microfluidic separation tools to isolate specific cell types or molecular analyte
1243 for their further analysis or on chip culture [224-227]. Furthermore, microfluidic tools can
1244 be employed also for the production of drug nanoformulations and injectable liposomes
1245 with therapeutic applications [228-230]. Although their discussion is not covered by this
1246 review, the interested researchers can find detailed reviews in literature for further
1247 readings.

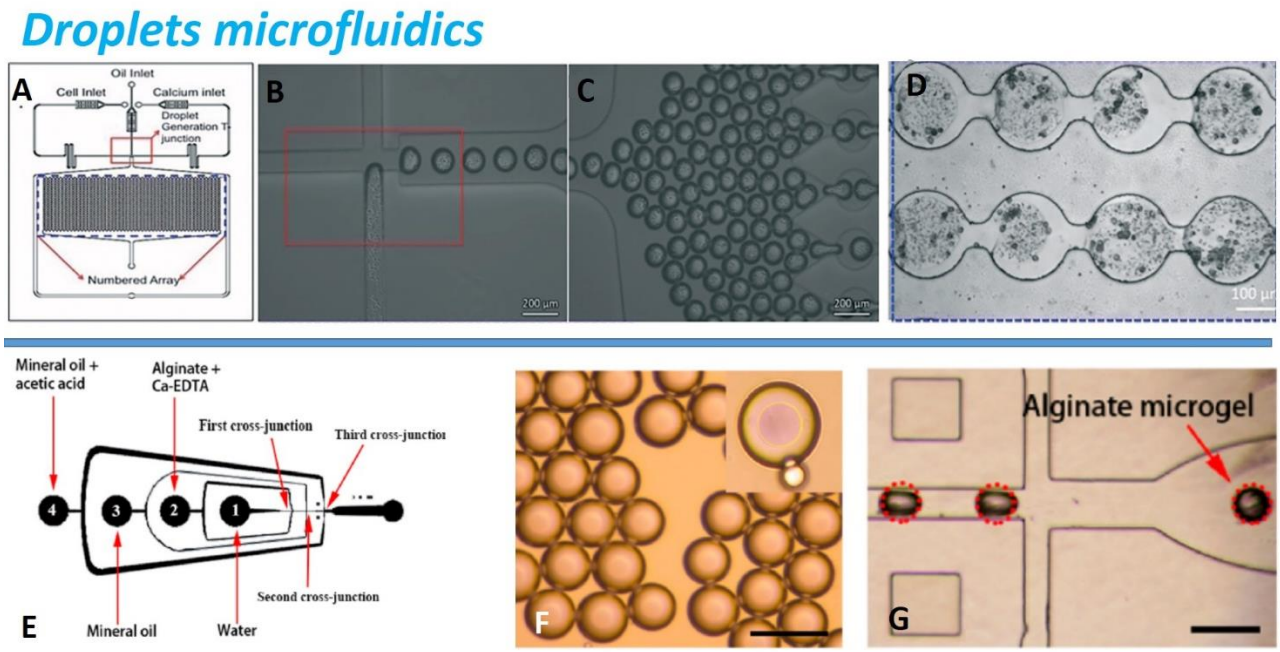

Figure 16. (A) *Layout of the microfluidic device for spheroid generation and docking array reported by Sabhachandani et al.[219].* ***(B)*** *T-junction for cell-laden alginate droplet formation. Scale bar: 200 µm.* ***(C)*** *Droplets entering the docking array after generation but before gelation. Scale bar: 200 µm.* ***(D)*** *Docking array with gelled cell-laden alginate spheroids. Scale bar: 100 µm. Adapted from Ref.[219].* ***(E)*** *Schematic of the flow-focusing device reported by Sun et al.[223] for producing core−shell alginate particles for encapsulating different cells in their core and the shell region.* ***(F)*** *Monodispersed core−shell alginate particles collected in mineral oil.* ***(G)*** *Cross-linking of alginate and microgel formation due to the injection of mineral oil containing acetic acid which triggers the release of* Ca^{2+} *from Ca-EDTA. Scale bars are 200 µm. Adapted from Ref.[223]*

1257 **3.2 Sensor integration for real-time analysis**

1258 Organs-on-chips provide effective microphysiological systems for biomedical studies
1259 and drug development. However, to take full advantage of their capabilities and accelerate
1260 research, they should be combined with efficient analytical methods. In this respect, we can
1261 distinguish among (1) endpoint analysis, (2) effluent collection and supernatant based
1262 assays, (3) in situ microscopy and imaging characterization and (4) real time analysis with
1263 integrated on-chip sensors. Concerning the first two categories, the small volumes in OOC
1264 platforms pose some challenges in the use of traditional methodologies such as a possible
1265 reduction in the low signal-to-noise ratios [9]. Within the third category, fluorescence and
1266 confocal microscopy provide powerful tools for investigating cellular arrangement,
1267 interactions and processes using appropriate fluorescent staining or tracers (as shown in the
1268 previous sections) but additional analytical assays may be required for further insight. In
1269 this respect, a recent trend consists in the on chip integration of in-line miniaturized sensors
1270 to replace off chip assays on manually extracted samples. This approach offers great
1271 opportunities for enabling continuous and automated data collection and in-situ monitoring
1272 of functional indicators and biological responses [13, 231]. It also facilitates real-time
1273 decision making. The range of monitorable parameters include barrier integrity, oxygen
1274 concentration and inflammation response (e.g., cytokines production) as well as electrical
1275 and mechanical signals [232, 233]. As a consequence, it is worth spending some words to
1276 present the most relevant sensing technologies.

1277 Miniaturized (bio)sensors are widely employed in diagnostics and automated lab on
1278 chip platforms, exploiting their high selectivity and sensitivity and integration in portable
1279 measurements systems [234-238]. In this respect, electrochemical / impedance read-out is
1280 particularly attractive for miniaturization. Electrochemical sensors in OOC models permit
1281 to monitor microenvironment conditions (such as pH and temperature) and analyze
1282 metabolic parameters (respiration rate, lactate levels and glucose consumption). Enzyme,

1283 protein, aptamers and antibodies can be immobilized on the sensor surface as recognition
1284 elements to detect specific markers. For example, oxygenation is an important physiological
1285 parameter that impacts on cell metabolism and functionality of a tissue [239]. In the gut,
1286 intestinal cells are subjected to different oxygen concentrations: low in the lumen center and
1287 high in the intestinal mucosa. Changes in oxygen distribution can be a symptom of bacterial
1288 infection and/or gut inflammation [240]. Amperometry with miniaturized electrodes
1289 permits to monitor dissolved oxygen levels by measuring the current produced via oxygen
1290 reduction reactions. For this purpose, Moya et al. [241] integrated multiple ink-jet sensors
1291 in a thin and porous membrane inside a Liver-On-a-Chip device (**Figure 17 A**). In tumor
1292 microtissues, instead, metabolic parameters provide information on cell growth and
1293 viability and in ref. [242] an amperometry sensor was implemented to monitor glucose and
1294 lactate levels secreted by a 3D human colon cancer microtissue.

1295 Electrochemical impedance spectroscopy (EIS) is a related transduction technique
1296 based on changes in the electrical properties near the electrode surface. From its
1297 introduction by Giaver and Keese [243], this method has been employed in lab-on-chip for
1298 facilitating several cell-based assays, including monitoring motion, attachment, growth,
1299 proliferation, spreading and differentiation of cultured cells [234, 244, 245], quantifying cell
1300 viability and heterogeneity [246, 247], assessing cell migration and invasive activities [248-
1301 250] and evaluating the effects of biochemical compounds and cytotoxicity [251-254].
1302 Furthermore, upon electrode functionalization with suitable recognition probes, EIS sensors
1303 consent the detection of biorecognition events [255-259]. Recently, Sorafenib efficacy in
1304 hepatocellular carcinoma treatment was assessed on chip through EIS sensors integrated in
1305 a miniaturized platform for cell proliferation assays and drug screening [260]. Within OOC
1306 field, in ref. [261], Ortega et al. used EIS sensors functionalized with enzyme-linked
1307 secondary antibodies to detect interleukin (IL)-6 and tumor necrosis factor (TNF), reaching
1308 limit of detection of the order of ng/ml. Zhang et al. monitored liver and heart in a multi-

1309 OOC platform (liver and heart) achieving a two orders of magnitude lower limit of detection
1310 (LOD) [262]. Moreover, impedance spectroscopy has been exploited to measure tumor
1311 spheroid size on-chip [263] and to study tumor spheroid viability throughout drug testing
1312 assays [264].

1313 The transepithelial/transendothelial electrical resistance (TEER) can be very useful to
1314 monitor in real time the integrity and the functionality of cellular barriers in OOC models
1315 such as the BBB, the intestinal epithelial barrier in gut-on-a-chip or the air-liquid interface
1316 in lung-on-a-chip. In ref. [157], Maoz and coworkers employed TEER measurements to
1317 simultaneously detect dynamic alterations of vascular permeability in heart-on-a-chip
1318 device. In the same chip, multi electrodes arrays (MEA) were integrated to measure field
1319 potentials of cardiomyocytes (**Figure 17 B**). In general, the electric/electrochemical
1320 techniques described above require electrode integration in the chambers/channels housing
1321 living cells or in contact with fluids passing through the cell compartments.

1322 Optical biosensors provide another, convenient in-situ monitoring approach [265].
1323 Refractive index changes near the sensor surface (due for example to cellular response or
1324 analyte secretion) are measured in surface plasmon resonance (SPR) [235, 236, 266, 267],
1325 optical waveguide light mode spectroscopy (OWLS), photonic crystals (PC) and resonant
1326 waveguide grating (RWG). In ref. [268], SPR based on nanoholes arrays were integrated in
1327 a microfluidic platform to detect vascular endothelial growth factor. Photonic crystals and
1328 structures fabricated by colloidal lithography were used as self-reporting tools for
1329 cardiomyocytes activity or microphysiological breath [158, 269] (**Figure 17 C1-C3**). Optical
1330 waveguides were fabricated in flexible PEG-based hydrogels to stimulate drug release from
1331 optogenetically engineered bacteria [270], whereas resonant waveguide grating biosensors
1332 have been used to study the role of plasma proteases on endothelial cell layers [271].

1333 Optical sensors have been also developed to investigate cell and tissue metabolism using
1334 sensitive opto-chemical tracer molecules. These sensors represent a valid alternative to

1335 electrical sensors to measure microenvironmental parameters such as pH and oxygen levels.
1336 Optical oxygen sensors exploit photoluminescence quenching produced by oxygen-sensitive
1337 dyes. Fluorophores based ruthenium- and metalloporphyrin were largely diffused due to
1338 their very high quenching constants [265]. For example, Shaegh et al. realized a bioreactor
1339 with integrated LED and photodetectors for monitoring of pH and oxygen levels [272]. By
1340 means of a similar approach, Khalid et al. measured the absorption light variation in cell
1341 media in the presence of phenol red to monitor pH in a lung cancer-on-a-chip platform
1342 (**Figure 17 C4**) [273].

1343 Mechanical sensors is another class which attracted attention due their potential
1344 applications in monitoring different physiological signals, mechanical (strain, pressure) or
1345 biological (for example detection of metabolic biomarkers) [274]. These sensors are used in
1346 OOC to study tissue stiffness and monitor dynamic deformations typical of the striatal
1347 muscular tissues (skeletal and cardiac muscle tissues). For example, Lind et al. developed
1348 some cantilevers that contained flexible thin-film strain gauges to detect beat rate and
1349 contractile stresses of the cardiac cells [155] (**Figure 17 D1-D2**). In ref. [275], Sidorov et al.
1350 designed a platform to grow 3D cardiac tissue constructs (ECTCs) and to perform
1351 measurements of their mechanical and electrophysiological parameters to evaluate the
1352 ECTCs functionality in both normal and pharmacologically modified conditions, using
1353 cantilever probes.

1354 Between mechanical sensors, surface acoustic wave are widely used since they are very
1355 sensitive toward mass loading, viscosity and conductivity variations occurring on the surface
1356 [276, 277], being the mechanical excitation strongly localized in the surface region [278].
1357 For example, Wang at al. used a shear horizontal-surface acoustic waves (SH-SAW) device
1358 comprising two pairs of resonators for detection and quantification of viability and growth
1359 of cells [279] (**Figure 17 D3-D4**). The same authors included SAW sensors in a gravitation
1360 microfluidic platform system for monitoring the proliferation and metabolism of tumoroids

[280]. Liu et al. [281] realized an integrated system of metal-enhanced fluorescence with SAW for cancer biomarker detection.

In some cases, gas sensors can provide other suitable monitoring and diagnostic tools as demonstrated by the increasing interest in their use for volatilomics and metabolomics [282-289]. Finally, some authors developed and integrated sensors in OOC devices, equipped with miniaturized models of laboratorial instruments. For example, a 3D-printed digital fluorescence type microscope was incorporated in a lung-cancer on chip platform for the visual monitoring of the cells on the chip [273]. In ref. [290], Mermoud et al. presented microimpedance tomography system integrated in a flexible printed circuit board to control cell activity and membrane movements in a breathing lung-on-chip.

In summary, the integration of miniaturized sensors for in situ, automated monitoring of relevant cellular and physiological parameters represents an important frontier for further increasing the throughput and content of OOC platforms.

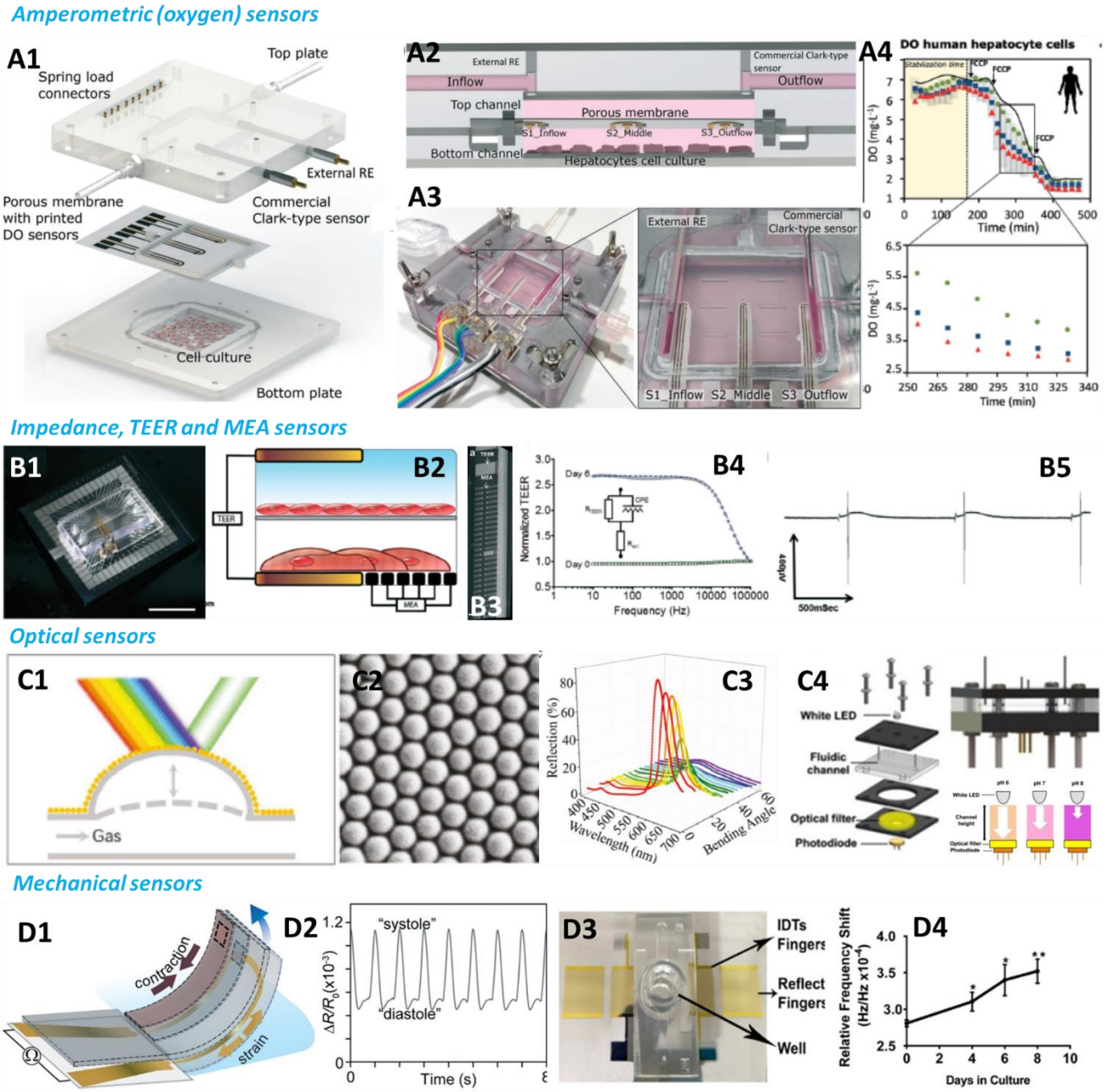

Figure 17. (A1-A4) *Schematic of the OOC system with the three printed electrochemical sensors along the microfluidic channel and sensor characterization data without primary cells, with primary rat hepatocytes cell culture, and with primary human hepatocytes [241].* ***(B1)*** *Transepithelial Electrical Resistance- Multi-Electrode Array chip.* ***(B2)*** *Schematic of experimental setup with endothelial layer grown on the top of membrane and cardiomyocytes on the top of MEA and among the two sets of TEER electrodes.****(B3)*** *Scanning electron microscope (SEM) image of the bottom layer electrodes.****(B4)*** *TEER measurements as a function of frequency* ***(B5)*** *MEA trace of single electrode* [157]. ***(C1)*** *Schematic diagram of sectional view of the pulmonary alveolus which activity is monitored using photonic nanoparticles* ***(C2-C3)*** *[269].****(C4)*** *Optical pH sensing in cell culture medium and sensor characterization data.[272].****(D1)*** *Cantilever strain-gauge sensor* ***(D2)*** *Micrograph of the sensor and typical response curve. [155]* ***(D3-D4)*** *Surface acoustic wave sensor for detection and quantification of viability and growth of cells [279].*

1387 **3.3 Materials for Organs-on-chips devices**

1388 Different materials are used to develop organs-on-chips depending on the specific
1389 features required in mimicking the in vivo structural and/or biochemical environment
1390 (**Table 1**). In this paragraph, the advantages and disadvantages of the most popular
1391 materials explored in the design of OOC are discussed.

1392 Glass is the oldest material employed in microfluidics. It is transparent, resistant to
1393 mechanical stress, hydrophilic, biocompatible and possess a low drug absorptivity. The
1394 major disadvantages which led to the experimentation of other materials concern its low
1395 gas permeability that does not allow long-term cell studies and the high cost of fabrication
1396 processes [291]. For these reasons, the use of polymeric materials became a mainstream.
1397 Launched many years after glass chips, polymeric-based devices can today be divided into
1398 three major groups: elastomers, thermoplastics and thermosets.

1399 Between elastomers, polyimethylsiloxane (PDMS) is the most employed for the
1400 realization of devices for life science applications [291]. It is flexible, optical transparent,
1401 gas permeable and biocompatible [292]. Its mechanical properties and its hydrophobicity
1402 are tunable respectively changing the ratio of PDMS base to curing agent and making
1403 surface plasma treatments [293]. It has a low autofluorescence and a good deformability
1404 that allows easy microfluidic connections [294, 295]. For its ease of use and its low cost, it
1405 is very useful in prototyping new devices [296]. PDMS elasticity is also exploited to mimic
1406 biological processes involving a mechanical deformation, such as breathing [297, 298] and
1407 gut peristalsis [17] or to measure mechanical properties of monolayer cells [299]. Other
1408 uses of PDMS are (i) in the form of membrane for cell culture at the interface between two
1409 compartments [297] and (ii) to produce microwell arrays to confine and induce 3D cell
1410 aggregation into spheroid, embryoid body or organoids [300]. Various fabrication
1411 methods are available for the fabrication of PDMS devices, from conventional soft
1412 lithography and micromolding techniques to new strategies such as hybrid stamp approach

1413 [301], sacrificial template methods [302], razor-printing [303] and 3D printing (using a
1414 PDMS resin) [304]. PDMS has some limits of applications due to its incompatibility with
1415 organic solvents (not particularly relevant for OOC applications) and its tendency to adsorb
1416 protein and small analytes [305]. Some treatment with plasma, UV or coatings are
1417 performed to improve the PDMS surface [292, 306]. Moreover, it can leach un-crosslinked
1418 oligomers that can cause toxicity in cells and affect their behavior, altering for example the
1419 predictions of pharmacokinetics/pharmacodynamics studies [307].

1420 Thermoplastics are a class of polymers that can be melted and reshaped many times
1421 through heating usually by means of thermomolding [308]. These materials are mostly
1422 optically transparent, more rigid than elastomers and resistant to the diffusion of small
1423 molecules [296], moderately resistant to alcool but dissoluble in most organic solvents
1424 [309]. Unfortunately, being lowly gas-permeable, thermoplastic sealed microchannel and
1425 microchamber are not suitable for long-term cell studies [309]. Moreover, their stiffness
1426 does not allow to realized diaphragm valves [309]. Depending on their application
1427 thermoplastics surface can be functionalized by means of surface grafting techniques or
1428 dynamic coating [309]. Thermoplastic polymers such as polystyrene (PS), polycarbonate
1429 (PC), polyurethane (PU), polymethylmethacrylate (PMMA) and polyethylene glycol
1430 diacrylate (PEGDA) are generally used in microfluidic systems [292, 310]. PS is highly
1431 biocompatible and used for cell growth and adhesion [311]. PC membranes are usually
1432 integrated among microchannels in OOC structures for modelling tissue-tissue interfaces
1433 [19, 312]. PU is a high mechanical strength material, resilient and resistant to abrasion,
1434 used in the fabrication of biomedical devices such as heart valves, pacemakers,
1435 haemodialysis membrane and artificial heart [313] but also as membrane in thermoplastic
1436 microfluidic devices [314]. PMMA has been employed as substrate for OOC due to its
1437 stiffness, good optical transparency and low auto-fluorescence background [315, 316].
1438 PEGDA thermoplastic is used to realize different type of microfluidic valve and pump [317,

318]. Thermoplastics are suitable for commercial production since fabrication techniques as thermomoulding can ensure high production-rate and low cost but they are not economic for prototyping [309]. For fast prototyping, photocurable soft lithography compatible liquid PS prepolymer and a fast curing PMMA prepolymer have been exploited as negative photoresists and shaped by means UV or visible light exposure [319, 320].

Differently from thermoplastics, in thermoset plastics the polymer chains cross-link into a rigid network structure that make difficult the reshaping of material. Thermosets, generally used as negative photoresists (e. g. SU-8) for microchannels fabrication, are optically transparent, resistant to heat degradation and to chemical attack of most solvents. Their mechanical strength permits the realization of high-aspect ratio and free-standing microstructures. However, their rigidity and high cost can limit their applications in biochips [309].

Paper is another material explored in microfluidics for its low cost, lightweight and ease to use. The porous structure of cellulose matrix is exploited for cell growth in 3D layout. In addition, sensor films can be integrated in paper-based devices for the monitoring of physiological microenvironment [321, 322]. 3D tumor cells have been growth in a paper roll device for the analysis of cellular environment and response [323, 324]. Although the manufacturing of paper-based microfluidic device is simple, few applications have been demonstrated on paper chips [309]. In these devices, the detection methods are relatively limited and it is difficult to integrate microcomponents such as valves.

Hydrogel is a hydrophilic macromolecular polymer gel constructed of a network of crosslinked polymer chains. The type and degree of crosslinking (depending on gelation and fabrication methods) affects the network properties, like swelling, elastic modulus porosity, permeability and degradability [325]. Physically or chemically cross linking can provide hydrogels a three dimensional network structure and make them insoluble, allowing immobilization and release of biomolecules. The ability of hydrogels to embed a

1465 large amount of water (more than 30% w/v) make them similar to natural soft tissues, while
1466 their properties to swell under specific biological conditions allow applications in
1467 biomedical fields, such as drug delivery and tissue engineering [325]. Hydrogels are also
1468 among the most used materials for mimicking the mechanics and biochemistry of native
1469 extracellular membrane [291]. These polymer networks, permeable to gas, water and
1470 solute, allow cell adhesion and migration, growth, differentiation and maturation of
1471 organoids [293]. ECM models in hydrogel are employed to study processes such as
1472 angiogenesis [326], cancer metastasis [327], and osteoblast migration [328]. Combining
1473 crosslinked strategies with lithography technique hydrogel scaffold are realized for 3D cell
1474 culture. Hydrogels have been likewise used to fabricate entire microfluidic devices for the
1475 study of blood vessel and to produce engineered tissue with functional vasculature [329].
1476 Hydrogels can be formed from natural polymers such as for example collagen, gelatin,
1477 matrigel, fibrin and alginate, or synthetic ones such as polyethylene glycol and its
1478 derivatives (PEG-DA), polycaprolactone (PCL) or synthetic/natural hybrids [296, 330].
1479 Remarkably, hydrogels are compatible with a variety of fabrication techniques, including
1480 soft lithography, 3D printing, micropatterning, electrospinning, UV curing, that enable the
1481 design of different structures [293].

1482 Collagens are the most common components of the native ECM and of connective
1483 tissues [296]. These natural hydrogels have several cell-binding sites for cell adhesion,
1484 growth and differentiation, that make them suitable for integration in platform model of
1485 heart, liver, skeletal muscle, neuronal network and tumor spheroids [331-334]. Moreover,
1486 collagen has been employed as structural component in microfluidic devices for the
1487 development of artificial microvessels [330]. Although Gelatin is similar to collagen in
1488 composition, it has a lower cost and is less antigenic. It is combined with other materials
1489 for supporting cell cultures in OOC platforms. Matrigel, a protein mixture extracted from
1490 mouse tumor cells, is used not only to model ECM in many tissue type, but also for cell

1491 adhesion, proliferation and for the formation of functional organoids [335].

1492 Within the category of natural compounds, Fibrin is an elastic protein involved in
1493 clotting, manly proposed for vascular network engineering but also used as scaffold for cell
1494 encapsulation and as artificial component of ECM. Alginate, a polysaccharide extracted
1495 from brown algae, is widely employed for several applications for its low-cost, low toxicity,
1496 easy functionalization and immediate gelation at mild condition. For example, Choi et al.
1497 [336] realized microfluidic channels in calcium alginate for mass transfer sensing and for
1498 detection of chemical environment control surrounding encapsulated cells.

1499 Natural hydrogels possess interesting properties for OOC applications such as high
1500 biocompatibility and biodegradability, but they have some limitations related to their
1501 relatively weak mechanical properties, limited long term stability and batch-to-batch
1502 variability. Synthetic hydrogel (and also hybrid) has been developed to provide materials
1503 with reproducible chemical and physical properties and tunable mechanical properties and
1504 degradation rate. Hydrogels based on PEG and its derivative (e.g. PEG-DA) are the most
1505 investigated synthetic hydrogel for tissue engineering. PCL found application in drug
1506 delivery and bone tissue scaffold. These synthetic biomaterials have some drawbacks
1507 related to the absence of cell adhesion ligands on the surface. To combine the advantages
1508 from both natural and synthetic biomaterials, hybrid hydrogels have been prepared. For
1509 example, as soft hydrogel is not suitable to mimic the hard and mineralized ECM of bone,
1510 fibrin incorporating hydroxyapatite [337] and mineralized collagen [338] are employed to
1511 study cancer metastatic into bone, bone angiogenesis and to investigate mechanical
1512 stimulation efficacy on bone formation. Finally, it is worth mentioning that “smart”
1513 responsive hydrogels able to respond to external stimuli are presently in the development
1514 phase.

1515

1516

Table 1. *Materials for OOC platforms.*

Categories	Materials	Advantages	Limitation	Applications
Glass		• transparency, • resistance to mechanical stress • hydrophilicity • biocompatibility • low drug absorptivity	low gas permeability,	• OOC substrate
Elastomers	PDMS	• flexible • optical transparent, • gas permeable • biocompatible, • low autofluorescent, • deformable, • ease of use , • low cost, • very useful in prototyping new devices	• hydrophobicity • incompatibility with organic solvents • tendency to adsorb protein and small analytes • leaching un-crosslinked oligomers	• OOC substrate • to mimic biological processes involving a mechanical deformation, (breathing [297, 298] and gut peristalsis [17]) • porous membrane to measure mechanical properties of monolayer cells[297] • to produce microwell arrays to induce 3D cell aggregation [300].
Thermoplastics	polystyrene (**PS**),	• optically transparent, • more rigid than elastomers and • resistant to the diffusion of small molecules, • moderate resistant to alcohol.	• lowly gas-permeability • inflexible • dissoluble in most organic solvents	• cell growth and adhesion [311]
	polycarbonate (**PC**)			• Membranes [19, 312].
	polyurethane (**PU**)			• heart valves, pacemakers, haemodialysis membrane and artificial heart [313] • membrane [314]
	polymethylmethacrylate (**PMMA**)			• OOC substrate
	polyethylene glycol diacrylate (**PEGDA**)			• microfluidic valve and pump [317, 318]
Thermosets		• optically transparent • resistant to heat degradation and to chemical attack of most solvents	• rigidity • high cost	• negative photoresists (es. SU-8) for microchannels fabrication • high-aspect ratio and free-standing microstructures
Paper		• low cost, • lightweight • ease to use	• limited detection method • difficulty to integrate microcomponents such as valves.	• cell growth
Natural Hydrogel	**Collagens**	• biocompatible, • permeable to gas, water and solute • low-cost • similar to natural soft tissue • non- or low-immunogenicity • alginate and gelatin have tunable properties • collagen present motifs for cell adhesion	• weak mechanical properties • limited long term stability • batch-to-batch variability	• ECM models [296] • cell adhesion, growth and differentiation, tumoroids [331-334] • artificial microvessels [330]
	Gelatin			• cell growth
	matrigel			• ECM models • cell adhesion, proliferation • formation of functional organoids [335].
	Fibrin			• vascular network engineering • scaffold for cell encapsulation • component of ECM
	Alginate			• microfluidic channels [336]
Synthetic Hydrogel	**PEG** and its derivative	• biocompatible, • permeable to gas, water and solute • low-cost • tunable mechanical properties and degradation rate	• absence of cell adhesion ligands on the surface	• tissue engineering
	PCL			• drug delivery and bone tissue scaffold

1518 **3.4 Cell Lines and technologies**

1519 For OOC implementation, various kinds of cells and cultures have been employed
1520 depending on the organ and the target application. In general, simple monocultures are
1521 limited under several aspects and the use of co-cultures is crucial to reproduce organotypic
1522 microenvironments encompassing homotypic and heterotypic cell-cell interactions.
1523 Critical parameters for co-cultures include the type of cells, culture media, order in which
1524 cells are cultured, and numbers/ratio of cell types [143].

1525 In terms of cells (**Table 2**), human primary cells have limited number of population
1526 doublings. Thus, immortalized cell lines are often employed to avoid senescence and
1527 improve availability, life span and reproducibility. However, while differentiating, they
1528 both show different characteristics after each passage and it is difficult to keep them in
1529 culture for long periods without changes [339]. In contrast, stem cells can differentiate into
1530 different cell types and exhibit the capacity for self-renewal. Among them induced
1531 pluripotent stem cells can be considered as the next-generation toolkit [39], in particular
1532 human-induced pluripotent stem cells (hiPSCs) which have been hailed as an effective
1533 replacement for human embryonic stem cells (hESCs). hiPSCs are represented by somatic
1534 cells, usually fibroblasts, that undergo a reprogramming process that converts already
1535 differentiated somatic cells into hiPSCs. Remarkably, the use of induced human stem cells
1536 is contributing to the development of patient-specific drugs and regenerative medicine
1537 [339, 340]. Beyond cell lines, spheroids and organoids have been integrated in microfluidic
1538 platform, e.g. for tumor models with perfusable channels. Biomaterial based scaffolds and
1539 3D cell bioprinting are also contributing in providing additional capacity for the fabrication
1540 of more advanced OOC models [48].

1541 In designing an OOC, both the cell-to-liquid ratio and the surface- to-volume ratio have
1542 to be considered since they can affect the response. In this respect, it is worth noting as
1543 OOC platforms differ from the in vivo case having large media volumes if compared to the

limited amount of tissues and this results in a continuous dilution of the metabolites. Furthermore, OOC also present a different surface-to-volume ratio which influences cell autocrine and paracrine signaling [31]. In various MOC studies, attention has been dedicated in building the devices maintaining ratios among the different organ masses as close as possible to the in vivo case. Vascularization, barrier functions, mechanical clues (e.g. associated to flow, breath or peristalsis), inflammatory processes, gas gradients and in particular oxygen concentrations are other important aspects to be carefully taken into account.

Table 2. *Cell lines for OOC platforms. [adapted from* https://promocell.com/in-the-lab/human-primary-cells-and-immortal-cell-lines/]

	Human primary cells	Cell lines	HiPSC (human induced pluripotent stem cell) and ESC (embryonic stem cells)
Senescence	Can replicate over a limited period of time	Can replicate over a long period of time	Have self-renewal
Culture	more demanding: Require more skills, special media and additives (growth factors) and adjustment for each cell type	Standard culture conditions easy to work with and keep alive	Sensitive, must be handled with care, require appropriate culture media with growth factors and extracellular matrix proteins.
Identity	Maintain the characteristics of the original tissue	Questionable, misidentification possible	ESC differentiate into different cell type, HiPSC derive from an adult somatic cell and is induced to convert into a stem cell that will give rise to a specifically differentiated cell
Morphology	Show healthy cell morphology	Loss of polarity, lack of key morphological features	
Phenotype	Maintain original phenotype for a limited number of passages depending on cell type and conditions	Change in phenotypes (need to be validated), functional alteration	
Genome	Genetically stable	Altered genomic content	Stable
Relevance *in vivo*	high	low	High
Reproducibility of results	Lower, donor-to-donor variations need to be considered	Higher, uniform cell type	
Cell availability	Limited	Unlimited	Unlimited (HiPSC) Limited (ESC)
Costs	High	Low	High
Ethics	Regulations for use of human tissues	Non relevant	Ethical issues relating to ESCs surmountable by HIPS

1556 ***Table 3.*** *Summary of discussed OOC and MOC platforms and their major characteristics.*

ORGAN-ON-CHIP	CULTURED CELLS IN DEVICE	Main scope / aim	Key features	Diseases	Drug	Barrier
1.1 Intestine	➢ Human colorectal adenocarcinoma cells (Caco2) [341] ➢ Co-colture of enterobacteria and Caco2 [341] ➢ HiPSC derived-human intestinal-like tubules [342]	➢ Drug absorption and bioavailability ➢ nutrient/biomolecules exchange ➢ environmental factors ➢ gut/host-microbiota interplay and alterations of gut microbiota composition and function (dysbiosis) ➢ gut inflammation, imbalance between pro-inflammatory and anti-inflammatory signals	➢ peristaltic movements ➢ villi microstructures, ➢ gut/host-microbiota interplay ➢ gut inflammation influence	➢ intestinal dysfunction, ➢ intestinal inflammation ➢ gut severe, chronic and cancerous diseases	➢ Drug absorption and bioavailability ➢ Efficacy ➢ toxicity and side effects	➢ intestinal epithelial barrier ➢ permeability, tightness of cell junctions
1.2 Lung	➢ Human small airway epithelial cells (SAEC) [343] ➢ Human pulmonary alveolar epithelial cells (HPAEpiC) and human pulmonary microvascular endothelial cells (HPMEC) [297] ➢ HiPSCs -derived lung cells [340] ➢ Human dermal microvascular endothelial cells (HDMEC) ➢ Human lung fibroblasts (HLF)	➢ Targeted instead than systemic administration ➢ influence of shear stress on paracellular and transcellular transport	➢ pulmonary microenvironment ➢ branching/breathing movements → cyclic strain and mechanical forces	➢ respiratory and pulmonary diseases ➢ viral and bacterial lung infections, ➢ chronic obstructive pulmonary disease (COPD) pulmonary edemas, tuberculosis and lung cancer, SARS-CoV and other respiratory virus infection injury ➢ airway repair after an injury ➢ Wound healing	➢ Drug absorption and bioavailability ➢ Efficacy drug-induced toxicity and side effects	➢ lung-blood barrier for inhaled agents ➢ alveolar-capillary barrier ➢ air-liquid interface (ALI)
1.3 Skin	➢ Human immortalized keratinocytes (HaCaT) [344] ➢ HiPSC-derived fibroblasts and keratinocytes[339] ➢ Melanocytes, Immune cells, Neurons ➢ + integration of biopsy and off chip models	➢ Risk assessment for external agents and cosmetic products ➢ Transdermal drug delivery/administration ➢ Drug penetration in bloodstream	➢ considerable differences vs animal skin in terms of structural and biochemical properties, lipid profile, hair density and stratum corneum thickness	➢ Dermatological studies ➢ Wound healing	➢ Transdermal drug delivery/administration ➢ Drug penetration in bloodstream	➢ skin barrier
1.4 Vasculature	➢ Human umbilical vein endothelial cells (HUVEC) [341] ➢ Porcine aortic endothelial cells (PAEC) [341] ➢ Human embryonic stem cell (hESC)-derived pericytes [339] ➢	➢ Intravenous administration and drug transport, ➢ recirculation at physiologically relevant perfusion rates and application of shear stress at in vivo levels ➢ vasculogenesis, sprouting angiogenesis and anastomosis ➢ blood organ barriers	➢ network of perfused microvessels ➢ Drug and nutrient transport (→increased lifespan for OOC) ➢ hemodynamic forces and vascular paarenchymal mechanotransduction vasculogenesis and angiogenesis	➢ diseases of the vascular system (i.e. atherosclerosis and deep vein thrombotic) ➢ vascularized micro organs (VMO) and micro tumors (VMT) ➢ tumor proliferation invasion, intravasation, extravasion	➢ Drug Transport, efficacy, ➢ anti-cancer and anti-angiogenic drugs	➢ blood organ barriers
2.1 Blood-Brain Barrier	➢ Human brain endothelial cells (hCMEC/D3) [341] ➢ Primary human-derived microvascular endothelial cells (HBMVEC) [339] ➢ HiPSC-derived neurons [339] ➢ HiPSC-derived brain microvascular endothelial cells (BMECs) ➢ Co-colture of neurons, glial cells, endothelial cells and skeletal muscle cells	➢ mimicking in vivo physiological brain microenvironment/barrier and relevant conditions/functions	➢ High-fidelity in mimicking in vivo physiological microenvironment	➢ neurodegenerative and brain diseases ➢	➢ Drug delivery through BBB junctions ➢ vascular network permeability	➢ functionality and disruption ➢ inflammatory disruption of BBB ➢ metabolic consequences and repair mechanisms
2.2 Tumor	➢ Patient-derived cells ➢ Tumor spheroids ➢ Variety of tumor cell lines	➢ vascularized tumor model ➢ use of (standard and liquid) biopsy & patient-derived samples, patient-specific tumor cell functions, ex vivo analysis of tumor cell dynamics and heterogeneity, ➢ microtumors arrays for testing combinatorial treatments with high throughput.	➢ 3D solid tumor tissues (tumor spheroids/organoids/ tumoroids) ➢ tumour microenvironment, extracellular matrix, cell–cell interactions, blood vasculature, and presence of nutrients, metabolites and oxygen gradients ➢ tumor angiogenesis and tumor and vasculature interactions ➢ metastatic cascade	➢ Cancer and metastatic cascade: proliferation invasion, intravasation, extravasion	➢ Drug development and screening ➢ Personalized therapies	➢ blood organ barriers
2.3.1 Heart	➢ Cardiomyocyte cells [341] ➢ Embryonic cardiomyoblast cell line(H9C2) [351] ➢ HiPSC-derived cardiomyocyte [339]	➢ influence of mechanical cues ➢ microtissue-generated contractile forces ➢ Studying cardiotoxicity and cardioprotective efficacy of cardiovascular drugs			➢ Efficacy ➢ toxicity and side effects	
2.3.2 Bone	➢ Human foetal osteoblast cell line (hFOB) ➢ Co-colture osteocyte and osteoclast ➢ Osteoblast-like cell line (MG63) ➢ Chondrocytes	➢ Recreating biomechanical structures of the bone with scaffold materials and co-coltures models ➢ mechanobiology and mechanotransduction			➢ Efficacy ➢ toxicity and side effects	
2.4.1 Liver	➢ Human liver carcinoma cesll (HEpG2) and Umbilical endothelial cells (HUVEC) [341] ➢ HiPSC -derived hepatic progenitor cells (HPC) and mesenchimal stem cells (MCSs) and enteroendocrine cells (ECs) [345] ➢ HiPSC- derived hepatocytes (iHep)	➢ Hepatotoxicity test of drugs and compounds ➢ Investigating drug-induced liver injury ➢ Studying hepatic drug metabolism changes in humans overcoming species-specific differences in ➢ hepatic drug metabolism	➢ drug metabolism ➢ multi-organ interactions ➢	➢ liver pathologies ➢ drug-induced liver injury (DILI)	➢ drug metabolism ➢ drug-induced liver toxicity	
2.4.2 Kidney	➢ Madin darby canine kidney(MDCK) [341] ➢ Human primary renal proximal tubule epithelial cell line (RPTEC) [346] ➢ Human renal epithelial cells (HREC) [347] ➢ hiPSC-derived human podocytes [348] ➢ Human immortalized proximal tubular epithelial cell with organic anion transporter 1 (CiPTEC-OAT1)	➢ Nephrotoxicity test of drugs and compounds ➢ Detecting drug-induced kidney injury	➢ drug clearance ➢ multi-organ interactions	➢ kidney pathologies ➢ drug-induced kidney injury (DIKI)	➢ drug-induced nephrotoxicity studies	
2.5 Multi-organ	➢ Hepatocellular carcinoma (HepG2/C3A) and Madin-Darby canine kidney (MDCK) [349] ➢ Hepatic cell line (HepaRG) and human epatic stellate cells (HHStec)[350]	➢ miniature 'body-on-a-chip' microphysiological systems ➢ organ-organ interaction/crosstalk, ➢ physiological relations, methabolic pathways, ➢ significant biological barriers ➢ whole-body drug response with in vivo-like sequential organ-to-organ transfer of media	➢ Drug development, toxicity tests and metabolism of xenobiotics ➢ Recapitulating metabolic pathways with ➢ intestine models accounting for absorption and metabolism of drugs, liver for their metabolism and kidney for clearance/excretion	➢ systemic studies on orally-administered or inhaled substances or transdermal administration and subsequent drug metabolism ➢ multi-organ platforms for predicting antitumor drug response and metastasis	➢ evaluation of systemic effectiveness, accuracy and safety of drugs	➢ By integrating relevant barrier models

1557

1558 **Perspectives and Conclusions**

1559 Current drug developments methodologies present severe limitations in their ability to
1560 appropriately take into account the complex in vivo physiopathology of human tissues. As
1561 a consequence, both conventional 2D culture and (costly) animal models fail to provide
1562 accurate predictions on human clinical outcomes with striking discrepancies in efficacy and
1563 side effects when compared to human trials [8, 156, 352]. This results in high costs and low
1564 success rate in translation to the clinic, which are responsible for the declining number of
1565 approved drugs, the increasing duration of the drug development process and a higher risk
1566 for drug withdrawal from the market at front of huge investments [353].

1567 To overcome these deficiencies, new platforms with enhanced predictive potential are
1568 under development. Exploiting advances in microfluidics and cell culture technologies, 3D-
1569 based models, microphysiological systems and organs-on-chips can recapitulate
1570 pathophysiology, in vivo biophysical conditions, cell-cell/cell-matrix interactions, organ-
1571 organ crosstalk and the underlying biochemical pathways of different diseases providing
1572 accurate and versatile in vitro models. The motivation for mimicking on chip natural
1573 tissues/organs microenvironments is twofold: (i) to accelerate high-content disease-related
1574 research and (ii) to enable high-throughput preclinical screening increasing predictability
1575 with human-based models.

1576 Advantages with respect to traditional methodologies have been discussed in **Figure 3**,
1577 while **Table 3** provides a summary of the state of the art for the OOC and MOC platforms
1578 which were discussed in details in the previous sections. Remarkably, recent advances have
1579 enabled to build relevant models of several human organs and diseases. Apart from drug
1580 efficacy and toxicity, enhanced in vitro models for micro-tissues vascularization and
1581 biological barriers have been optimized for investigating drug transport and barriers'
1582 permeability with increased accuracy and for developing novel drugs delivery systems
1583 across relevant in-vivo barriers (e.g. exploiting nanodelivery). Remarkably, microfluidic
1584 technologies offer great suitability to be readily adapted and easily scaled up for

1585 combinatorial approaches to assay relevant libraries of drug candidates and evaluate
1586 toxicity against multiple tissues in a more adequate and predictive way than previously
1587 possible. In addition, miniaturized sensor integration opens the way to further automation
1588 and number up of the assays. Remarkably, a recent trend consists now in coupling multiple
1589 organ modules linked by vascular perfusion in order to recapitulate organ-level structures
1590 and simulate multi-organ interactions in a comprehensive 'body-on-a-chip' platform [355].

1591 These huge progresses have been facilitated by cutting-edge techniques, spanning from
1592 microfabrication processes inherited from microelectronics to soft lithographies,
1593 micromachining, rapid prototyping techniques, laser-assisted stereolithography, 3D
1594 printing and bioprinting. A further relevant building block was the emergence of protocols
1595 for the efficient directed differentiation of human induced pluripotent stem cells at high
1596 quantity and quality [354], in order to make available the pertinent and supporting cells
1597 necessary for accurate disease and barrier models.

1598 In conclusion, drug research is rapidly advancing with novel technologies at the disposal
1599 of researchers and companies. Today, more predictive drug screening assays based on
1600 accurate in vitro replicas of human tissues, specific disease and multi-organ models can
1601 respond to the pressing need for filling a gap in effective drug screening and discovery as
1602 well as drug development improving the throughput, augmenting conventional 2D culture
1603 systems and minimizing animal testing with their related ethical issues. Furthermore,
1604 modern organ-on-chip systems offer also tremendous promise for elucidating the
1605 mechanisms responsible for several currently-incurable diseases. Several milestones were
1606 already achieved in this direction and future challenges are expected to regard achieving
1607 compromises between standardization, reproducibility and reliability in recapitulating
1608 disease microenvironment and drug response [360] as well as to proceed toward patient-
1609 derived testing platform for personalized precision medicine.

1610

1611

References

1. Low, L. A.; Mummery, C.; Berridge, B. R.; Austin, C. P.; Tagle, D. A., *Nature Reviews Drug Discovery* **2021,** *20* (5), 345-361. DOI 10.1038/s41573-020-0079-3.
2. Bhatia, S. N.; Ingber, D. E., *Nat. Biotechnol.* **2014,** *32* (8), 760-772. DOI 10.1038/nbt.2989.
3. Huh, D.; Hamilton, G. A.; Ingber, D. E., *Trends in Cell Biology* **2011,** *21* (12), 745-754. DOI 10.1016/j.tcb.2011.09.005.
4. Huh, D.; Matthews, B. D.; Mammoto, A.; Montoya-Zavala, M.; Hsin, H. Y.; Ingber, D. E., *Science* **2010,** *328* (5986), 1662-1668. DOI 10.1126/science.1188302.
5. Skardal, A.; Shupe, T.; Atala, A., *Drug Discov. Today* **2016,** *21* (9), 1399-1411. DOI 10.1016/j.drudis.2016.07.003.
6. Caplin, J. D.; Granados, N. G.; James, M. R.; Montazami, R.; Hashemi, N., *Advanced Healthcare Materials* **2015,** *4* (10), 1426-1450. DOI 10.1002/adhm.201500040.
7. Benam, K. H.; Dauth, S.; Hassell, B.; Herland, A.; Jain, A.; Jang, K. J.; Karalis, K.; Kim, H. J.; MacQueen, L.; Mahmoodian, R.; Musah, S.; Torisawa, Y. S.; van der Meer, A. D.; Villenave, R.; Yadid, M.; Parker, K. K.; Ingber, D. E., Engineered In Vitro Disease Models. In *Annual Review of Pathology: Mechanisms of Disease, Vol 10*, Abbas, A. K.; Galli, S. J.; Howley, P. M., Eds. Annual Reviews: Palo Alto, 2015; Vol. 10, pp 195-262.
8. Dhiman, N.; Kingshott, P.; Sumer, H.; Sharma, C. S.; Rath, S. N., *Biosens. Bioelectron.* **2019,** *137*, 236-254. DOI 10.1016/j.bios.2019.02.070.
9. Bennet, T. J.; Randhawa, A.; Hua, J.; Cheung, K. C., *Cells* **2021,** *10* (7), 51. DOI 10.3390/cells10071602.
10. Ashammakhi, N.; Darabi, M. A.; Celebi-Saltik, B.; Tutar, R.; Hartel, M. C.; Lee, J.; Hussein, S. M.; Goudie, M. J.; Cornelius, M. B.; Dokmeci, M. R.; Khademhosseini, A., *Small Methods* **2020,** *4* (1). DOI 10.1002/smtd.201900589.
11. Fois, C. A. M.; Le, T. Y. L.; Schindeler, A.; Naficy, S.; McClure, D. D.; Read, M. N.; Valtchev, P.; Khademhosseini, A.; Dehghani, F., *Advanced Healthcare Materials* **2019,** *8* (21), 1900968. DOI https://doi.org/10.1002/adhm.201900968.
12. Hewes, S. A.; Wilson, R. L.; Estes, M. K.; Shroyer, N. F.; Blutt, S. E.; Grande-Allen, K. J., *Tissue Engineering Part B-Reviews* **2020,** *26* (4), 313-326. DOI 10.1089/ten.teb.2019.0334.
13. Marrero, D.; Pujol-Vila, F.; Vera, D.; Gabriel, G.; Illa, X.; Elizalde-Torrent, A.; Alvarez, M.; Villa, R., *Biosens Bioelectron* **2021,** *181*, 113156. DOI 10.1016/j.bios.2021.113156.
14. Bein, A.; Shin, W.; Jalili-Firoozinezhad, S.; Park, M. H.; Sontheimer-Phelps, A.; Tovaglieri, A.; Chalkiadaki, A.; Kim, H. J.; Ingber, D. E., *Cell. Mol. Gastroenterol. Hepatol.* **2018,** *5* (4), 659-668. DOI 10.1016/j.jcmgh.2017.12.010.
15. Maurer, M.; Gresnigt, M. S.; Last, A.; Wollny, T.; Berlinghof, F.; Pospich, R.; Cseresnyes, Z.; Medyukhina, A.; Graf, K.; Gröger, M.; Raasch, M.; Siwczak, F.; Nietzsche, S.; Jacobsen, I. D.; Figge, M. T.; Hube, B.; Huber, O.; Mosig, A. S., *Biomaterials* **2019,** *220*, 119396. DOI https://doi.org/10.1016/j.biomaterials.2019.119396.
16. Marrero, D.; Pujol-Vila, F.; Vera, D.; Gabriel, G.; Illa, X.; Elizalde-Torrent, A.; Alvarez, M.; Villa, R., *Biosens. Bioelectron.* **2021,** *181*, 15. DOI 10.1016/j.bios.2021.113156.
17. Kim, H. J.; Huh, D.; Hamilton, G.; Ingber, D. E., *Lab on a Chip* **2012,** *12* (12), 2165-2174. DOI 10.1039/C2LC40074J.
18. Kimura, H.; Yamamoto, T.; Sakai, H.; Sakai, Y.; Fujii, T., *Lab on a Chip* **2008,** *8* (5), 741-746. DOI 10.1039/B717091B.
19. Pocock, K.; Delon, L.; Bala, V.; Rao, S.; Priest, C.; Prestidge, C.; Thierry, B., *Acs Biomaterials Science & Engineering* **2017,** *3* (6), 951-959. DOI 10.1021/acsbiomaterials.7b00023.
20. Kulthong, K.; Duivenvoorde, L.; Sun, H.; Confederat, S.; Wu, J.; Spenkelink, B.; de Haan, L.; Marin, V.; van der Zande, M.; Bouwmeester, H., *Toxicology in vitro : an international journal published in association with BIBRA* **2020,** *65*, 104815. DOI 10.1016/j.tiv.2020.104815.
21. Beaurivage, C.; Naumovska, E.; Chang, Y. X.; Elstak, E. D.; Nicolas, A.; Wouters, H.; van Moolenbroek, G.; Lanz, H. L.; Trietsch, S. J.; Joore, J.; Vulto, P.; Janssen, R. A. J.; Erdmann, K. S.; Stallen, J.; Kurek, D., *International Journal of Molecular Sciences* **2019,** *20* (22), 5661.

22. Kim, H. J.; Li, H.; Collins, J. J.; Ingber, D. E., *Proc. Natl. Acad. Sci. U. S. A.* **2016,** *113* (1), E7-E15. DOI 10.1073/pnas.1522193112.
23. Neurath, M. F., *Nat. Rev. Immunol.* **2014,** *14* (5), 329-342. DOI 10.1038/nri3661.
24. Wang, L.; Wu, J.; Chen, J.; Dou, W.; Zhao, Q.; Han, J.; Liu, J.; Su, W.; Li, A.; Liu, P.; An, Z.; Xu, C.; Sun, Y., *Talanta* **2021,** *226*, 122097. DOI 10.1016/j.talanta.2021.122097.
25. Ashammakhi, N.; Nasiri, R.; Barros, N. R.; Tebon, P.; Thakor, J.; Goudie, M.; Shamloo, A.; Martin, M. G.; Khademhosseini, A., *Biomaterials* **2020,** *255*, 120196. DOI 10.1016/j.biomaterials.2020.120196.
26. World Health Organisation [WHO]. The Top 10 Causes of Death. Geneva: World Health Organization.
27. Cidem, A.; Bradbury, P.; Traini, D.; Ong, H. X., *Frontiers in Bioengineering and Biotechnology* **2020,** *8*. DOI 10.3389/fbioe.2020.581995.
28. Borghardt, J. M.; Kloft, C.; Sharma, A., *Canadian Respiratory Journal* **2018,** *2018*, 2732017. DOI 10.1155/2018/2732017.
29. Ainslie, G. R.; Davis, M.; Ewart, L.; Lieberman, L. A.; Rowlands, D. J.; Thorley, A. J.; Yoder, G.; Ryan, A. M., *Lab on a Chip* **2019,** *19* (19), 3152-3161. DOI 10.1039/c9lc00492k.
30. Khedoe, P.; Marges, E.; Hiemstra, P.; Ninaber, M.; Geelhoed, M., *Frontiers in Immunology* **2020,** *11*. DOI 10.3389/fimmu.2020.01990.
31. Barros, A. S.; Costa, A.; Sarmento, B., *Advanced Drug Delivery Reviews* **2021,** *170*, 386-395. DOI 10.1016/j.addr.2020.09.008.
32. Campillo, N.; Oliveira, V. R.; da Palma, R. K., *Chemosensors* **2021,** *9* (9), 17. DOI 10.3390/chemosensors9090248.
33. Frost, T. S.; Jiang, L. A.; Lynch, R. M.; Zohar, Y., *Micromachines* **2019,** *10* (8), 18. DOI 10.3390/mi10080533.
34. Ishahak, M.; Hill, J.; Amin, Q.; Wubker, L.; Hernandez, A.; Mitrofanova, A.; Sloan, A.; Fornoni, A.; Agarwal, A., *Frontiers in Bioengineering and Biotechnology* **2020,** *8* (1311). DOI 10.3389/fbioe.2020.581163.
35. Henry, O. Y. F.; Villenave, R.; Cronce, M. J.; Leineweber, W. D.; Benz, M. A.; Ingber, D. E., *Lab on a Chip* **2017,** *17* (13), 2264-2271. DOI 10.1039/c7lc00155j.
36. Stucki, J. D.; Hobi, N.; Galimov, A.; Stucki, A. O.; Schneider-Daum, N.; Lehr, C. M.; Huwer, H.; Frick, M.; Funke-Chambour, M.; Geiser, T.; Guenat, O. T., *Sci Rep* **2018,** *8*, 13. DOI 10.1038/s41598-018-32523-x.
37. Huh, D.; Leslie, D. C.; Matthews, B. D.; Fraser, J. P.; Jurek, S.; Hamilton, G. A.; Thorneloe, K. S.; McAlexander, M. A.; Ingber, D. E., *Science Translational Medicine* **2012,** *4* (159). DOI 10.1126/scitranslmed.3004249.
38. Felder, M.; Trueeb, B.; Stucki, A. O.; Borcard, S.; Stucki, J. D.; Schnyder, B.; Geiser, T.; Guenat, O. T., *Frontiers in Bioengineering and Biotechnology* **2019,** *7*, 5. DOI 10.3389/fbioe.2019.00003.
39. Huang, D.; Liu, T. T.; Liao, J. L.; Maharjan, S.; Xie, X.; Perez, M.; Anaya, I.; Wang, S. W.; Mayer, A. T.; Kang, Z. X.; Kong, W. J.; Mainardi, V. L.; Garciamendez-Mijares, C. E.; Martinez, G. G.; Moretti, M.; Zhang, W. J.; Gu, Z. Z.; Ghaemmaghami, A. M.; Zhang, Y. S., *Proc. Natl. Acad. Sci. U. S. A.* **2021,** *118* (19), 10. DOI 10.1073/pnas.2016146118.
40. Douville, N. J.; Tung, Y. C.; Li, R.; Wang, J. D.; El-Sayed, M. E. H.; Takayama, S., *Anal. Chem.* **2010,** *82* (6), 2505-2511. DOI 10.1021/ac9029345.
41. Jain, A.; Barrile, R.; van der Meer, A.; Mammoto, A.; Mammoto, T.; De Ceunynck, K.; Aisiku, O.; Otieno, M.; Louden, C.; Hamilton, G.; Flaumenhaft, R.; Ingber, D., *Clin Pharmacol Ther* **2018,** *103* (2), 332-340. DOI https://doi.org/10.1002/cpt.742.
42. Stucki, A. O.; Stucki, J. D.; Hall, S. R. R.; Felder, M.; Mermoud, Y.; Schmid, R. A.; Geiser, T.; Guenat, O. T., *Lab on a Chip* **2015,** *15* (5), 1302-1310. DOI 10.1039/c4lc01252f.
43. Zamprogno, P.; Wuthrich, S.; Achenbach, S.; Thoma, G.; Stucki, J. D.; Hobi, N.; Schneider-Daum, N.; Lehr, C. M.; Huwer, H.; Geiser, T.; Schmid, R. A.; Guenat, O. T., *Communications Biology* **2021,** *4* (1), 10. DOI 10.1038/s42003-021-01695-0.
44. Benam, K. H.; Villenave, R.; Lucchesi, C.; Varone, A.; Hubeau, C.; Lee, H. H.; Alves, S. E.; Salmon, M.; Ferrante, T. C.; Weaver, J. C.; Bahinski, A.; Hamilton, G. A.; Ingber, D. E., *Nature Methods* **2016,** *13* (2), 151-+. DOI 10.1038/nmeth.3697.
45. Humayun, M.; Chow, C. W.; Young, E. W. K., *Lab on a Chip* **2018,** *18* (9), 1298-1309. DOI 10.1039/c7lc01357d.

46. Sellgren, K. L.; Butala, E. J.; Gilmour, B. P.; Randell, S. H.; Grego, S., *Lab on a Chip* **2014,** *14* (17), 3349-3358. DOI 10.1039/C4LC00552J.
47. Barkal, L. J.; Procknow, C. L.; Álvarez-García, Y. R.; Niu, M.; Jiménez-Torres, J. A.; Brockman-Schneider, R. A.; Gern, J. E.; Denlinger, L. C.; Theberge, A. B.; Keller, N. P.; Berthier, E.; Beebe, D. J., *Nature Communications* **2017,** *8* (1), 1770. DOI 10.1038/s41467-017-01985-4.
48. Park, J. Y.; Ryu, H.; Lee, B.; Ha, D.-H.; Ahn, M.; Kim, S.; Kim, J. Y.; Jeon, N. L.; Cho, D.-W., *Biofabrication* **2018,** *11* (1), 015002. DOI 10.1088/1758-5090/aae545.
49. Lin, K. C.; Yen, C. Z.; Yang, J. W.; Chung, J. H. Y.; Chen, G. Y., *Materials Today Advances* **2022,** *14*, 10. DOI 10.1016/j.mtadv.2022.100216.
50. Zhang, M.; Xu, C.; Jiang, L.; Qin, J. H., *Toxicol. Res.* **2018,** *7* (6), 13. DOI 10.1039/c8tx00156a.
51. van den Berge, M.; Ten Hacken, N. H. T.; Cohen, J.; Douma, W. R.; Postma, D. S., *Chest* **2011,** *139* (2), 412-423. DOI 10.1378/chest.10-1210.
52. Nawroth, J. C.; Lucchesi, C.; Cheng, D.; Shukla, A.; Ngyuen, J.; Shroff, T.; Varone, A.; Karalis, K.; Lee, H. H.; Alves, S.; Hamilton, G. A.; Salmon, M.; Villenave, R., *American Journal of Respiratory Cell and Molecular Biology* **2020,** *63* (5), 591-600. DOI 10.1165/rcmb.2020-0010MA.
53. Jain, A.; Barrile, R.; van der Meer, A. D.; Mammoto, A.; Mammoto, T.; De Ceunynck, K.; Aisiku, O.; Otieno, M. A.; Louden, C. S.; Hamilton, G. A.; Flaumenhaft, R.; Ingber, D., *Clin Pharmacol Ther* **2018,** *103* (2), 332-340. DOI 10.1002/cpt.742.
54. Bovard, D.; Sandoz, A.; Luettich, K.; Frentzel, S.; Iskandar, A.; Marescotti, D.; Trivedi, K.; Guedj, E.; Dutertre, Q.; Peitsch, M. C.; Hoeng, J., *Lab on a Chip* **2018,** *18* (24), 3814-3829. DOI 10.1039/c8lc01029c.
55. Mejias, J. C.; Nelson, M. R.; Liseth, O.; Roy, K., *Lab on a Chip* **2020,** *20* (19), 3601-3611. DOI 10.1039/d0lc00644k.
56. Thacker, V. V.; Sharma, K.; Dhar, N.; Mancini, G. F.; Sordet-Dessimoz, J.; McKinney, J. D., *Embo Reports* **2021,** *22* (6), 19. DOI 10.15252/embr.202152744.
57. Si, L. L.; Bai, H. Q.; Oh, C. Y.; Jin, L.; Prantil-Baun, R.; Ingber, D. E., *Microbiol. Spectr.* **2021,** *9* (2), 10. DOI 10.1128/Spectrum.00257-21.
58. Yang, X. Y.; Li, K. Y.; Zhang, X.; Liu, C.; Guo, B. K.; Wen, W. J.; Gao, X. H., *Lab on a Chip* **2018,** *18* (3), 486-495. DOI 10.1039/c7lc01224a.
59. van den Broek, L. J.; Bergers, L.; Reijnders, C. M. A.; Gibbs, S., *Stem Cell Reviews and Reports* **2017,** *13* (3), 418-429. DOI 10.1007/s12015-017-9737-1.
60. Cui, M. Y.; Wiraja, C.; Zheng, M. J.; Singh, G.; Yong, K. T.; Xu, C. J., *Adv. Therap.* **2022,** *5* (1), 13. DOI 10.1002/adtp.202100138.
61. Nitsche, K. S.; Muller, I.; Malcomber, S.; Carmichael, P. L.; Bouwmeester, H., *Arch. Toxicol.* **2022,** *96* (3), 711-741. DOI 10.1007/s00204-022-03234-0.
62. Zoio, P.; Oliva, A., *Pharmaceutics* **2022,** *14* (3), 30. DOI 10.3390/pharmaceutics14030682.
63. Risueno, I.; Valencia, L.; Jorcano, J. L.; Velasco, D., *Apl Bioengineering* **2021,** *5* (3), 12. DOI 10.1063/5.0046376.
64. Mathes, S. H.; Ruffner, H.; Graf-Hausner, U., *Advanced Drug Delivery Reviews* **2014,** *69*, 81-102. DOI 10.1016/j.addr.2013.12.006.
65. Gibbs, S.; Corsini, E.; Spiekstra, S. W.; Galbiati, V.; Fuchs, H. W.; DeGeorge, G.; Troese, M.; Hayden, P.; Deng, W.; Roggen, E., *Toxicology and Applied Pharmacology* **2013,** *272* (2), 529-541. DOI https://doi.org/10.1016/j.taap.2013.07.003.
66. Jain, P.; Sonti, S.; Garruto, J.; Mehta, R.; Banga, A. K., *Journal of Cosmetic Dermatology* **2012,** *11* (2), 101-110. DOI https://doi.org/10.1111/j.1473-2165.2012.00610.x.
67. Asbill, C.; Kim, N.; El-Kattan, A.; Creek, K.; Wertz, P.; Michniak, B., *Pharm. Res.* **2000,** *17* (9), 1092-1097. DOI 10.1023/A:1026405712870.
68. *Tissue Engineering Part C: Methods* **2012,** *18* (12), 947-957. DOI 10.1089/ten.tec.2011.0676.
69. Ouwehand, K.; Spiekstra, S. W.; Waaijman, T.; Scheper, R. J.; de Gruijl, T. D.; Gibbs, S., *Journal of Leukocyte Biology* **2011,** *90* (5), 1027-1033. DOI https://doi.org/10.1189/jlb.0610374.
70. Nissan, X.; Larribere, L.; Saidani, M.; Hurbain, I.; Delevoye, C.; Feteira, J.; Lemaitre, G.; Peschanski, M.; Baldeschi, C., *Proceedings of the National Academy of Sciences* **2011,** *108* (36), 14861-14866. DOI doi:10.1073/pnas.1019070108.

71. Michel, M.; L'Heureux, N.; Pouliot, R.; Xu, W.; Auger, F. A.; Germain, L., *In Vitro Cellular & Developmental Biology - Animal* **1999,** *35* (6), 318. DOI 10.1007/s11626-999-0081-x.
72. Abaci, H. E.; Gledhill, K.; Guo, Z.; Christiano, A. M.; Shuler, M. L., *Lab on a Chip* **2015,** *15* (3), 882-888. DOI 10.1039/C4LC00999A.
73. Kim, J. J.; Ellett, F.; Thomas, C. N.; Jalali, F.; Anderson, R. R.; Irimia, D.; Raff, A. B., *Lab on a Chip* **2019,** *19* (18), 3094-3103. DOI 10.1039/C9LC00399A.
74. Lee, S.; Jin, S. P.; Kim, Y. K.; Sung, G. Y.; Chung, J. H.; Sung, J. H., *Biomedical Microdevices* **2017,** *19* (2), 14. DOI 10.1007/s10544-017-0156-5.
75. Song, H. J.; Lim, H. Y.; Chun, W.; Choi, K. C.; Sung, J. H.; Sung, G. Y., *J. Ind. Eng. Chem.* **2017,** *56*, 375-381. DOI https://doi.org/10.1016/j.jiec.2017.07.034.
76. Song, H. J.; Lim, H. Y.; Chun, W.; Choi, K. C.; Lee, T.-y.; Sung, J. H.; Sung, G. Y., *J. Ind. Eng. Chem.* **2018,** *60*, 355-359. DOI https://doi.org/10.1016/j.jiec.2017.11.022.
77. Jeon, H. M.; Kim, K.; Choi, K. C.; Sung, G. Y., *J. Ind. Eng. Chem.* **2020,** *82*, 71-80. DOI https://doi.org/10.1016/j.jiec.2019.09.044.
78. Kim, J.; Kim, K.; Sung, G. Y., *International Journal of Molecular Sciences* **2020,** *21* (22), 8475.
79. Sriram, G.; Alberti, M.; Dancik, Y.; Wu, B.; Wu, R. G.; Feng, Z. X.; Ramasamy, S.; Bigliardi, P. L.; Bigliardi-Qi, M.; Wang, Z. P., *Mater Today* **2018,** *21* (4), 326-340. DOI 10.1016/j.mattod.2017.11.002.
80. Ramadan, Q.; Ting, F. C. W., *Lab on a Chip* **2016,** *16* (10), 1899-1908. DOI 10.1039/C6LC00229C.
81. Wufuer, M.; Lee, G.; Hur, W.; Jeon, B.; Kim, B. J.; Choi, T. H.; Lee, S., *Sci Rep* **2016,** *6* (1), 37471. DOI 10.1038/srep37471.
82. Au - Risueño, I.; Au - Valencia, L.; Au - Holgado, M.; Au - Jorcano, J. L.; Au - Velasco, D., *JoVE* **2021,** (171), e62353. DOI doi:10.3791/62353.
83. Mohammadi, M. H.; Heidary Araghi, B.; Beydaghi, V.; Geraili, A.; Moradi, F.; Jafari, P.; Janmaleki, M.; Valente, K. P.; Akbari, M.; Sanati-Nezhad, A., *Adv Healthc Mater* **2016,** *5* (19), 2459-2480. DOI 10.1002/adhm.201600439.
84. Zhang, J.; Chen, Z. Z.; Zhang, Y. Y.; Wang, X. C.; Ouyang, J.; Zhu, J. F.; Yan, Y. C.; Sun, X. W.; Wang, F.; Li, X. R.; Ye, H.; Sun, S. Q.; Yu, Q. D.; Sun, J. W.; Ge, J. J.; Li, Q. W.; Han, Q. Q.; Pu, Y. P.; Gu, Z. Z., *Lab on a Chip* **2021,** *21* (19), 3804-3818. DOI 10.1039/d1lc00099c.
85. Alberti, M.; Dancik, Y.; Sriram, G.; Wu, B.; Teo, Y. L.; Feng, Z.; Bigliardi-Qi, M.; Wu, R. G.; Wang, Z. P.; Bigliardi, P. L., *Lab on a Chip* **2017,** *17* (9), 1625-1634. DOI 10.1039/C6LC01574C.
86. Li, Y.; Wang, S.; Huang, R.; Huang, Z.; Hu, B.; Zheng, W.; Yang, G.; Jiang, X., *Biomacromolecules* **2015,** *16* (3), 780-789. DOI 10.1021/bm501680s.
87. Biglari, S.; Le, T. Y. L.; Tan, R. P.; Wise, S. G.; Zambon, A.; Codolo, G.; De Bernard, M.; Warkiani, M.; Schindeler, A.; Naficy, S.; Valtchev, P.; Khademhosseini, A.; Dehghani, F., *Advanced Healthcare Materials* **2019,** *8* (1), 12. DOI 10.1002/adhm.201801307.
88. *Applied In Vitro Toxicology* **2015,** *1* (2), 165-171. DOI 10.1089/aivt.2015.0002.
89. Valencia, L.; Canalejas-Tejero, V.; Clemente, M.; Fernaud, I.; Holgado, M.; Jorcano, J. L.; Velasco, D., *Sci Rep* **2021,** *11* (1), 14. DOI 10.1038/s41598-021-91875-z.
90. Varone, A.; Nguyen, J. K.; Leng, L.; Barrile, R.; Sliz, J.; Lucchesi, C.; Wen, N. R.; Gravanis, A.; Hamilton, G. A.; Karalis, K.; Hinojosa, C. D., *Biomaterials* **2021,** *275*, 12. DOI 10.1016/j.biomaterials.2021.120957.
91. Atac, B.; Wagner, I.; Horland, R.; Lauster, R.; Marx, U.; Tonevitsky, A. G.; Azar, R. P.; Lindner, G., *Lab on a Chip* **2013,** *13* (18), 3555-3561. DOI 10.1039/c3lc50227a.
92. Wagner, I.; Materne, E. M.; Brincker, S.; Sussbier, U.; Fradrich, C.; Busek, M.; Sonntag, F.; Sakharov, D. A.; Trushkin, E. V.; Tonevitsky, A. G.; Lauster, R.; Marx, U., *Lab on a Chip* **2013,** *13* (18), 3538-3547. DOI 10.1039/c3lc50234a.
93. Maschmeyer, I.; Lorenz, A. K.; Schimek, K.; Hasenberg, T.; Ramme, A. P.; Hubner, J.; Lindner, M.; Drewell, C.; Bauer, S.; Thomas, A.; Sambo, N. S.; Sonntag, F.; Lauster, R.; Marx, U., *Lab on a Chip* **2015,** *15* (12), 2688-2699. DOI 10.1039/c5lc00392j.
94. Maschmeyer, I.; Hasenberg, T.; Jaenicke, A.; Lindner, M.; Lorenz, A. K.; Zech, J.; Garbe, L. A.; Sonntag, F.; Hayden, P.; Ayehunie, S.; Lauster, R.; Marx, U.; Materne, E. M., *Eur. J. Pharm. Biopharm.* **2015,** *95*, 77-87. DOI 10.1016/j.ejpb.2015.03.002.
95. Chen, Z. K.; Kheiri, S.; Gevorkian, A.; Young, E. W. K.; Andre, V.; Deisenroth, T.; Kumacheva, E., *Lab on a Chip* **2021,** *21* (20), 3952-3962. DOI 10.1039/d1lc00619c.

96. Pradhan, S.; Banda, O. A.; Farino, C. J.; Sperduto, J. L.; Keller, K. A.; Taitano, R.; Slater, J. H., *Advanced Healthcare Materials* **2020,** *9* (8). DOI 10.1002/adhm.201901255.
97. Osaki, T.; Sivathanu, V.; Kamm, R. D., *Curr. Opin. Biotechnol.* **2018,** *52*, 116-123. DOI 10.1016/j.copbio.2018.03.011.
98. Dellaquila, A.; Le Bao, C.; Letourneur, D.; Simon-Yarza, T., *Advanced Science* **2021,** *8* (19), 2100798. DOI https://doi.org/10.1002/advs.202100798.
99. Lin, D. S. Y.; Guo, F.; Zhang, B. Y., *Nanotechnology* **2019,** *30* (2). DOI 10.1088/1361-6528/aae7de.
100. Vailhé, B.; Vittet, D.; Feige, J.-J., *Laboratory Investigation* **2001,** *81* (4), 439-452. DOI 10.1038/labinvest.3780252.
101. Risau, W., *Nature* **1997,** *386* (6626), 671-674. DOI 10.1038/386671a0.
102. Sekine, H.; Shimizu, T.; Sakaguchi, K.; Dobashi, I.; Wada, M.; Yamato, M.; Kobayashi, E.; Umezu, M.; Okano, T., *Nature Communications* **2013,** *4* (1), 1399. DOI 10.1038/ncomms2406.
103. Du, Y.; Li, N.; Yang, H.; Luo, C.; Gong, Y.; Tong, C.; Gao, Y.; Lü, S.; Long, M., *Lab on a Chip* **2017,** *17* (5), 782-794. DOI 10.1039/C6LC01374K.
104. Miller, J. S.; Stevens, K. R.; Yang, M. T.; Baker, B. M.; Nguyen, D.-H. T.; Cohen, D. M.; Toro, E.; Chen, A. A.; Galie, P. A.; Yu, X.; Chaturvedi, R.; Bhatia, S. N.; Chen, C. S., *Nat. Mater.* **2012,** *11* (9), 768-774. DOI 10.1038/nmat3357.
105. Abaci, H. E.; Guo, Z.; Coffman, A.; Gillette, B.; Lee, W.-h.; Sia, S. K.; Christiano, A. M., *Advanced Healthcare Materials* **2016,** *5* (14), 1800-1807. DOI https://doi.org/10.1002/adhm.201500936.
106. Mori, N.; Morimoto, Y.; Takeuchi, S., *Biomaterials* **2017,** *116*, 48-56. DOI https://doi.org/10.1016/j.biomaterials.2016.11.031.
107. Kim, B. S.; Gao, G.; Kim, J. Y.; Cho, D.-W., *Advanced Healthcare Materials* **2019,** *8* (7), 1801019. DOI https://doi.org/10.1002/adhm.201801019.
108. Kim, S.; Lee, H.; Chung, M.; Jeon, N. L., *Lab on a Chip* **2013,** *13* (8), 1489-1500. DOI 10.1039/c3lc41320a.
109. Wang, X.; Phan, D. T. T.; Sobrino, A.; George, S. C.; Hughes, C. C. W.; Lee, A. P., *Lab on a Chip* **2016,** *16* (2), 282-290. DOI 10.1039/C5LC01050K.
110. Sobrino, A.; Phan, D. T. T.; Datta, R.; Wang, X. L.; Hachey, S. J.; Romero-Lopez, M.; Gratton, E.; Lee, A. P.; George, S. C.; Hughes, C. C. W., *Sci Rep* **2016,** *6*, 11. DOI 10.1038/srep31589.
111. Chen, M. B.; Whisler, J. A.; Fröse, J.; Yu, C.; Shin, Y.; Kamm, R. D., *Nature Protocols* **2017,** *12* (5), 865-880. DOI 10.1038/nprot.2017.018.
112. van der Helm, M. W.; van der Meer, A. D.; Eijkel, J. C. T.; van den Berg, A.; Segerink, L. I., *Tissue Barriers* **2016,** *4* (1). DOI 10.1080/21688370.2016.1142493.
113. Osaki, T.; Shin, Y.; Sivathanu, V.; Campisi, M.; Kamm, R. D., *Advanced Healthcare Materials* **2018,** *7* (2), 29. DOI 10.1002/adhm.201700489.
114. Wang, Y. I.; Abaci, H. E.; Shuler, M. L., *Biotechnology and Bioengineering* **2017,** *114* (1), 184-194. DOI 10.1002/bit.26045.
115. Jeong, S.; Kim, S.; Buonocore, J.; Park, J.; Welsh, C. J.; Li, J. R.; Han, A., *Ieee Transactions on Biomedical Engineering* **2018,** *65* (2), 431-439. DOI 10.1109/tbme.2017.2773463.
116. Park, T. E.; Mustafaoglu, N.; Herland, A.; Hasselkus, R.; Mannix, R.; FitzGerald, E. A.; Prantil-Baun, R.; Watters, A.; Henry, O.; Benz, M.; Sanchez, H.; McCrea, H. J.; Goumnerova, L. C.; Song, H. W.; Palecek, S. P.; Shusta, E.; Ingber, D. E., *Nature Communications* **2019,** *10*, 12. DOI 10.1038/s41467-019-10588-0.
117. Arik, Y. B.; van der Helm, M. W.; Odijk, M.; Segerink, L. I.; Passier, R.; van den Berg, A.; van der Meer, A. D., *Biomicrofluidics* **2018,** *12* (4). DOI 10.1063/1.5023041.
118. Srinivasan, B.; Kolli, A. R.; Esch, M. B.; Abaci, H. E.; Shuler, M. L.; Hickman, J. J., *Jala* **2015,** *20* (2), 107-126. DOI 10.1177/2211068214561025.
119. Wong, J. F.; Simmons, C. A., *Lab on a Chip* **2019,** *19* (6), 1060-1070. DOI 10.1039/c8lc01321g.
120. Bang, S.; Lee, S.-R.; Ko, J.; Son, K.; Tahk, D.; Ahn, J.; Im, C.; Jeon, N. L., *Sci Rep* **2017,** *7* (1), 8083. DOI 10.1038/s41598-017-07416-0.
121. Brown, J. A.; Codreanu, S. G.; Shi, M.; Sherrod, S. D.; Markov, D. A.; Neely, M. D.; Britt, C. M.; Hoilett, O. S.; Reiserer, R. S.; Samson, P. C.; McCawley, L. J.; Webb, D. J.; Bowman, A. B.; McLean, J. A.; Wikswo, J. P., *Journal of Neuroinflammation* **2016,** *13*. DOI 10.1186/s12974-016-0760-y.
122. Kwapiszewska, K.; Michalczuk, A.; Rybka, M.; Kwapiszewski, R.; Brzózka, Z., *Lab on a Chip* **2014,** *14* (12), 2096-2104. DOI 10.1039/C4LC00291A.

123. Mollica, H.; Palomba, R.; Primavera, R.; Decuzzi, P., *ACS Biomaterials Science & Engineering* **2019,** *5* (9), 4834-4843. DOI 10.1021/acsbiomaterials.9b00697.
124. Du, Z.; Mi, S.; Yi, X.; Xu, Y.; Sun, W., *Biofabrication* **2018,** *10* (3), 034102. DOI 10.1088/1758-5090/aac70c.
125. Chen, M. B.; Lamar, J. M.; Li, R.; Hynes, R. O.; Kamm, R. D., *Cancer research* **2016,** *76* (9), 2513-24. DOI 10.1158/0008-5472.can-15-1325.
126. Song, J.; Miermont, A.; Lim, C. T.; Kamm, R. D., *Scientific Reports* **2018,** *8* (1), 17949. DOI 10.1038/s41598-018-36381-5.
127. Xiao, Y.; Kim, D.; Dura, B.; Zhang, K.; Yan, R.; Li, H.; Han, E.; Ip, J.; Zou, P.; Liu, J.; Chen, A. T.; Vortmeyer, A. O.; Zhou, J.; Fan, R., *Advanced Science* **2019,** *6* (8), 1801531. DOI https://doi.org/10.1002/advs.201801531.
128. Sobrino, A.; Phan, D. T. T.; Datta, R.; Wang, X.; Hachey, S. J.; Romero-López, M.; Gratton, E.; Lee, A. P.; George, S. C.; Hughes, C. C. W., *Scientific Reports* **2016,** *6* (1), 31589. DOI 10.1038/srep31589.
129. Phan, D. T. T.; Wang, X. L.; Craver, B. M.; Sobrino, A.; Zhao, D.; Chen, J. C.; Lee, L. Y. N.; George, S. C.; Lee, A. P.; Hughes, C. C. W., *Lab on a Chip* **2017,** *17* (3), 511-520. DOI 10.1039/c6lc01422d.
130. Marturano-Kruik, A.; Nava, M. M.; Yeager, K.; Chramiec, A.; Hao, L.; Robinson, S.; Guo, E.; Raimondi, M. T.; Vunjak-Novakovic, G., *Proceedings of the National Academy of Sciences* **2018,** *115* (6), 1256-1261. DOI doi:10.1073/pnas.1714282115.
131. Xu, H.; Li, Z.; Yu, Y.; Sizdahkhani, S.; Ho, W. S.; Yin, F.; Wang, L.; Zhu, G.; Zhang, M.; Jiang, L.; Zhuang, Z.; Qin, J., *Scientific Reports* **2016,** *6* (1), 36670. DOI 10.1038/srep36670.
132. Lim, J.; Ching, H.; Yoon, J.-K.; Jeon, N. L.; Kim, Y., *Nano Convergence* **2021,** *8* (1), 12. DOI 10.1186/s40580-021-00261-y.
133. Zhang, X.; Karim, M.; Hasan, M. M., **2022,** *14* (3). DOI 10.3390/cancers14030648.
134. Lin, Z.; Luo, G.; Du, W.; Kong, T.; Liu, C.; Liu, Z., *Small* **2020,** *16* (9), 1903899. DOI https://doi.org/10.1002/smll.201903899.
135. Del Piccolo, N.; Shirure, V. S.; Bi, Y.; Goedegebuure, S. P.; Gholami, S.; Hughes, C. C. W.; Fields, R. C.; George, S. C., *Advanced drug delivery reviews* **2021,** *175*, 113798. DOI 10.1016/j.addr.2021.05.008.
136. Imparato, G.; Urciuolo, F.; Netti, P. A., *Bioengineering* **2022,** *9* (1), 28.
137. Lee, S. W.; Kwak, H. S.; Kang, M.-H.; Park, Y.-Y.; Jeong, G. S., *Scientific Reports* **2018,** *8* (1), 2365. DOI 10.1038/s41598-018-20886-0.
138. Chung, M.; Ahn, J.; Son, K.; Kim, S.; Jeon, N. L., *Advanced healthcare materials* **2017,** *6* (15). DOI 10.1002/adhm.201700196.
139. Ayuso, J. M.; Truttschel, R.; Gong, M. M.; Humayun, M.; Virumbrales-Munoz, M.; Vitek, R.; Felder, M.; Gillies, S. D.; Sondel, P.; Wisinski, K. B.; Patankar, M.; Beebe, D. J.; Skala, M. C., *Oncoimmunology* **2018,** *8* (3), 1553477-1553477. DOI 10.1080/2162402X.2018.1553477.
140. Nashimoto, Y.; Okada, R.; Hanada, S.; Arima, Y.; Nishiyama, K.; Miura, T.; Yokokawa, R., *Biomaterials* **2020,** *229*, 119547. DOI https://doi.org/10.1016/j.biomaterials.2019.119547.
141. Haase, K.; Offeddu, G. S.; Gillrie, M. R.; Kamm, R. D., *Advanced Functional Materials* **2020,** *30* (48), 2002444. DOI https://doi.org/10.1002/adfm.202002444.
142. Nashimoto, Y.; Hayashi, T.; Kunita, I.; Nakamasu, A.; Torisawa, Y.-s.; Nakayama, M.; Takigawa-Imamura, H.; Kotera, H.; Nishiyama, K.; Miura, T.; Yokokawa, R., *Integrative Biology* **2017,** *9* (6), 506-518. DOI 10.1039/c7ib00024c.
143. Hodgkinson, T.; Amado, I. N.; O'Brien, F. J.; Kennedy, O. D., *Apl Bioengineering* **2022,** *6* (1), 17. DOI 10.1063/5.0068277.
144. Middleton, K.; Al-Dujaili, S.; Mei, X.; Günther, A.; You, L., *J. Biomech.* **2017,** *59*, 35-42. DOI https://doi.org/10.1016/j.jbiomech.2017.05.012.
145. Tang, Q. Q.; Li, X. Y.; Lai, C.; Li, L.; Wu, H. K.; Wang, Y. J.; Shi, X. T., *Bioactive Materials* **2021,** *6* (1), 169-178. DOI 10.1016/j.bioactmat.2020.07.016.
146. Scialla, S.; Palazzo, B.; Barca, A.; Carbone, L.; Fiore, A.; Monteduro, A. G.; Maruccio, G.; Sannino, A.; Gervaso, F., *Materials Science & Engineering C-Materials for Biological Applications* **2017,** *76*, 1166-1174. DOI 10.1016/j.msec.2017.03.060.
147. Whelan, I. T.; Moeendarbary, E.; Hoey, D. A.; Kelly, D. J., *Biofabrication* **2021,** *13* (3), 22. DOI 10.1088/1758-5090/ac04f7.

148. Neto, E.; Monteiro, A. C.; Leite Pereira, C.; Simões, M.; Conde, J. P.; Chu, V.; Sarmento, B.; Lamghari, M., *Advanced Healthcare Materials n/a* (n/a), 2102305. DOI https://doi.org/10.1002/adhm.202102305.
149. Galvan-Chacon, V. P.; Zampouka, A.; Hesse, B.; Bohner, M.; Habibovic, P.; Barata, D., *Adv Eng Mater*, 13. DOI 10.1002/adem.202101467.
150. Savoji, H.; Mohammadi, M. H.; Rafatian, N.; Toroghi, M. K.; Wang, E. Y.; Zhao, Y. M.; Korolj, A.; Ahadian, S.; Radisic, M., *Biomaterials* **2019,** *198*, 3-26. DOI 10.1016/j.biomaterials.2018.09.036.
151. Meyer, T.; Tiburcy, M.; Zimmermann, W. H., *Advanced Drug Delivery Reviews* **2019,** *140*, 93-100. DOI 10.1016/j.addr.2019.03.002.
152. Legant, W. R.; Pathak, A.; Yang, M. T.; Deshpande, V. S.; McMeeking, R. M.; Chen, C. S., *Proceedings of the National Academy of Sciences* **2009,** *106* (25), 10097-10102. DOI doi:10.1073/pnas.0900174106.
153. Agarwal, A.; Goss, J. A.; Cho, A.; McCain, M. L.; Parker, K. K., *Lab on a Chip* **2013,** *13* (18), 3599-3608. DOI 10.1039/c3lc50350j.
154. Lind, J. U.; Busbee, T. A.; Valentine, A. D.; Pasqualini, F. S.; Yuan, H. Y.; Yadid, M.; Park, S. J.; Kotikian, A.; Nesmith, A. P.; Campbell, P. H.; Vlassak, J. J.; Lewis, J. A.; Parker, K. K., *Nat. Mater.* **2017,** *16* (3), 303-+. DOI 10.1038/nmat4782.
155. Lind, J. U.; Yadid, M.; Perkins, I.; O'Connor, B. B.; Eweje, F.; Chantre, C. O.; Hemphill, M. A.; Yuan, H. Y.; Campbell, P. H.; Vlassak, J. J.; Parker, K. K., *Lab on a Chip* **2017,** *17* (21), 3692-3703. DOI 10.1039/c7lc00740j.
156. Ren, L.; Zhou, X. W.; Nasiri, R.; Fang, J.; Jiang, X.; Wang, C. R.; Qu, M. Y.; Ling, H. N.; Chen, Y. H.; Xue, Y. M.; Hartel, M. C.; Tebon, P.; Zhang, S. M.; Kim, H. J.; Yuan, X. C.; Shamloo, A.; Dokmeci, M. R.; Li, S.; Khademhosseini, A.; Ahadian, S.; Sun, W. J., *Small Methods* **2020,** *4* (10). DOI 10.1002/smtd.202000438.
157. Maoz, B. M.; Herland, A.; Henry, O. Y. F.; Leineweber, W. D.; Yadid, M.; Doyle, J.; Mannix, R.; Kujala, V. J.; FitzGerald, E. A.; Parker, K. K.; Ingber, D. E., *Lab on a Chip* **2017,** *17* (13), 2294-2302. DOI 10.1039/c7lc00412e.
158. Shang, Y. X.; Chen, Z. Y.; Zhang, Z. H.; Yang, Y. Z.; Zhao, Y. J., *Bio-Design and Manufacturing* **2020,** *3* (3), 266-280. DOI 10.1007/s42242-020-00073-9.
159. Zhang, Y. S.; Arneri, A.; Bersini, S.; Shin, S. R.; Zhu, K.; Goli-Malekabadi, Z.; Aleman, J.; Colosi, C.; Busignani, F.; Dell'Erba, V.; Bishop, C.; Shupe, T.; Demarchi, D.; Moretti, M.; Rasponi, M.; Dokmeci, M. R.; Atala, A.; Khademhosseini, A., *Biomaterials* **2016,** *110*, 45-59. DOI 10.1016/j.biomaterials.2016.09.003.
160. Abudupataer, M.; Zhu, S. C.; Yan, S. Q.; Xu, K. H.; Zhang, J. J.; Luo, S. M.; Ma, W. R.; Alam, M. F.; Tang, Y. Y.; Huang, H.; Chen, N.; Wang, L.; Yan, G. Q.; Li, J.; Lai, H.; Wang, C. S.; Zhu, K.; Zhang, W. J., *eLife* **2021,** *10*, 26. DOI 10.7554/eLife.69310; 10.7554/eLife.69310.sa1; 10.7554/eLife.69310.sa2.
161. Osaki, T.; Uzel, S. G. M.; Kamm, R. D., *Science Advances* **2018,** *4* (10), 15. DOI 10.1126/sciadv.aat5847.
162. Arjmand, B.; Hamidpour, S. K.; Rabbani, Z.; Tayanloo-Beik, A.; Rahim, F.; Aghayan, H. R.; Larijani, B., *Front. Neurol.* **2022,** *12*, 17. DOI 10.3389/fneur.2021.788462.
163. Fralish, Z.; Lotz, E. M.; Chavez, T.; Khodabukus, A.; Bursac, N., *Frontiers in Cell and Developmental Biology* **2021,** *09*, 35. DOI 10.3389/fcell.2021.764732.
164. De Gregorio, V.; Telesco, M.; Corrado, B.; Rosiello, V.; Urciuolo, F.; Netti, P. A.; Imparato, G., *Frontiers in Bioengineering and Biotechnology* **2020,** *8*, 19. DOI 10.3389/fbioe.2020.00163.
165. Foster, A. J.; Chouhan, B.; Regan, S. L.; Rollison, H.; Amberntsson, S.; Andersson, L. C.; Srivastava, A.; Darnell, M.; Cairns, J.; Lazic, S. E.; Jang, K. J.; Petropolis, D. B.; Kodella, K.; Rubins, J. E.; Williams, D.; Hamilton, G. A.; Ewart, L.; Morgan, P., *Arch. Toxicol.* **2019,** *93* (4), 1021-1037. DOI 10.1007/s00204-019-02427-4.
166. Christoffersson, J.; Aronsson, C.; Jury, M.; Selegard, R.; Aili, D.; Mandenius, C. F., *Biofabrication* **2019,** *11* (1), 13. DOI 10.1088/1758-5090/aaf657.
167. Tan, K.; Keegan, P.; Rogers, M.; Lu, M. J.; Gosset, J. R.; Charest, J.; Bale, S. S., *Lab on a Chip* **2019,** *19* (9), 1556-1566. DOI 10.1039/c8lc01262h.
168. Decsi, B.; Krammer, R.; Hegedus, K.; Ender, F.; Gyarmati, B.; Szilagyi, A.; Totos, R.; Katona, G.; Paizs, C.; Balogh, G. T.; Poppe, L.; Balogh-Weiser, D., *Micromachines* **2019,** *10* (10), 13. DOI 10.3390/mi10100668.
169. Deng, J.; Wei, W. B.; Chen, Z. Z.; Lin, B. C.; Zhao, W. J.; Luo, Y.; Zhang, X. L., *Micromachines* **2019,** *10* (10), 26. DOI 10.3390/mi10100676.

170. Theobald, J.; Maaty, M. A. A.; Kusterer, N.; Wetterauer, B.; Wink, M.; Cheng, X. L.; Wolfl, S., *Sci Rep* **2019,** *9*, 11. DOI 10.1038/s41598-019-40851-9.
171. Theobald, J.; Ghanem, A.; Wallisch, P.; Banaeiyan, A. A.; Andrade-Navarro, M. A.; Taskova, K.; Haltmeier, M.; Kurtz, A.; Becker, H.; Reuter, S.; Mrowka, R.; Cheng, X. L.; Wolfl, S., *Acs Biomaterials Science & Engineering* **2018,** *4* (1), 78-89. DOI 10.1021/acsbiomaterials.7b00417.
172. Lee, S. Y.; Sung, J. H., *Biotechnology and Bioengineering* **2018,** *115* (11), 2817-2827. DOI 10.1002/bit.26793.
173. Ong, L. J. Y.; Ching, T.; Chong, L. H.; Arora, S.; Li, H.; Hashimoto, M.; DasGupta, R.; Yuen, P. K.; Toh, Y. C., *Lab on a Chip* **2019,** *19* (13), 2178-2191. DOI 10.1039/c9lc00160c.
174. Vernetti, L.; Gough, A.; Baetz, N.; Blutt, S.; Broughman, J. R.; Brown, J. A.; Foulke-Abel, J.; Hasan, N.; In, J.; Kelly, E.; Kovbasnjuk, O.; Repper, J.; Senutovitch, N.; Stabb, J.; Yeung, C.; Zachos, N. C.; Donowitz, M.; Estes, M.; Himmelfarb, J.; Truskey, G.; Wikswo, J. P.; Taylor, D. L., *Sci Rep* **2017,** *7*. DOI 10.1038/srep42296.
175. Bavli, D.; Prill, S.; Ezra, E.; Levy, G.; Cohen, M.; Vinken, M.; Vanfleteren, J.; Jaeger, M.; Nahmias, Y., *Proc. Natl. Acad. Sci. U. S. A.* **2016,** *113* (16), E2231-E2240. DOI 10.1073/pnas.1522556113.
176. No, D. Y.; Lee, K. H.; Lee, J.; Lee, S. H., *Lab on a Chip* **2015,** *15* (19), 3822-3837. DOI 10.1039/c5lc00611b.
177. Bale, S. S.; Vernetti, L.; Senutovitch, N.; Jindal, R.; Hegde, M.; Gough, A.; McCarty, W. J.; Bakan, A.; Bhushan, A.; Shun, T. Y.; Golberg, I.; DeBiasio, R.; Usta, O. B.; Taylor, D. L.; Yarmush, M. L., *Exp. Biol. Med.* **2014,** *239* (9), 1180-1191. DOI 10.1177/1535370214531872.
178. Esch, M. B.; Mahler, G. J.; Stokor, T.; Shuler, M. L., *Lab on a Chip* **2014,** *14* (16), 3081-3092. DOI 10.1039/c4lc00371c.
179. Shintu, L.; Baudoin, R.; Navratil, V.; Prot, J. M.; Pontoizeau, C.; Defernez, M.; Blaise, B. J.; Domange, C.; Pery, A. R.; Toulhoat, P.; Legallais, C.; Brochot, C.; Leclerc, E.; Dumas, M. E., *Anal. Chem.* **2012,** *84* (4), 1840-1848. DOI 10.1021/ac2011075.
180. Zhang, C.; Zhao, Z. Q.; Rahim, N. A. A.; van Noort, D.; Yu, H., *Lab on a Chip* **2009,** *9* (22), 3185-3192. DOI 10.1039/b915147h.
181. Fabre, K.; Berridge, B.; Proctor, W. R.; Ralston, S.; Will, Y.; Baran, S. W.; Yoder, G.; Van Vleet, T. R., *Lab on a Chip* **2020,** *20* (6), 1049-1057. DOI 10.1039/c9lc01168d.
182. Phillips, J. A.; Grandhi, T. S. P.; Davis, M.; Gautier, J. C.; Hariparsad, N.; Keller, D.; Sura, R.; Van Vleet, T. R., *Lab on a Chip* **2020,** *20* (3), 468-476. DOI 10.1039/c9lc00925f.
183. Peel, S.; Corrigan, A. M.; Ehrhardt, B.; Jang, K. J.; Caetano-Pinto, P.; Boeckeler, M.; Rubins, J. E.; Kodella, K.; Petropolis, D. B.; Ronxhi, J.; Kulkarni, G.; Foster, A. J.; Williams, D.; Hamilton, G. A.; Ewart, L., *Lab on a Chip* **2019,** *19* (3), 410-421. DOI 10.1039/c8lc00829a.
184. Musah, S.; Dimitrakak, N.; Camacho, D. M.; Church, G. M.; Ingber, D. E., *Nature Protocols* **2018,** *13* (7), 1662-1685. DOI 10.1038/s41596-018-0007-8.
185. Musah, S.; Mammoto, A.; Ferrante, T. C.; Jeanty, S. S. F.; Hirano-Kobayashi, M.; Mammoto, T.; Roberts, K.; Chung, S.; Novak, R.; Ingram, M.; Fatanat-Didar, T.; Koshy, S.; Weaver, J. C.; Church, G. M.; Ingber, D. E., *Nat. Biomed. Eng* **2017,** *1* (5), 12. DOI 10.1038/s41551-017-0069.
186. Wilmer, M. J.; Ng, C. P.; Lanz, H. L.; Vulto, P.; Suter-Dick, L.; Masereeuw, R., *Trends Biotechnol.* **2016,** *34* (2), 156-170. DOI 10.1016/j.tibtech.2015.11.001.
187. Jang, K. J.; Mehr, A. P.; Hamilton, G. A.; McPartlin, L. A.; Chung, S. Y.; Suh, K. Y.; Ingber, D. E., *Integrative Biology* **2013,** *5* (9), 1119-1129. DOI 10.1039/c3ib40049b.
188. Miller, P. G.; Shuler, M. L., *Biotechnology and Bioengineering* **2016,** *113* (10), 2213-2227. DOI 10.1002/bit.25989.
189. Ware, B. R.; Khetani, S. R., *Trends Biotechnol* **2017,** *35* (2), 172-183. DOI 10.1016/j.tibtech.2016.08.001.
190. Jang, K. J.; Otieno, M. A.; Ronxhi, J.; Lim, H. K.; Ewart, L.; Kodella, K. R.; Petropolis, D. B.; Kulkarni, G.; Rubins, J. E.; Conegliano, D.; Nawroth, J.; Simic, D.; Lam, W.; Singer, M.; Barale, E.; Singh, B.; Sonee, M.; Streeter, A. J.; Manthey, C.; Jones, B.; Srivastava, A.; Andersson, L. C.; Williams, D.; Park, H.; Barrile, R.; Sliz, J.; Herland, A.; Haney, S.; Karalis, K.; Ingber, D. E.; Hamilton, G. A., *Sci Transl Med* **2019,** *11* (517). DOI 10.1126/scitranslmed.aax5516.
191. Gough, A.; Soto-Gutierrez, A.; Vernetti, L.; Ebrahimkhani, M. R.; Stern, A. M.; Taylor, D. L., *Nature reviews. Gastroenterology & hepatology* **2021,** *18* (4), 252-268. DOI 10.1038/s41575-020-00386-1.

192. Bircsak, K. M.; DeBiasio, R.; Miedel, M.; Alsebahi, A.; Reddinger, R.; Saleh, A.; Shun, T.; Vernetti, L. A.; Gough, A., *Toxicology* **2021,** *450*, 152667. DOI 10.1016/j.tox.2020.152667.
193. Tsamandouras, N.; Kostrzewski, T.; Stokes, C. L.; Griffith, L. G.; Hughes, D. J.; Cirit, M., *The Journal of pharmacology and experimental therapeutics* **2017,** *360* (1), 95-105. DOI 10.1124/jpet.116.237495.
194. Farooqi, H. M. U.; Kang, B.; Khalid, M. A. U.; Salih, A. R. C.; Hyun, K.; Park, S. H.; Huh, D.; Choi, K. H., *Nano convergence* **2021,** *8* (1), 3-3. DOI 10.1186/s40580-021-00253-y.
195. Li, Z.; Su, W.; Zhu, Y.; Tao, T.; Li, D.; Peng, X.; Qin, J., *Biomicrofluidics* **2017,** *11* (3), 034114. DOI 10.1063/1.4984768.
196. Cohen, A.; Ioannidis, K.; Ehrlich, A.; Regenbaum, S.; Cohen, M.; Ayyash, M.; Tikva, S. S.; Nahmias, Y., *Sci Transl Med* **2021,** *13* (582). DOI 10.1126/scitranslmed.abd6299.
197. Perazella, M. A., *Clinical journal of the American Society of Nephrology : CJASN* **2009,** *4* (7), 1275-83. DOI 10.2215/CJN.02050309.
198. Ashammakhi, N.; Wesseling-Perry, K.; Hasan, A.; Elkhammas, E.; Zhang, Y. S., *Kidney Int* **2018,** *94* (6), 1073-1086. DOI 10.1016/j.kint.2018.06.034.
199. Yin, L.; Du, G.; Zhang, B.; Zhang, H.; Yin, R.; Zhang, W.; Yang, S. M., *Sci Rep* **2020,** *10* (1), 6568. DOI 10.1038/s41598-020-63096-3.
200. Vormann, M. K.; Vriend, J.; Lanz, H. L.; Gijzen, L.; van den Heuvel, A.; Hutter, S.; Joore, J.; Trietsch, S. J.; Stuut, C.; Nieskens, T. T. G.; Peters, J. G. P.; Ramp, D.; Caj, M.; Russel, F. G. M.; Jacobsen, B.; Roth, A.; Lu, S.; Polli, J. W.; Naidoo, A. A.; Vulto, P.; Masereeuw, R.; Wilmer, M. J.; Suter-Dick, L., *Journal of pharmaceutical sciences* **2021,** *110* (4), 1601-1614. DOI 10.1016/j.xphs.2021.01.028.
201. Li, X.; Tian, T., *Frontiers in pharmacology* **2018,** *9*, 1067. DOI 10.3389/fphar.2018.01067.
202. de Haan, P.; Santbergen, M. J. C.; van der Zande, M.; Bouwmeester, H.; Nielen, M. W. F.; Verpoorte, E., *Sci Rep* **2021,** *11* (1), 4920. DOI 10.1038/s41598-021-84187-9.
203. Miller, P. G.; Chen, C. Y.; Wang, Y. I.; Gao, E.; Shuler, M. L., *Biotechnology and Bioengineering* **2020,** *117* (2), 486-497. DOI 10.1002/bit.27188.
204. Li, Z.; Li, D.; Guo, Y.; Wang, Y.; Su, W., *Biotechnology Letters* **2021,** *43* (2), 383-392. DOI 10.1007/s10529-020-03043-4.
205. Yin, F. C.; Zhang, X.; Wang, L.; Wang, Y. Q.; Zhu, Y. J.; Li, Z. Y.; Tao, T. T.; Chen, W. W.; Yu, H.; Qin, J. H., *Lab on a Chip* **2021,** *21* (3), 571-581. DOI 10.1039/d0lc00921k.
206. Liu, W. W.; Song, J.; Du, X. H.; Zhou, Y.; Li, Y.; Li, R.; Lyu, L.; He, Y. T.; Hao, J. X.; Ben, J.; Wang, W.; Shi, H. B.; Wang, Q., *Acta Biomaterialia* **2019,** *91*, 195-208. DOI 10.1016/j.actbio.2019.04.053.
207. Khot, M. I.; Levenstein, M. A.; de Boer, G. N.; Armstrong, G.; Maisey, T.; Svavarsdottir, H. S.; Andrew, H.; Perry, S. L.; Kapur, N.; Jayne, D. G., *Sci Rep* **2020,** *10* (1). DOI 10.1038/s41598-020-72952-1.
208. Ai, X. N.; Wu, Y.; Lu, W. B.; Zhang, X. R.; Zhao, L.; Tu, P. F.; Wang, K. W.; Jiang, Y., *Advanced Science* **2020,** *7* (11). DOI 10.1002/advs.202000111.
209. Ai, X. N.; Zhao, L.; Lu, Y. Y.; Hou, Y.; Lv, T.; Jiang, Y.; Tu, P. F.; Guo, X. Y., *Anal. Chem.* **2020,** *92* (17), 11696-11704. DOI 10.1021/acs.analchem.0c01590.
210. Mondal, S.; Hegarty, E.; Martin, C.; Gokce, S. K.; Ghorashian, N.; Ben-Yakar, A., *Nature Communications* **2016,** *7*. DOI 10.1038/ncomms13023.
211. Chung, K.; Zhan, M.; Srinivasan, J.; Sternberg, P. W.; Gong, E.; Schroeder, F. C.; Lu, H., *Lab on a Chip* **2011,** *11* (21), 3689-3697. DOI 10.1039/c1lc20400a.
212. Popova, A. A.; Marcato, D.; Peravali, R.; Wehl, I.; Schepers, U.; Levkin, P. A., *Adv. Funct. Mater.* **2018,** *28* (3). DOI 10.1002/adfm.201703486.
213. Fan, Y. T.; Nguyen, D. T.; Akay, Y.; Xu, F.; Akay, M., *Sci Rep* **2016,** *6*. DOI 10.1038/srep25062.
214. Yang, W. G.; Cai, S. X.; Yuan, Z.; Lai, Y. B.; Yu, H. B.; Wang, Y. C.; Liu, L. Q., *Materials & Design* **2019,** *183*. DOI 10.1016/j.matdes.2019.108182.
215. Mazzocchi, A. R.; Rajan, S. A. P.; Votanopoulos, K. I.; Hall, A. R.; Skardal, A., *Sci Rep* **2018,** *8*. DOI 10.1038/s41598-018-21200-8.
216. Liu, W. M.; Sun, M. L.; Han, K.; Wang, J. Y., *Anal. Chem.* **2019,** *91* (21), 13601-13610. DOI 10.1021/acs.analchem.9b02768.
217. Lee, J. M.; Choi, J. W.; Ahrberg, C. D.; Choi, H. W.; Ha, J. H.; Mun, S. G.; Mo, S. J.; Chung, B. G., *Microsystems & Nanoengineering* **2020,** *6* (1). DOI 10.1038/s41378-020-0167-x.

218. Kwak, B.; Lee, Y.; Lee, J.; Lee, S.; Lim, J., *Journal of Controlled Release* **2018,** *275*, 201-207. DOI 10.1016/j.jconrel.2018.02.029.
219. Sabhachandani, P.; Motwani, V.; Cohen, N.; Sarkar, S.; Torchilin, V.; Konry, T., *Lab on a Chip* **2016,** *16* (3), 497-505. DOI 10.1039/c5lc01139f.
220. Jang, M.; Koh, I.; Lee, S. J.; Cheong, J. H.; Kim, P., *Scientific Reports* **2017,** *7*. DOI 10.1038/srep41541.
221. Wu, Z. H.; Gong, Z. Y.; Ao, Z.; Xu, J. H.; Cai, H. W.; Muhsen, M.; Heaps, S.; Bondesson, M.; Guo, S. S.; Guo, F., *Acs Applied Bio Materials* **2020,** *3* (9), 6273-6283. DOI 10.1021/acsabm.0c00768.
222. Karamikamkar, S.; Behzadfar, E.; Cheung, K. C., *Biomedical Microdevices* **2018,** *20* (2). DOI 10.1007/s10544-018-0260-1.
223. Sun, Q.; Tan, S. H.; Chen, Q. S.; Ran, R.; Hui, Y.; Chen, D.; Zhao, C. X., *Acs Biomaterials Science & Engineering* **2018,** *4* (12), 4425-4433. DOI 10.1021/acsbiomaterials.8b00904.
224. Nagrath, S.; Sequist, L. V.; Maheswaran, S.; Bell, D. W.; Irimia, D.; Ulkus, L.; Smith, M. R.; Kwak, E. L.; Digumarthy, S.; Muzikansky, A.; Ryan, P.; Balis, U. J.; Tompkins, R. G.; Haber, D. A.; Toner, M., *Nature* **2007,** *450* (7173), 1235-1239. DOI http://www.nature.com/nature/journal/v450/n7173/suppinfo/nature06385_S1.html.
225. Chen, Y.; Li, P.; Huang, P.-H.; Xie, Y.; Mai, J. D.; Wang, L.; Nam-Trung, N.; Huang, T. J., *Lab on a Chip* **2014,** *14* (4), 626-645. DOI 10.1039/c3lc90136j.
226. Wu, M. X.; Ouyang, Y. S.; Wang, Z. Y.; Zhang, R.; Huang, P. H.; Chen, C. Y.; Li, H.; Li, P.; Quinn, D.; Dao, M.; Suresh, S.; Sadovsky, Y.; Huang, T. J., *Proc. Natl. Acad. Sci. U. S. A.* **2017,** *114* (40), 10584-10589. DOI 10.1073/pnas.1709210114.
227. Contreras-Naranjo, J. C.; Wu, H. J.; Ugaz, V. M., *Lab on a Chip* **2017,** *17* (21), 3558-3577. DOI 10.1039/c7lc00592j.
228. Zizzari, A.; Bianco, M.; Carbone, L.; Perrone, E.; Amato, F.; Maruccio, G.; Rendina, F.; Arima, V., *Materials* **2017,** *10* (12). DOI 10.3390/ma10121411.
229. Shah, R. K.; Shum, H. C.; Rowat, A. C.; Lee, D.; Agresti, J. J.; Utada, A. S.; Chu, L. Y.; Kim, J. W.; Fernandez-Nieves, A.; Martinez, C. J.; Weitz, D. A., *Mater Today* **2008,** *11* (4), 18-27. DOI 10.1016/s1369-7021(08)70053-1.
230. Shum, H. C.; Lee, D.; Yoon, I.; Kodger, T.; Weitz, D. A., *Langmuir* **2008,** *24* (15), 7651-7653. DOI 10.1021/la801833a.
231. Young, A. T.; Rivera, K. R.; Erb, P. D.; Daniele, M. A., *Acs Sensors* **2019,** *4* (6), 1454-1464. DOI 10.1021/acssensors.8b01549.
232. Li, X.; Tian, T., *Analytical Methods* **2018,** *10* (26), 3122-3130. DOI 10.1039/c8ay00970h.
233. Soucy, J. R.; Bindas, A. J.; Koppes, A. N.; Koppes, R. A., *iScience* **2019,** *21*, 521-548. DOI 10.1016/j.isci.2019.10.052.
234. Arndt, S.; Seebach, J.; Psathaki, K.; Galla, H. J.; Wegener, J., *Biosens. Bioelectron.* **2004,** *19* (6), 583-594. DOI 10.1016/s0956-5663(03)00269-0.
235. Nguyen, H. H.; Park, J.; Kang, S.; Kim, M., *Sensors* **2015,** *15* (5), 10481-10510. DOI 10.3390/s150510481.
236. Haes, A. J.; Hall, W. P.; Chang, L.; Klein, W. L.; Van Duyne, R. P., *Nano Lett.* **2004,** *4* (6), 1029-1034. DOI 10.1021/nl049670j.
237. Baselt, D. R.; Lee, G. U.; Natesan, M.; Metzger, S. W.; Sheehan, P. E.; Colton, R. J., *Biosens. Bioelectron.* **1998,** *13* (7-8), 731-739.
238. Rizzato, S.; Leo, A.; Monteduro, A. G.; Chiriacò, M. S.; Primiceri, E.; Sirsi, F.; Milone, A.; Maruccio, G., *Micromachines* **2020,** *11* (5), 491. DOI 10.3390/mi11050491.
239. Atkuri, K. R.; Herzenberg, L. A.; Niemi, A.-K.; Cowan, T.; Herzenberg, L. A., *Proceedings of the National Academy of Sciences* **2007,** *104* (11), 4547-4552. DOI doi:10.1073/pnas.0611732104.
240. Zeitouni, N. E.; Chotikatum, S.; von Köckritz-Blickwede, M.; Naim, H. Y., *Molecular and Cellular Pediatrics* **2016,** *3* (1), 14. DOI 10.1186/s40348-016-0041-y.
241. Moya, A.; Ortega-Ribera, M.; Guimerà, X.; Sowade, E.; Zea, M.; Illa, X.; Ramon, E.; Villa, R.; Gracia-Sancho, J.; Gabriel, G., *Lab on a Chip* **2018,** *18* (14), 2023-2035. DOI 10.1039/C8LC00456K.
242. Misun, P. M.; Rothe, J.; Schmid, Y. R. F.; Hierlemann, A.; Frey, O., *Microsystems & Nanoengineering* **2016,** *2* (1), 16022. DOI 10.1038/micronano.2016.22.
243. Giaever, I.; Keese, C. R., *Nature* **1993,** *366* (6455), 591-592. DOI 10.1038/366591a0.
244. Wegener, J.; Keese, C. R.; Giaever, I., *Experimental cell research* **2000,** *259* (1), 158-166.

245. Bagnaninchi, P. O.; Drummond, N., *Proc. Natl. Acad. Sci. U. S. A.* **2011,** *108* (16), 6462-6467. DOI 10.1073/pnas.1018260108.
246. Han, A.; Yang, L.; Frazier, A. B., *Clin Cancer Res* **2007,** *13* (1), 139-143. DOI 10.1158/1078-0432.ccr-06-1346.
247. Swami, P.; Sharma, A.; Anand, S.; Gupta, S., *Biosens. Bioelectron.* **2021,** *182*, 113190. DOI 10.1016/j.bios.2021.113190.
248. Rodriguez, L. G.; Wu, X.; Guan, J.-L., Wound-healing assay. In *Cell Migration*, Springer: 2005; pp 23-29.
249. Primiceri, E.; Chiriacò, M. S.; Dioguardi, F.; Monteduro, A. G.; D'Amone, E.; Rinaldi, R.; Giannelli, G.; Maruccio, G., *Lab on a Chip* **2011,** *11* (23), 4081-4086. DOI 10.1039/c1lc20540d.
250. Keese, C. R.; Bhawe, K.; Wegener, J.; Giaever, I., *Biotechniques* **2002,** *33* (4), 842-850. DOI 10.2144/02334rr01.
251. Xiao, C.; Luong, J. H., *Biotechnology progress* **2003,** *19* (3), 1000-1005.
252. Primiceri, E.; Chiriacò, M. S.; D'Amone, E.; Urso, E.; Ionescu, R. E.; Rizzello, A.; Maffia, M.; Cingolani, R.; Rinaldi, R.; Maruccio, G., *Biosens. Bioelectron.* **2010,** *25* (12), 2711-2716. DOI 10.1016/j.bios.2010.04.032.
253. Kustermann, S.; Boess, F.; Buness, A.; Schmitz, M.; Watzele, M.; Weiser, T.; Singer, T.; Suter, L.; Roth, A., *Toxicology in Vitro* **2013,** *27* (5), 1589-1595. DOI 10.1016/j.tiv.2012.08.019.
254. Ramis, G.; Martinez-Alarcon, L.; Quereda, J. J.; Mendonca, L.; Majado, M. J.; Gomez-Coelho, K.; Mrowiec, A.; Herrero-Medrano, J. M.; Abellaneda, J. M.; Pallares, F. J.; Rios, A.; Ramirez, P.; Munoz, A., *Biomedical Microdevices* **2013,** *15* (6), 985-995. DOI 10.1007/s10544-013-9790-8.
255. Katz, E.; Willner, I., *Electroanalysis* **2003,** *15* (11), 913-947.
256. Chiriacò, M. S.; de Feo, F.; Primiceri, E.; Monteduro, A. G.; de Benedetto, G. E.; Pennetta, A.; Rinaldi, R.; Maruccio, G., *Talanta* **2015,** *142*, 57-63. DOI 10.1016/j.talanta.2015.04.040.
257. Chiriacò, M. S.; Primiceri, E.; De Feo, F.; Montanaro, A.; Monteduro, A. G.; Tinelli, A.; Megha, M.; Carati, D.; Maruccio, G., *Biosensors and Bioelectronics* **2016,** *79*, 9-14. DOI 10.1016/j.bios.2015.11.100.
258. Chiriacò, M. S.; Primiceri, E.; Monteduro, A. G.; Bove, A.; Leporatti, S.; Capello, M.; Ferri-Borgogno, S.; Rinaldi, R.; Novelli, F.; Maruccio, G., *Lab on a Chip* **2013,** *13* (4), 730-734. DOI 10.1039/c2lc41127j.
259. Buja, I.; Sabella, E.; Monteduro, A. G.; Rizzato, S.; Bellis, L. D.; Elicio, V.; Formica, L.; Luvisi, A.; Maruccio, G., *Biosensors* **2022,** *12* (3), 147.
260. Piccinno, E.; Monteduro, A. G.; Dituri, F.; Rizzato, S.; Giannelli, G.; Maruccio, G., *International Journal of Molecular Sciences* **2021,** *22* (23), 13090. DOI 10.3390/ijms222313090.
261. Ortega, M. A.; Fernández-Garibay, X.; Castaño, A. G.; De Chiara, F.; Hernández-Albors, A.; Balaguer-Trias, J.; Ramón-Azcón, J., *Lab on a Chip* **2019,** *19* (15), 2568-2580. DOI 10.1039/C9LC00285E.
262. Zhang, Y. S.; Aleman, J.; Shin, S. R.; Kilic, T., **2017,** *114* (12), E2293-e2302. DOI 10.1073/pnas.1612906114.
263. Schmid, Y. R. F.; Bürgel, S. C.; Misun, P. M.; Hierlemann, A.; Frey, O., *ACS Sensors* **2016,** *1* (8), 1028-1035. DOI 10.1021/acssensors.6b00272.
264. Wu, Q.; Wei, X.; Pan, Y.; Zou, Y.; Hu, N.; Wang, P., *Biomedical Microdevices* **2018,** *20* (4), 82. DOI 10.1007/s10544-018-0329-x.
265. Kavand, H.; Nasiri, R.; Herland, A., *Advanced Materials n/a* (n/a), 2107876. DOI https://doi.org/10.1002/adma.202107876.
266. Colombelli, A.; Primiceri, E.; Rizzato, S.; Monteduro, A. G.; Maruccio, G.; Rella, R.; Manera, M. G., *Chemosensors* **2021,** *9* (1), 10.
267. Rizzato, S.; Primiceri, E.; Monteduro, A. G.; Colombelli, A.; Leo, A.; Manera, M. G.; Rella, R.; Maruccio, G., *Beilstein Journal of Nanotechnology* **2018,** *9*, 1582-1593. DOI 10.3762/bjnano.9.150.
268. Li, X.; Soler, M.; Belushkin, A.; Yesilköy, F.; Altug, H., *Optofluidic nanoplasmonic biosensor for label-free live cell analysis in real time*. SPIE: **2018**; Vol. 10509.
269. Zhu, Y. J.; Sun, L. Y.; Wang, Y.; Cai, L. J.; Zhang, Z. H.; Shang, Y. X.; Zhao, Y. J., *Adv. Mater.*, 10. DOI 10.1002/adma.202108972.
270. Feng, J.; Zheng, Y.; Bhusari, S.; Villiou, M.; Pearson, S.; del Campo, A., *Advanced Functional Materials* **2020,** *30* (45), 2004327. DOI https://doi.org/10.1002/adfm.202004327.
271. Debreczeni, M. L.; Szekacs, I.; Kovacs, B.; Saftics, A.; Kurunczi, S.; Gál, P.; Dobó, J.; Cervenak, L.; Horvath, R., *Scientific Reports* **2020,** *10* (1), 3303. DOI 10.1038/s41598-020-60158-4.

272. Shaegh, S. A. M.; Ferrari, F. D.; Zhang, Y. S.; Nabavinia, M.; Mohammad, N. B.; Ryan, J.; Pourmand, A.; Laukaitis, E.; Sadeghian, R. B.; Nadhman, A.; Shin, S. R.; Nezhad, A. S.; Khademhosseini, A.; Dokmeci, M. R., *Biomicrofluidics* **2016,** *10* (4), 044111. DOI 10.1063/1.4955155.
273. Khalid, M. A. U.; Kim, Y. S.; Ali, M.; Lee, B. G.; Cho, Y.-J.; Choi, K. H., *Biochemical Engineering Journal* **2020,** *155*, 107469. DOI https://doi.org/10.1016/j.bej.2019.107469.
274. Ferrari, E.; Palma, C., **2020,** *10* (9). DOI 10.3390/bios10090110.
275. Sidorov, V. Y.; Samson, P. C.; Sidorova, T. N.; Davidson, J. M.; Lim, C. C.; Wikswo, J. P., *Acta Biomaterialia* **2017,** *48*, 68-78. DOI https://doi.org/10.1016/j.actbio.2016.11.009.
276. Chiriacò, M. S.; Rizzato, S.; Primiceri, E.; Spagnolo, S.; Monteduro, A. G.; Ferrara, F.; Maruccio, G., *Microelectron. Eng.* **2018,** *202*, 31-36. DOI 10.1016/j.mee.2018.10.008.
277. Rizzato, S.; Scigliuzzo, M.; Chiriacò, M. S.; Scarlino, P.; Monteduro, A. G.; Maruccio, C.; Tasco, V.; Maruccio, G., *Journal of Micromechanics and Microengineering* **2017,** *27* (12), 125002. DOI 10.1088/1361-6439/aa8186.
278. Maruccio, C.; Scigliuzzo, M.; Rizzato, S.; Scarlino, P.; Quaranta, G.; Chiriaco, M. S.; Monteduro, A. G.; Maruccio, G., *Journal of Intelligent Material Systems and Structures* **2018**, 1045389X18803461. DOI 10.1177/1045389X18803461.
279. Wang, T.; Green, R.; Nair, R. R.; Howell, M.; Mohapatra, S.; Guldiken, R.; Mohapatra, S. S., *Sensors (Basel, Switzerland)* **2015,** *15* (12), 32045-32055. DOI 10.3390/s151229909.
280. Wang, T.; Green, R.; Howell, M.; Martinez, T.; Dutta, R.; Mohapatra, S.; Mohapatra, S. S., *Nanomedicine: Nanotechnology, Biology and Medicine* **2020,** *30*, 102294. DOI https://doi.org/10.1016/j.nano.2020.102294.
281. Liu, J.; Li, S.; Bhethanabotla, V. R., *ACS Sensors* **2018,** *3* (1), 222-229. DOI 10.1021/acssensors.7b00876.
282. Milone, A.; Monteduro, A. G.; Rizzato, S.; Leo, A.; Di Natale, C.; Kim, S. S.; Maruccio, G., *Advanced Sustainable Systems n/a* (n/a), 2200083. DOI https://doi.org/10.1002/adsu.202200083.
283. Serasanambati, M.; Broza, Y. Y.; Marmur, A.; Haick, H., *iScience* **2019,** *11*, 178-188. DOI 10.1016/j.isci.2018.12.008.
284. Dummer, J.; Storer, M.; Swanney, M.; McEwan, M.; Scott-Thomas, A.; Bhandari, S.; Chambers, S.; Dweik, R.; Epton, M., *TrAC Trends in Analytical Chemistry* **2011,** *30* (7), 960-967. DOI https://doi.org/10.1016/j.trac.2011.03.011.
285. Phillips, M.; Basa-Dalay, V.; Blais, J.; Bothamley, G.; Chaturvedi, A.; Modi, K. D.; Pandya, M.; Natividad, M. P.; Patel, U.; Ramraje, N. N.; Schmitt, P.; Udwadia, Z. F., *Tuberculosis (Edinb)* **2012,** *92* (4), 314-20. DOI 10.1016/j.tube.2012.04.002.
286. Einoch Amor, R.; Nakhleh, M. K.; Barash, O.; Haick, H., *European Respiratory Review* **2019,** *28* (152), 190002. DOI 10.1183/16000617.0002-2019.
287. Di Natale, C.; Macagnano, A.; Martinelli, E.; Paolesse, R.; D'Arcangelo, G.; Roscioni, C.; Finazzi-Agro, A.; D'Amico, A., *Biosens. Bioelectron.* **2003,** *18* (10), 1209-1218. DOI 10.1016/s0956-5663(03)00086-1.
288. Murdocca, M.; Torino, F.; Pucci, S.; Costantini, M.; Capuano, R.; Greggi, C.; Polidoro, C.; Somma, G.; Pasqualetti, V.; Ketchanji Mougang, Y.; Catini, A.; Simone, G.; Paolesse, R.; Orlandi, A.; Mauriello, A.; Roselli, M.; Magrini, A.; Novelli, G.; Di Natale, C.; Sangiuolo, F. C., *Cancers* **2021,** *13* (16), 4213.
289. Mougang, Y. K.; Di Zazzo, L.; Minieri, M.; Capuano, R.; Catini, A.; Legramante, J. M.; Paolesse, R.; Bernardini, S.; Di Natale, C., *iScience* **2021,** *24* (8), 102851. DOI https://doi.org/10.1016/j.isci.2021.102851.
290. Mermoud, Y.; Felder, M.; Stucki, J. D.; Stucki, A. O.; Guenat, O. T., *Sensors and Actuators B: Chemical* **2018,** *255*, 3647-3653. DOI https://doi.org/10.1016/j.snb.2017.09.192.
291. Ding, C.; Chen, X.; Kang, Q.; Yan, X., *Frontiers in bioengineering and biotechnology* **2020,** *8*, 823-823. DOI 10.3389/fbioe.2020.00823.
292. Ning, R.; Wang, F.; Lin, L., *TrAC Trends in Analytical Chemistry* **2016,** *80*, 255-265. DOI https://doi.org/10.1016/j.trac.2015.08.017.
293. Guttenplan, A. P. M.; Tahmasebi Birgani, Z.; Giselbrecht, S.; Truckenmüller, R. K.; Habibović, P., *Advanced Healthcare Materials* **2021,** *10* (14), 2100371. DOI https://doi.org/10.1002/adhm.202100371.
294. Piruska, A.; Nikcevic, I.; Lee, S. H.; Ahn, C.; Heineman, W. R.; Limbach, P. A.; Seliskar, C. J., *Lab on a Chip* **2005,** *5* (12), 1348-1354.

295. Amani Wan Salim, W. W.; H Park, J.; Ul Haque, A.; Marshall Porterfield, D., *Recent Patents on Space Technology* **2013,** *3* (1), 24-39.
296. Hassan, S.; Heinrich, M.; Cecen, B.; Prakash, J.; Zhang, Y. S., 26 - Biomaterials for on-chip organ systems. In *Biomaterials for Organ and Tissue Regeneration*, Vrana, N. E.; Knopf-Marques, H.; Barthes, J., Eds. Woodhead Publishing: 2020; pp 669-707.
297. Huh, D.; Matthews, B. D.; Mammoto, A.; Montoya-Zavala, M.; Hsin, H. Y.; Ingber, D. E., *Science* **2010,** *328* (5986), 1662-8. DOI 10.1126/science.1188302.
298. Huh, D. D., *Ann Am Thorac Soc* **2015,** *12 Suppl 1* (Suppl 1), S42-4. DOI 10.1513/AnnalsATS.201410-442MG.
299. Sorba, F.; Poulin, A.; Ischer, R.; Shea, H.; Martin-Olmos, C., *Lab Chip* **2019,** *19* (12), 2138-2146. DOI 10.1039/c9lc00075e.
300. Lee, J. M.; Park, D. Y.; Yang, L., **2018,** *8* (1), 17145. DOI 10.1038/s41598-018-35216-7.
301. Kung, Y.-C.; Huang, K.-W.; Fan, Y.-J.; Chiou, P.-Y., *Lab on a Chip* **2015,** *15* (8), 1861-1868. DOI 10.1039/C4LC01211A.
302. Cheng, S.-B.; Xie, M.; Xu, J.-Q.; Wang, J.; Lv, S.-W.; Guo, S.; Shu, Y.; Wang, M.; Dong, W.-G.; Huang, W.-H., *Analytical Chemistry* **2016,** *88* (13), 6773-6780. DOI 10.1021/acs.analchem.6b01130.
303. Cosson, S.; Aeberli, L. G.; Brandenberg, N.; Lutolf, M. P., *Lab on a Chip* **2015,** *15* (1), 72-76. DOI 10.1039/C4LC00848K.
304. Bhattacharjee, N.; Parra-Cabrera, C.; Kim, Y. T.; Kuo, A. P.; Folch, A., *Advanced Materials* **2018,** *30* (22), 1800001. DOI https://doi.org/10.1002/adma.201800001.
305. Toepke, M. W.; Beebe, D. J., *Lab on a Chip* **2006,** *6* (12), 1484-1486. DOI 10.1039/B612140C.
306. Khetani, S.; Yong, K. W.; Guan, K.; Singh, A.; Phani, A.; Kollath, V. O.; Kim, S.; Karan, K.; Sen, A.; Sanati-Nezhad, A., *Applied Materials Today* **2020,** *20*, 100721. DOI https://doi.org/10.1016/j.apmt.2020.100721.
307. Carter, S.-S. D.; Atif, A.-R.; Kadekar, S.; Lanekoff, I.; Engqvist, H.; Varghese, O. P.; Tenje, M.; Mestres, G., *Organs-on-a-Chip* **2020,** *2*, 100004. DOI https://doi.org/10.1016/j.ooc.2020.100004.
308. Becker, H.; Gärtner, C., *Analytical and Bioanalytical Chemistry* **2008,** *390* (1), 89-111. DOI 10.1007/s00216-007-1692-2.
309. Ren, K.; Zhou, J.; Wu, H., *Accounts of Chemical Research* **2013,** *46* (11), 2396-2406. DOI 10.1021/ar300314s.
310. van Midwoud, P. M.; Janse, A.; Merema, M. T.; Groothuis, G. M.; Verpoorte, E., *Anal Chem* **2012,** *84* (9), 3938-44. DOI 10.1021/ac300771z.
311. Lee, S.; Lim, J.; Yu, J.; Ahn, J.; Lee, Y.; Jeon, N. L., *Lab on a Chip* **2019,** *19* (12), 2071-2080. DOI 10.1039/C9LC00148D.
312. Shah, P.; Fritz, J. V.; Glaab, E.; Desai, M. S.; Greenhalgh, K.; Frachet, A.; Niegowska, M.; Estes, M.; Jäger, C.; Seguin-Devaux, C.; Zenhausern, F.; Wilmes, P., *Nature communications* **2016,** *7* (1), 11535. DOI 10.1038/ncomms11535.
313. Piccin, E.; Coltro, W. K. T.; Fracassi da Silva, J. A.; Neto, S. C.; Mazo, L. H.; Carrilho, E., *Journal of Chromatography A* **2007,** *1173* (1), 151-158. DOI https://doi.org/10.1016/j.chroma.2007.09.081.
314. Pourmand, A.; Shaegh, S. A. M.; Ghavifekr, H. B.; Najafi Aghdam, E.; Dokmeci, M. R.; Khademhosseini, A.; Zhang, Y. S., *Sensors and Actuators B: Chemical* **2018,** *262*, 625-636. DOI https://doi.org/10.1016/j.snb.2017.12.132.
315. Chen, X.; Shen, J.; Zhou, M., *Journal of Micromechanics and Microengineering* **2016,** *26* (10), 107001. DOI 10.1088/0960-1317/26/10/107001.
316. Miller, P. G.; Shuler, M. L., *Biotechnol Bioeng* **2016,** *113* (10), 2213-27. DOI 10.1002/bit.25989.
317. Rogers, C. I.; Oxborrow, J. B.; Anderson, R. R.; Tsai, L.-F.; Nordin, G. P.; Woolley, A. T., *Sensors and Actuators B: Chemical* **2014,** *191*, 438-444. DOI https://doi.org/10.1016/j.snb.2013.10.008.
318. Rogers, C. I.; Pagaduan, J. V.; Nordin, G. P.; Woolley, A. T., *Analytical Chemistry* **2011,** *83* (16), 6418-6425. DOI 10.1021/ac201539h.
319. Nargang, T. M.; Brockmann, L.; Nikolov, P. M.; Schild, D.; Helmer, D.; Keller, N.; Sachsenheimer, K.; Wilhelm, E.; Pires, L.; Dirschka, M.; Kolew, A.; Schneider, M.; Worgull, M.; Giselbrecht, S.; Neumann, C.; Rapp, B. E., *Lab on a Chip* **2014,** *14* (15), 2698-2708. DOI 10.1039/C4LC00045E.

320. Kotz, F.; Arnold, K.; Wagner, S.; Bauer, W.; Keller, N.; Nargang, T. M.; Helmer, D.; Rapp, B. E., *Advanced Engineering Materials* **2018,** *20* (2), 1700699. DOI https://doi.org/10.1002/adem.201700699.
321. Boyce, M. W.; Kenney, R. M.; Truong, A. S.; Lockett, M. R., *Analytical and Bioanalytical Chemistry* **2016,** *408* (11), 2985-2992. DOI 10.1007/s00216-015-9189-x.
322. Mosadegh, B.; Lockett, M. R.; Minn, K. T.; Simon, K. A.; Gilbert, K.; Hillier, S.; Newsome, D.; Li, H.; Hall, A. B.; Boucher, D. M.; Eustace, B. K.; Whitesides, G. M., *Biomaterials* **2015,** *52*, 262-71. DOI 10.1016/j.biomaterials.2015.02.012.
323. Young, M.; Rodenhizer, D.; Dean, T.; D'Arcangelo, E.; Xu, B.; Ailles, L.; McGuigan, A. P., *Biomaterials* **2018,** *164*, 54-69. DOI 10.1016/j.biomaterials.2018.01.038.
324. Rodenhizer, D.; Gaude, E.; Cojocari, D.; Mahadevan, R.; Frezza, C.; Wouters, B. G.; McGuigan, A. P., *Nature Materials* **2016,** *15* (2), 227-234. DOI 10.1038/nmat4482.
325. Maitra, J.; Shukla, V. K., *Am. J. Polym. Sci* **2014,** *4* (2), 25-31.
326. Natividad-Diaz, S. L.; Browne, S.; Jha, A. K.; Ma, Z.; Hossainy, S.; Kurokawa, Y. K.; George, S. C.; Healy, K. E., *Biomaterials* **2019,** *194*, 73-83. DOI 10.1016/j.biomaterials.2018.11.032.
327. Lugo-Cintrón, K. M.; Ayuso, J. M.; White, B. R.; Harari, P. M.; Ponik, S. M.; Beebe, D. J.; Gong, M. M.; Virumbrales-Muñoz, M., *Lab on a Chip* **2020,** *20* (9), 1586-1600. DOI 10.1039/D0LC00099J.
328. Movilla, N.; Borau, C.; Valero, C.; García-Aznar, J. M., *Bone* **2018,** *107*, 10-17. DOI 10.1016/j.bone.2017.10.025.
329. Cabodi, M.; Choi, N. W.; Gleghorn, J. P.; Lee, C. S. D.; Bonassar, L. J.; Stroock, A. D., *Journal of the American Chemical Society* **2005,** *127* (40), 13788-13789. DOI 10.1021/ja054820t.
330. Liu, J.; Zheng, H.; Poh, P. S.; Machens, H. G.; Schilling, A. F., *Int J Mol Sci* **2015,** *16* (7), 15997-6016. DOI 10.3390/ijms160715997.
331. Tasoglu, S.; Demirci, U., *Trends in Biotechnology* **2013,** *31* (1), 10-19. DOI https://doi.org/10.1016/j.tibtech.2012.10.005.
332. Elomaa, L.; Yang, Y. P., *Tissue Eng Part B Rev* **2017,** *23* (5), 436-450. DOI 10.1089/ten.TEB.2016.0348.
333. Fedorovich, N. E.; Schuurman, W.; Wijnberg, H. M.; Prins, H.-J.; Van Weeren, P. R.; Malda, J.; Alblas, J.; Dhert, W. J., *Tissue Engineering Part C: Methods* **2012,** *18* (1), 33-44.
334. Roseti, L.; Parisi, V.; Petretta, M.; Cavallo, C.; Desando, G.; Bartolotti, I.; Grigolo, B., *Materials Science and Engineering: C* **2017,** *78*, 1246-1262. DOI https://doi.org/10.1016/j.msec.2017.05.017.
335. Hoang, P.; Ma, Z., *Acta Biomater* **2021,** *132*, 23-36. DOI 10.1016/j.actbio.2021.01.026.
336. Choi, N. W.; Cabodi, M.; Held, B.; Gleghorn, J. P.; Bonassar, L. J.; Stroock, A. D., *Nat Mater* **2007,** *6* (11), 908-15. DOI 10.1038/nmat2022.
337. Jusoh, N.; Oh, S.; Kim, S.; Kim, J.; Jeon, N. L., *Lab on a Chip* **2015,** *15* (20), 3984-3988. DOI 10.1039/C5LC00698H.
338. Hao, S.; Ha, L.; Cheng, G.; Wan, Y.; Xia, Y.; Sosnoski, D. M.; Mastro, A. M.; Zheng, S. Y., **2018,** *14* (12), e1702787. DOI 10.1002/smll.201702787.
339. Geraili, A.; Jafari, P.; Hassani, M. S.; Araghi, B. H.; Mohammadi, M. H.; Ghafari, A. M.; Tamrin, S. H.; Modarres, H. P.; Kolahchi, A. R.; Ahadian, S.; Sanati-Nezhad, A., *Adv Healthc Mater* **2018,** *7* (2). DOI 10.1002/adhm.201700426.
340. Zakrzewski, W.; Dobrzynski, M.; Szymonowicz, M.; Rybak, Z., *Stem cell research & therapy* **2019,** *10* (1), 68. DOI 10.1186/s13287-019-1165-5.
341. Caplin, J. D.; Granados, N. G.; James, M. R.; Montazami, R.; Hashemi, N., *Adv Healthc Mater* **2015,** *4* (10), 1426-50. DOI 10.1002/adhm.201500040.
342. Naumovska, E.; Aalderink, G.; Wong Valencia, C.; Kosim, K.; Nicolas, A.; Brown, S.; Vulto, P.; Erdmann, K. S.; Kurek, D., *International journal of molecular sciences* **2020,** *21* (14). DOI 10.3390/ijms21144964.
343. Huh, D.; Fujioka, H.; Tung, Y. C.; Futai, N.; Paine, R., 3rd; Grotberg, J. B.; Takayama, S., *Proceedings of the National Academy of Sciences of the United States of America* **2007,** *104* (48), 18886-91. DOI 10.1073/pnas.0610868104.
344. Ren, X.; Getschman, A. E.; Hwang, S.; Volkman, B. F.; Klonisch, T.; Levin, D.; Zhao, M.; Santos, S.; Liu, S.; Cheng, J.; Lin, F., *Lab Chip* **2021,** *21* (8), 1527-1539. DOI 10.1039/d0lc01194k.
345. Giobbe, G. G.; Michielin, F.; Luni, C.; Giulitti, S.; Martewicz, S.; Dupont, S.; Floreani, A.; Elvassore, N., *Nature methods* **2015,** *12* (7), 637-40. DOI 10.1038/nmeth.3411.

346. Frohlich, E. M.; Zhang, X.; Charest, J. L., *Integrative biology : quantitative biosciences from nano to macro* **2012,** *4* (1), 75-83. DOI 10.1039/c1ib00096a.
347. Ferrell, N.; Desai, R. R.; Fleischman, A. J.; Roy, S.; Humes, H. D.; Fissell, W. H., *Biotechnol Bioeng* **2010,** *107* (4), 707-16. DOI 10.1002/bit.22835.
348. Musah, S.; Mammoto, A.; Ferrante, T. C.; Jeanty, S. S. F.; Hirano-Kobayashi, M.; Mammoto, T.; Roberts, K.; Chung, S.; Novak, R.; Ingram, M.; Fatanat-Didar, T.; Koshy, S.; Weaver, J. C.; Church, G. M.; Ingber, D. E., *Nature biomedical engineering* **2017,** *1*. DOI 10.1038/s41551-017-0069.
349. Shintu, L.; Baudoin, R.; Navratil, V.; Prot, J. M.; Pontoizeau, C.; Defernez, M.; Blaise, B. J.; Domange, C.; Pery, A. R.; Toulhoat, P.; Legallais, C.; Brochot, C.; Leclerc, E.; Dumas, M. E., *Analytical chemistry* **2012,** *84* (4), 1840-8. DOI 10.1021/ac2011075.
350. Wagner, I.; Materne, E. M.; Brincker, S.; Sussbier, U.; Fradrich, C.; Busek, M.; Sonntag, F.; Sakharov, D. A.; Trushkin, E. V.; Tonevitsky, A. G.; Lauster, R.; Marx, U., *Lab Chip* **2013,** *13* (18), 3538-47. DOI 10.1039/c3lc50234a.
351. Giridharan, G. A.; Nguyen, M. D.; Estrada, R.; Parichehreh, V.; Hamid, T.; Ismahil, M. A.; Prabhu, S. D.; Sethu, P., *Analytical chemistry* **2010,** *82* (18), 7581-7. DOI 10.1021/ac1012893.
352. Nam, K. H.; Smith, A. S. T.; Lone, S.; Kwon, S.; Kim, D. H., *Jala* **2015,** *20* (3), 201-215. DOI 10.1177/2211068214557813.
353. Radhakrishnan, J.; Varadaraj, S.; Dash, S. K.; Sharma, A.; Verma, R. S., *Drug Discov. Today* **2020,** *25* (5), 879-890. DOI 10.1016/j.drudis.2020.03.002.
354. Zhang, B. Y.; Korolj, A.; Lai, B. F. L.; Radisic, M., *Nat. Rev. Mater.* **2018,** *3* (8), 257-278. DOI 10.1038/s41578-018-0034-7.
355. Wang, Y. I.; Carmona, C.; Hickman, J. J.; Shuler, M. L., *Advanced Healthcare Materials* **2018,** *7* (2). DOI 10.1002/adhm.201701000.
356. Raimondi, M. T.; Albani, D.; Giordano, C., *Trends Mol Med* **2019,** *25* (9), 737-740. DOI https://doi.org/10.1016/j.molmed.2019.07.006.
357. Raimondi, I.; Izzo, L.; Tunesi, M.; Comar, M.; Albania, D.; Giordano, C., *Frontiers in Bioengineering and Biotechnology* **2020,** *7*. DOI 10.3389/fbioe.2019.00435.
358. van Dijk, C. G. M.; Brandt, M. M.; Poulis, N.; Anten, J.; van der Moolen, M.; Kramer, L.; Homburg, E.; Louzao-Martinez, L.; Pei, J. Y.; Krebber, M. M.; van Balkom, B. W. M.; de Graaf, P.; Duncker, D. J.; Verhaar, M. C.; Luttge, R.; Cheng, C., *Lab on a Chip* **2020,** *20* (10), 1827-1844. DOI 10.1039/d0lc00059k.
359. Sun, W. J.; Luo, Z. M.; Lee, J.; Kim, H. J.; Lee, K.; Tebon, P.; Feng, Y. D.; Dokmeci, M. R.; Sengupta, S.; Khademhosseini, A., *Advanced Healthcare Materials* **2019,** *8* (4), 12. DOI 10.1002/adhm.201801363.
360. Brancato, V.; Oliveira, J. M.; Correlo, V. M.; Reis, R. L.; Kundu, S. C., *Biomaterials* **2020,** *232*. DOI 10.1016/j.biomaterials.2019.119744.
361. Oddo, A.; Peng, B.; Tong, Z. Q.; Wei, Y. K.; Tong, W. Y.; Thissen, H.; Voelcker, N. H., *Trends Biotechnol.* **2019,** *37* (12), 1295-1314. DOI 10.1016/j.tibtech.2019.04.006.